

## CHAPTER 2

# General and theoretical aspects of the cyclopropyl group

DIETER CREMER, ELFI KRAKA and KALMAN JOSEF SZABO

*Department of Theoretical Chemistry, University of Göteborg, Kemigården 3,  
S-41296 Göteborg, Sweden*

---

I. INTRODUCTION	44
II. STRUCTURE AND TOPOLOGY	45
III. ELECTRONIC STRUCTURE—ORBITAL DESCRIPTION	48
A. Walsh Orbitals and Refined Walsh Orbitals	49
B. Förster–Coulson–Moffitt Orbitals and Non-orthogonal Valence Bond Hybrid Orbitals	55
C. SCF Orbitals, Orbital Energies and Ionization Potentials	60
IV. ELECTRON DENSITY DISTRIBUTION AND CHEMICAL BONDING	61
A. Analysis of the Difference Electron Density Distribution	62
B. Analysis of the Electron Density Distribution	64
C. Analysis of the Laplacian of the Electron Density Distribution	68
D. Surface Delocalization, $\pi$ -Complexes and Bonding	68
V. ENERGY AND STABILITY	73
A. Analysis of Ring Strain in Terms of Atomic Energies	74
B. Analysis of Ring Strain in Terms of Bond Energies	75
C. Dissection of the Molecular Energy into Strain Contributions	77
D. Dissection of the Molecular Wave Function	79
E. Strain Energy, $\sigma$ -Aromaticity and Surface Delocalization	82
VI. GEOMETRY	83
A. Geometry of Cyclopropane	85
B. Substituent Effects on the Geometry of the Cyclopropyl Group	86
1. The molecular orbital description	87
2. The electron density description	90
3. Substituted cyclopropanes	93
C. Rationalization of the Geometry of Three-membered Rings	96
VII. VIBRATIONAL SPECTRA	98
VIII. ONE-ELECTRON PROPERTIES	106
IX. NMR SPECTRA	109

---

*The Chemistry of the Cyclopropyl Group.* Volume 2. Edited by Zvi Rappoport  
Copyright © 1995 John Wiley & Sons, Ltd. ISBN: 0-471-94074-7

X. EXCITED STATES AND ULTRAVIOLET ABSORPTION SPECTRA	111
XI. CHARGED CYCLOPROPYL GROUPS	113
A. Cyclopropyl Anion	113
B. Protonated Cyclopropane	114
C. Cyclopropyl Radical Cation	116
D. Cyclopropyl Cation	117
XII. THE CYCLOPROPYL RADICAL	120
XIII. FUSED CYCLOPROPANES	123
A. Bicyclo[1.1.0]butane	123
B. [1.1.1]Propellane	124
XIV. FORMATION AND REACTIVITY	125
A. Formation Reactions	125
B. Thermal Ring-opening and Stereomutation Reactions	126
C. Electrophilic Ring-opening Reactions and Insertion Reactions	126
XV. ACKNOWLEDGEMENTS	129
XVI. REFERENCES	129

## I. INTRODUCTION

The chemical and physical properties of cyclopropane (**1**) and the cyclopropyl group significantly differ from those of other alkanes or cycloalkanes. Best known is the double-bond-like behaviour of a cyclopropane ring in conjugation with a  $\pi$ -system. Also unusual are the length of its CC and CH bonds, upfield shifts of its proton and  $^{13}\text{C}$  NMR signals, its UV spectrum and its (for a three-membered ring) relatively large stability. Contrary to other cycloalkanes, **1** undergoes ring opening upon attack by an electrophile, but resists substitution.

Many of the peculiarities of cyclopropane and the cyclopropyl group have been described in detail in previous review articles<sup>1-5</sup> and in many theoretical investigations that focused on the electronic structure of **1**<sup>6-13</sup>. A considerable part of the *ab initio* work on **1** up to the year 1987 has been reviewed by Wiberg in the previous volume on the *Chemistry of the Cyclopropyl Group*<sup>14</sup>. Some other theoretical work has also been covered in review articles by Runge (on the chiroptical properties of the cyclopropyl group)<sup>15</sup>, by Morris (on the NMR and infrared spectra of cyclopropanes)<sup>16</sup>, by Ballard (on the photoelectron spectra of cyclopropanes)<sup>17</sup>, by Battiste and Coxon (on the acidity and basicity of cyclopropanes)<sup>18</sup> and by Tidwell (on conjugation and substituent properties of cyclopropanes)<sup>19</sup>, which appeared also in the previous volume on the *Chemistry of the Cyclopropyl Group*. However, since these articles were written, a considerable amount of new research on **1** has been published that will be covered in the present article. Also, in each of the previous articles a particular aspect of the theory of the cyclopropyl group was presented since a general account on the theoretical work of **1** was not intended. For example, Wiberg<sup>14</sup> concentrated in particular on his own work on **1** and its derivatives to get a consistent presentation of the theory of the cyclopropyl group.

In the present article, *ab initio* investigations on **1** and the cyclopropyl group published in the last seven years are summarized. But apart from this, we will also include some of the theoretical work that appeared before 1987, but were not mentioned in Wiberg's review. We will also shortly repeat some of the theoretical aspects of the cyclopropyl group already included in Wiberg's work, because this is necessary for a readable presentation. Finally, we will stress electronic features of the cyclopropyl group that have an impact on the general understanding of phenomena such as the delocalization of electrons or chemical bonding. For example, investigation of the electronic structure of **1** is essential for a

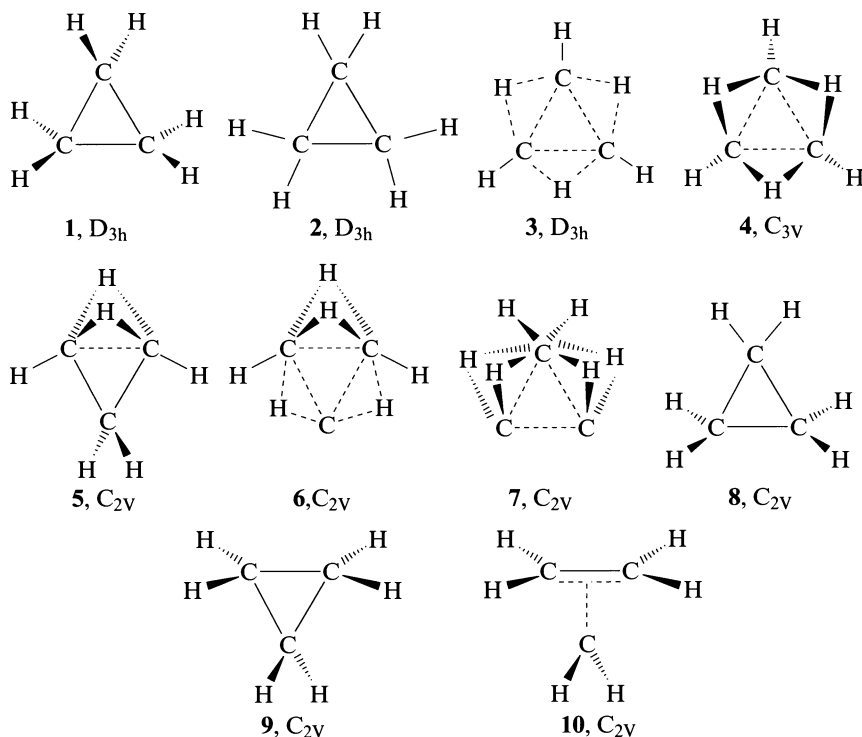


FIGURE 1. Possible structural formulas for a molecule with a  $C_3$ -ring and the stoichiometric formula  $C_3H_6$

critical evaluation of new concepts such as surface delocalization of electrons (as opposed to ribbon or volume delocalization) or  $\sigma$ -aromaticity (as opposed to  $\pi$ -aromaticity)<sup>8-13, 20</sup>.

In this way, we attempt to present a state-of-the-art account of the theoretical work on the cyclopropyl group that also leaves room for controversial descriptions even if we have to sacrifice the quality of consistency in the presentation. The inclusion of conflicting results will show an important point: although the cyclopropyl group is one of the best investigated functional groups (both experimentally and theoretically), there are still open questions with regard to its electronic structure, molecular properties and reactivity. It is the purpose of this chapter to give a fair presentation of all theoretical aspects of the cyclopropyl group, not only those that are no longer subject to theoretical discussions. To fulfill this objective, we have covered the literature up to July 1994.

## II. STRUCTURE AND TOPOLOGY

Cyclopropane,  $C_3H_6$ , is the smallest cycloalkane. If one considers that the three C atoms have to form a ring, then only few chemically reasonable possibilities will remain to attach the H atoms to the carbon ring. In structures 1 and 2 shown in Figure 1, all C atoms are tetravalent while in structures 3, 4 and 5 some or all C atoms are penta-coordinated because H atoms take a bridge position between the C atoms thus leading to non-classical cycloalkane structures. Structures 6 and 7 lead to hexa- and octa-coordinated C with the H atoms clustering in one region of the molecule.

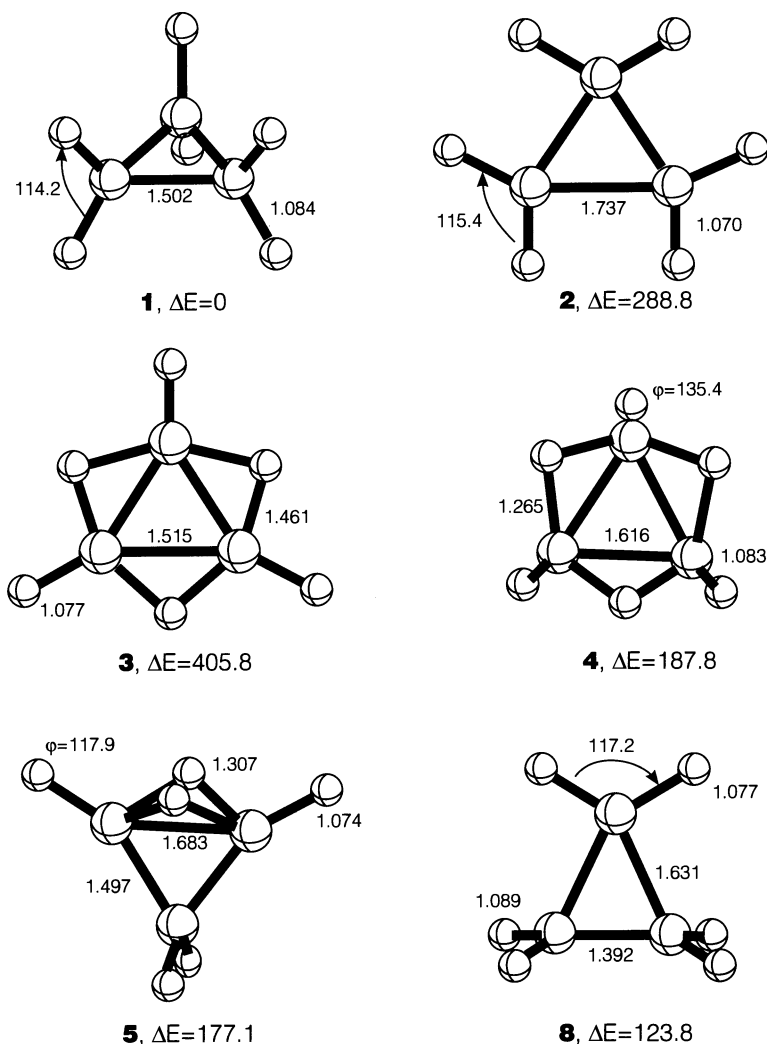


FIGURE 2. Geometries (bond lengths in Å, angles in deg) and relative energies (in kcal mol<sup>-1</sup>) of possible structures of C<sub>3</sub>H<sub>6</sub> [MP2/6-31G(d) calculations]. Structure **3** has a triplet ground state while all other structures possess singlet ground states. Angle  $\varphi$  denotes the folding of the plane CH<sub>bridge</sub>C out of the ring plane

Considering that cyclopropane possesses  $D_{3h}$  symmetry, structures **4**, **5**, **6** and **7** can be excluded. Considering further that all C atoms in cyclopropane are tetravalent, only **1** and **2** remain as possible cyclopropane structures. Finally, structure **1** is left as the only possibility if one considers that each CH<sub>2</sub> group in the molecule has to be perpendicular to the ring plane.

Although structures **2–7** are rather unusual alternatives for **1**, it is interesting to compare their properties with those of **1**. As shown in Figure 2, structure **2** with all CH<sub>2</sub> groups in the plane of the carbon ring possesses a relatively high energy [289 kcal mol<sup>-1</sup>, MP2/6-

31G(d) calculations] that would be sufficient to break not just one CC (CH) but several CC (CH) bonds. This is because structure **2** contains three times a 'planar C atom' (i.e. all four bonds of tetravalent C lying in a plane) which is a configuration that leads to two rather than four bonding electrons and two non-bonding  $p\pi$ -electrons. In the case of **2**, there would be just six electrons for 12 CC and CH bonds, thus leading to a highly electron-deficient hydrocarbon with rather long CC bonds (1.74 Å, Figure 2). These are also weakened by electron repulsion between six  $\pi$ -type lone-pair electrons located at the C atoms. Hence, **2** is not an electronically feasible structure. Even if only one CH<sub>2</sub> group in cyclopropane is rotated into the ring plane as in structure **8** (Figure 1), the energy increases to 124 kcal mol<sup>-1</sup> (Figure 2) as has been shown by Schleyer and coworkers<sup>21</sup>. A planar C atom in a three-membered ring can only be stabilized if hetero atoms with (a)  $\pi$ -electron acceptor and (b)  $\sigma$ -electron donor ability are incorporated into the ring. This is accomplished for diboracyclopropane, which is more stable by 13 kcal mol<sup>-1</sup> in the planar structure than in the non-planar structure<sup>22</sup>.

Structure **3** may be thought of as containing sp<sup>2</sup>-hybridized C atoms connected by three H bridges. There would be six electrons from the C atoms and three from the bridging H atoms for cyclic bonding, which means that one  $\sigma$ -electron would be unpaired. Similarly, one of the three  $\pi$ -electrons would be also unpaired, thus leading to a triplet biradical if the two unpaired electrons would have parallel spin or an open-shell singlet biradical if the  $\sigma$ - and the  $\pi$ -electron would obtain parallel spins. In any case, structure **3** would be highly unstable [ $\Delta E = 406$  kcal mol<sup>-1</sup> for the triplet ground state, UMP2/6-31G(d) calculations, Figure 2]. Calculations suggest CC distances of 1.52 Å and CH<sub>bridge</sub> distances of 1.46 Å.

Structure **3** is considerably stabilized if the H bridges and the normal CH bonds can bend out of the C plane thus leading to the C<sub>3v</sub>-symmetrical structure **4**. In **4**,  $\sigma$ - and  $\pi$ -orbitals mix and, as a consequence, there is pairing of all electrons and an involvement of all electrons into bonding. This decreases the relative energy to 188 kcal mol<sup>-1</sup>, which is still too high to compete with structure **1** since CC and CH bond dissociation energies are much smaller than 188 kcal mol<sup>-1</sup>. The three CC distances increase to 1.62 Å while CH<sub>bridge</sub> distances decrease to 1.27 Å (Figure 2). The CH<sub>bridge</sub> C plane is folded by the angle  $\varphi = 135^\circ$  out of the ring plane.

In structure **5**, one normal CH<sub>2</sub> group is included into the ring with the HCH plane standing orthogonal to the ring plane. The adjacent CC bonds are normal, which is confirmed by bond lengths of 1.50 Å close to the values found for **1** (Figure 2). The third CC bond is bridged by two H atoms, which leads to some lengthening of the interaction distances (CC: 1.68 Å, CH<sub>bridge</sub>: 1.31 Å). Structure **5** is somewhat more stable than **4** ( $\Delta E = 177$  kcal mol<sup>-1</sup>), but still too unstable to be of any relevance.

Since both structures **6** and **7** are highly unstable, we can conclude that the cyclopropane structure **1** is by far the most stable cyclic C<sub>3</sub>H<sub>6</sub> system possible. It complies with the rules of classical carbon chemistry [tetravalent C, (distorted) tetragonal geometries] and, therefore, it is relatively stable.

In Figure 3, the chemical relationship of **1** to other compounds is indicated by simple changes in its structure. Ionization will lead to the cyclopropyl radical cation (reaction 1, Section XI. C), homolytic or heterolytic CH bond dissociation (reactions 2,3,4) to cyclopropyl radical (Section XII), cation (Section XI. D) and anion (Section XI. A) and CC bond rupture to the trimethylene biradical (reaction 5, Section XIV. B) and propene (reaction 6). Reaction 7 is actually more interesting in the reverse mode as the ethene-carbene cycloaddition reaction leading to **1** (Section XIV. A). Reaction 8 is just formal (Section V. A) and reactions 9,10 and 11 bring **1** into relation with its carbene, with cyclopropene and cyclopropyne, which will not be discussed in this chapter. The protonation reaction 12 (Section XI. B) can lead to edge or corner protonated **1** while the CH<sub>2</sub> insertion reaction 13 sets **1** into relation with its higher homologue cyclobutane (Section XIV. C). Most of these reactions will be discussed in this review article, but a comment with regard to reaction 7



The Förster–Coulson–Moffitt orbitals<sup>23,24</sup>, on the other hand, are considered to represent localized (bond) orbitals that help to visualize the bent bond character of the CC bonds of **1** and to explain its ring strain. They seem to be less suited to analyse substituent–ring interactions or the conjugative properties of **1**.

However, these views are largely incorrect. Walsh orbitals suffer from a number of deficiencies that one has to know before using them.

1. Heilbronner and coworkers<sup>31</sup> have shown that Walsh orbitals and Förster–Coulson–Moffitt orbitals are not equivalent. For example, only the Förster–Coulson–Moffitt orbitals but not the Walsh orbitals are part of the manifold of bonding cyclopropane orbitals. Therefore, a correct description of bonding in **1** in terms of Walsh orbitals is not possible.

2. Because of this, interactions between CH<sub>2</sub> apex group and CH<sub>2</sub>CH<sub>2</sub> basal fragment cannot correctly be described using Walsh orbitals. For example, the  $\sigma$ -bridged- $\pi$ -character<sup>32</sup> of HOMO 12 (see Section VI. C) is lost and, by this, also the possibility of describing the exact relationship between three-membered rings and  $\pi$ -complexes<sup>9,11–13,34–44</sup>.

3. It is not possible to describe the properties of the cyclopropyl radical cation correctly on the basis of the Walsh orbitals (see Section XI. C and, there, Reference 233).

4. The hybridization scheme used by Walsh (sp<sup>2</sup>, p for C) disguises the pseudo- $\pi$ -character of some of the CH<sub>2</sub> orbitals of **1**<sup>29,30</sup>.

5. It is not possible to describe the interactions of **1** with  $\pi$ -donor substituents (let alone  $\sigma$ -donor/ $\sigma$ -acceptor substituents) on the basis of Walsh orbitals. For this purpose one has to retreat to the full set of SCF orbitals<sup>33</sup>.

6. The conjugative propensity of the cyclopropyl group is wrongly explained to depend only on the overlap between Walsh orbitals and adjacent  $\pi$ -orbitals while in reality it is also a consequence of the HOMO energies of **1** that facilitate delocalization of electrons into low-lying  $\pi^*$  orbitals<sup>31</sup>.

If one wants to use Walsh orbitals for discussing the properties of the cyclopropyl group, one has to refine them.

## A. Walsh Orbitals and Refined Walsh Orbitals

Walsh<sup>25</sup> derived the CC MOs for **1** by considering that the molecule is made up of CH<sub>2</sub> units, each of which has a set of sp<sup>2</sup> hybrid orbitals and a p-orbital. However, a somewhat more realistic picture of the MOs is obtained by assuming a set of sp hybrid orbitals complemented by two p orbitals for each C atom. In Figure 4, these orbitals are classified<sup>11,12</sup> as radially oriented (with regard to the centre of the ring) sp<sub>in</sub> and sp<sub>out</sub> orbitals and tangentially oriented (with regard to the perimeter of the ring) p<sub>ip</sub> (in-plane) and p<sub>op</sub> (out-of-plane) orbitals. Orbitals sp<sub>out</sub> and p<sub>op</sub> form together with the in-phase and the out-of-phase combination of the two 1s orbitals of the H···H unit the  $\sigma$ (CH<sub>2</sub>) and  $\pi$ (CH<sub>2</sub>) orbitals of **1** while sp<sub>in</sub> and p<sub>ip</sub> lead to CC  $\sigma$ - and  $\pi$ -orbitals of the ring. In Figure 4 it is shown that the orbital set {sp<sub>in</sub>, sp<sub>out</sub>, p<sub>ip</sub>, p<sub>op</sub>} can be used for the construction of the MOs of any cycloalkane, where ethene is included as a ‘two-membered cycloalkane’. The radially oriented CC orbitals are  $\sigma$ -type for ethene and **1** (formally, they enclose angles of 30° with the internuclear connection lines in the case of **1**), while the tangentially oriented CC orbitals have  $\pi$ -character (they enclose angles of 60° with the internuclear connection line for **1**). Cremer<sup>11,12</sup> pointed out that the nature of the CC orbitals changes when going from small to larger rings: The  $\sigma$ (CC) orbitals of ethene and **1** become the  $\pi$ -type ribbon orbitals of a larger ring and the  $\pi$ -orbitals become  $\sigma$ -type ribbon orbitals. In this case, there is a close relationship between ethene and **1** since for these molecules orbitals differ from those of a normal cycloalkane.

The tangential p<sub>ip</sub> orbitals form a Hückel system for even-membered rings but a Möbius system for odd-membered rings. However, this seems to be of little consequence because it has been shown that both Hückel and Möbius orbital systems have always an aromatic

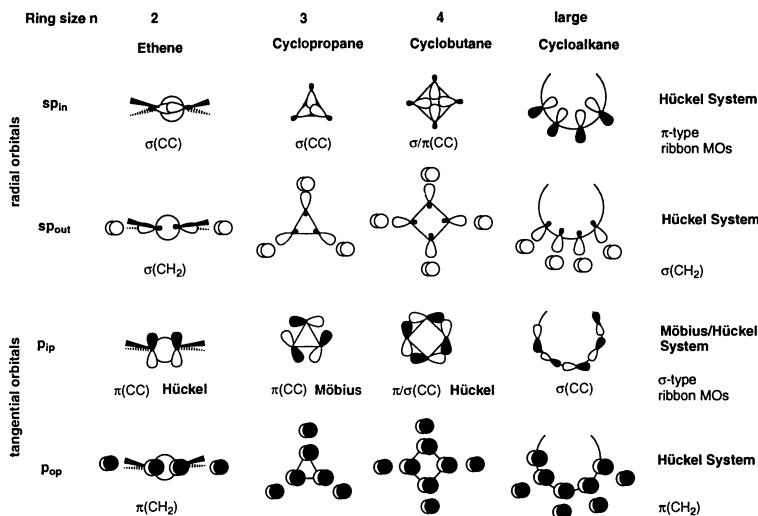


FIGURE 4. Basis orbitals for (planar) cycloalkanes with ring size  $n$ . Basis orbitals comprise the radially oriented  $sp_{in}$  and  $sp_{out}$  hybrid orbitals at C, the tangentially oriented  $p_{ip}$  (in plane) and  $p_{op}$  (out of plane) orbitals at C as well as in-phase and out-of-phase combinations of the two  $1s(H)$  orbitals, which combine with  $sp_{out}$  and  $p_{op}$  orbitals, respectively. Note that ethene is included as a 'two-membered ring' where the ring is symbolized by two bent bonds and the CH bonds are shown to define the orientation of the ring plane (parallel to the drawing plane). The nature of each orbital set ( $\sigma$  or  $\pi$ , CC or  $CH_2$  bonding, Hückel or Möbius type) is given

electron configuration ( $n = 2$ : 2;  $n = 3$ : 4;  $n = 4$ : 6 electrons, etc.) Molecule **1** as any other cycloalkane possesses only subshells with aromatic electron ensembles (see Figure 4) and, therefore, an aromatic/antiaromatic classification of cycloalkanes is not possible on a topological basis<sup>11, 12</sup>.

In Figure 5, an orbital interaction diagram is shown, in which radial and tangential orbitals are combined to the MOs of **1**. The orbital interaction diagram is based on a SCF calculation with a large basis set and differs with regard to the order of the unoccupied MOs considerably from previously published diagrams and orbital sets that were based on Extended Hückel type or minimal basis set SCF calculations<sup>29-31</sup>. It is well known that the virtual (unoccupied) MOs of a SCF calculation have little chemical significance because virtual MOs are just a by-product of the mathematical procedure to calculate the occupied MOs. Nevertheless, one uses the virtual MOs of minimal basis set calculations to illustrate energy ordering, shape and nodal properties of unoccupied MOs. In this spirit, all previous presentations of the MOs of **1** have been made.

However, it seems to us more interesting to present unoccupied MOs in the way they are suggested by large basis set HF calculations. This, of course, leads to the inclusion of diffuse virtual orbitals (Rydberg orbitals) with orbital energies close to zero into the set of unoccupied MOs, but diffuse virtual MOs are needed to reproduce the measured ultraviolet absorption spectrum of **1** in a CI calculation (see Section X). Therefore, the ordering of virtual orbitals given in Figures 5 and 6 (below) has some justification, although it may be generally criticized on the basis that virtual MOs have no physical meaning.

The six Walsh orbitals of **1** are formed from the (radial)  $sp_{in}$  and (tangential)  $p_{ip}$  starting orbitals. They may be denoted as  $\omega_O$ ,  $\omega_S$ ,  $\omega_A$  (CC bonding) and  $\omega_O^*$ ,  $\omega_S^*$ ,  $\omega_A^*$  orbital (CC antibonding). Two important improvements of the original Walsh orbitals  $\omega$  are indicated in Figure 5:



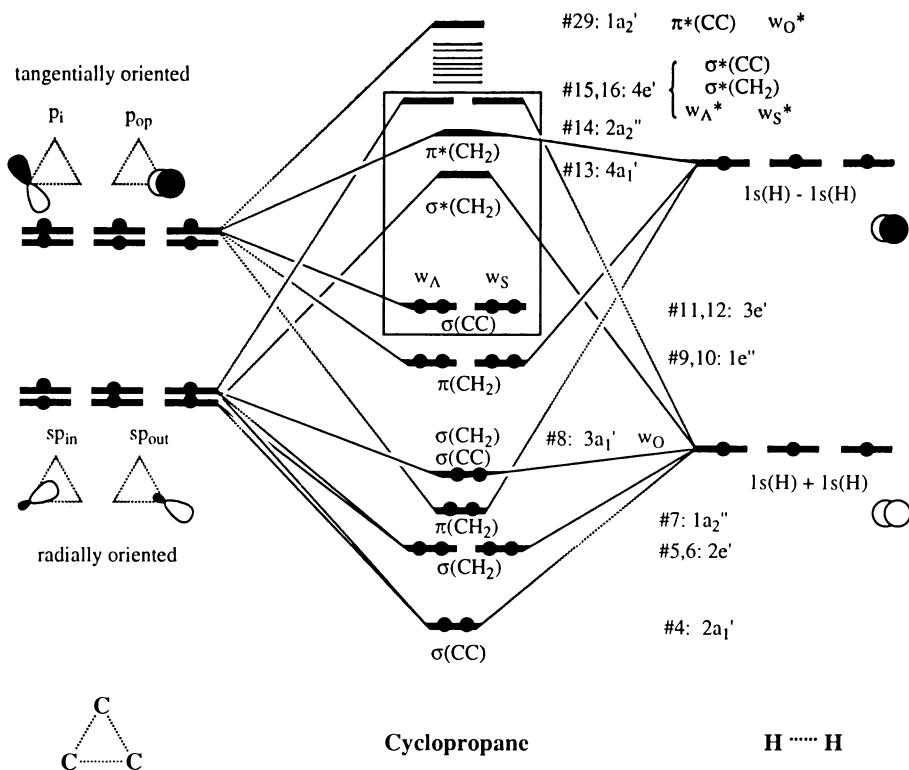


FIGURE 5. Orbital interaction diagram for cyclopropane according to SCF calculations with a large basis set. Basis orbitals for the three C atoms and for the three H...H units are given on the left and the right side, respectively. Resulting MOs are characterized with regard to their symmetry,  $\sigma/\pi$  character and their bonding nature (stars indicate antibonding nature). They are numbered including core orbitals  $1a_1'$  and  $1e'$ . Orbital mixing between  $3e'$  and  $4e'$  MOs is indicated by a frame around the corresponding orbital levels. CC bonding and antibonding MOs that correspond to one of the refined Walsh orbitals are denoted by the appropriate symbol, namely  $w_O$ ,  $w_A$ ,  $w_S$ ,  $w_O^*$ ,  $w_A^*$  or  $w_S^*$

1. The  $\sigma(\text{CC})$  and  $\sigma(\text{CH}_2)$  orbitals of  $a_1'$  symmetry can mix. As a result, the  $2a_1'$  (MO 4) orbital obtains more s-character and becomes almost pure CC bonding while the  $3a_1'$  (MO 8,  $w_O$ ) orbital gets more p-character, mixes with the in-phase combination of the HH orbitals and adopts both CC and  $\text{CH}_2$  bonding character.

2. The refined Walsh orbitals  $3e'$  (MOs 11, 12;  $w_A$  and  $w_S$ ) and  $4e'$  (MOs 15, 16;  $w_A^*$  and  $w_S^*$ ) result from mixing between the original Walsh orbitals  $\omega$  (indicated in Figure 5 by a frame around these orbitals) as shown in equations 1–4:

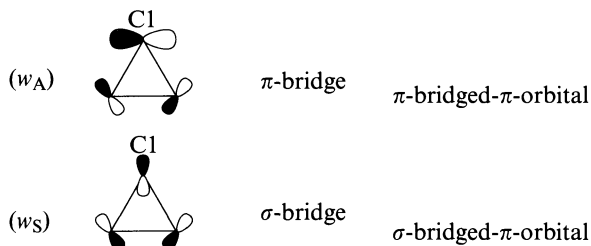
$$\text{MO 11:} \quad w_A = N_A (\omega_A + \lambda \omega_A^*) \quad (1)$$

$$\text{MO 15:} \quad w_A^* = N_A^* (\omega_A - \lambda \omega_A^*) \quad (2)$$

$$\text{MO 12:} \quad w_S = N_S (\omega_S + \lambda \omega_S^*) \quad (3)$$

$$\text{MO 16:} \quad w_S^* = N_S^* (\omega_S - \lambda \omega_S^*) \quad (4)$$

where  $N$  is a normalization factor and  $\lambda$  a mixing coefficient. As a result of the mixing, HOMOs  $3e'$  ( $w_A$  and  $w_S$ ) can be classified as ' $\pi$ -bridged- $\pi$  orbital' ( $\pi$ -orbital bridge at C1) and ' $\sigma$ -bridged- $\pi$ -orbital' ( $\sigma$ -orbital bridge at C1, see Scheme 1)<sup>32</sup>.



SCHEME 1

Mixing of  $3e'$  and  $4e'$  orbitals increases (a) the  $\pi$ -character (in the C2C3 bond) of the original  $w_A$  and the  $w_S^*$  orbitals and adds (b) the  $\sigma$ -orbital bridge to orbitals  $w_S$  and  $w_A^*$ . This is shown more clearly in Figure 6, where both the refined Walsh orbitals  $w$  (in the form of simple orbital pictures) and the final canonical SCF MOs (in the form of perspective three-dimensional drawings) of **1** are given. The electronic structure of **1** can only be rationalized if the full set of MOs derived from  $\{sp_{in}, sp_{out}, p_{ip}, p_{op}\}$  by appropriate orbital mixing (i.e. including refined Walsh orbitals  $w$ ) is used.

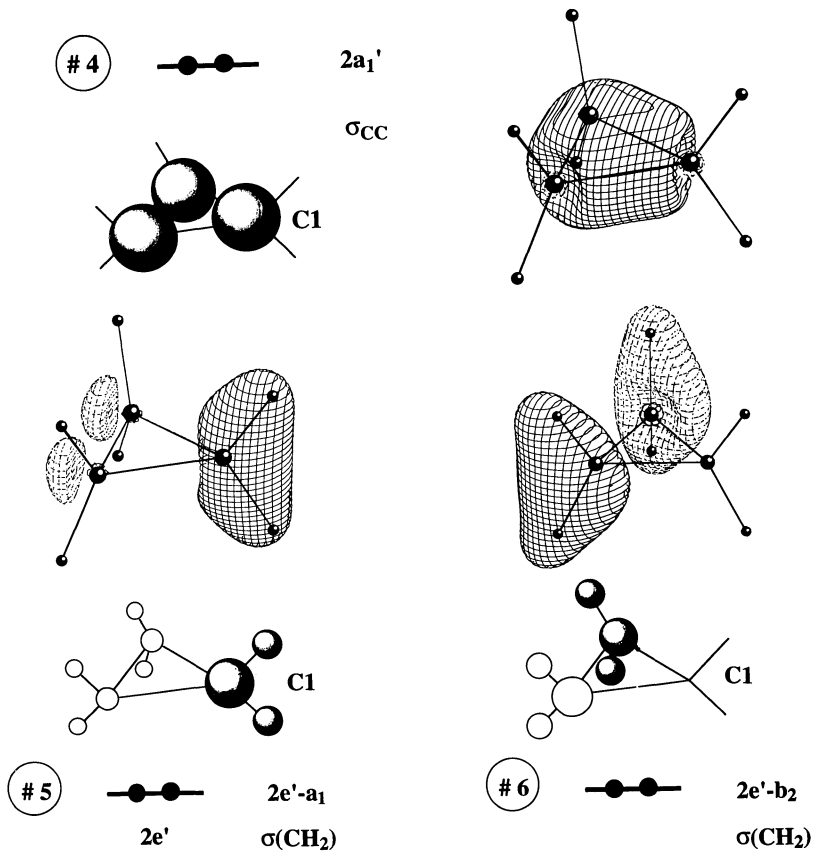


FIGURE 6. (Caption on page 55)

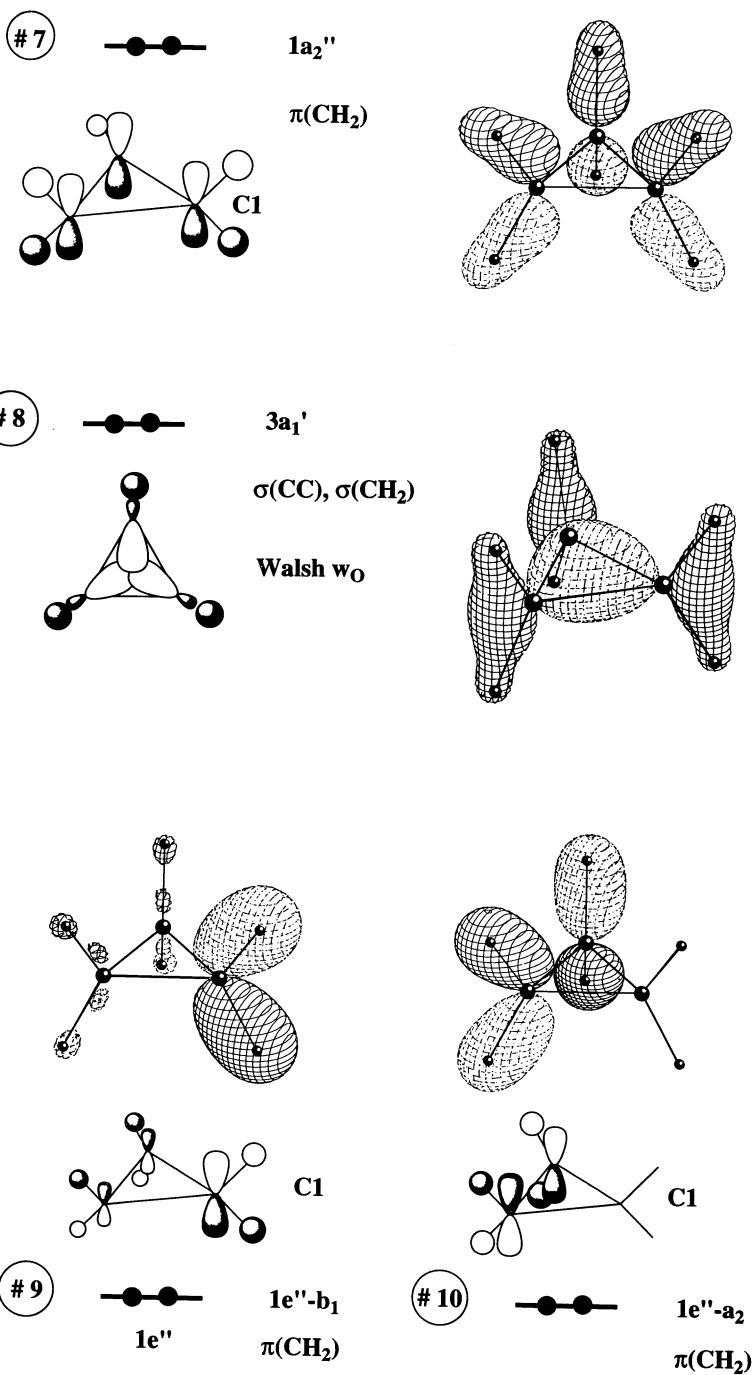


FIGURE 6. (continued)

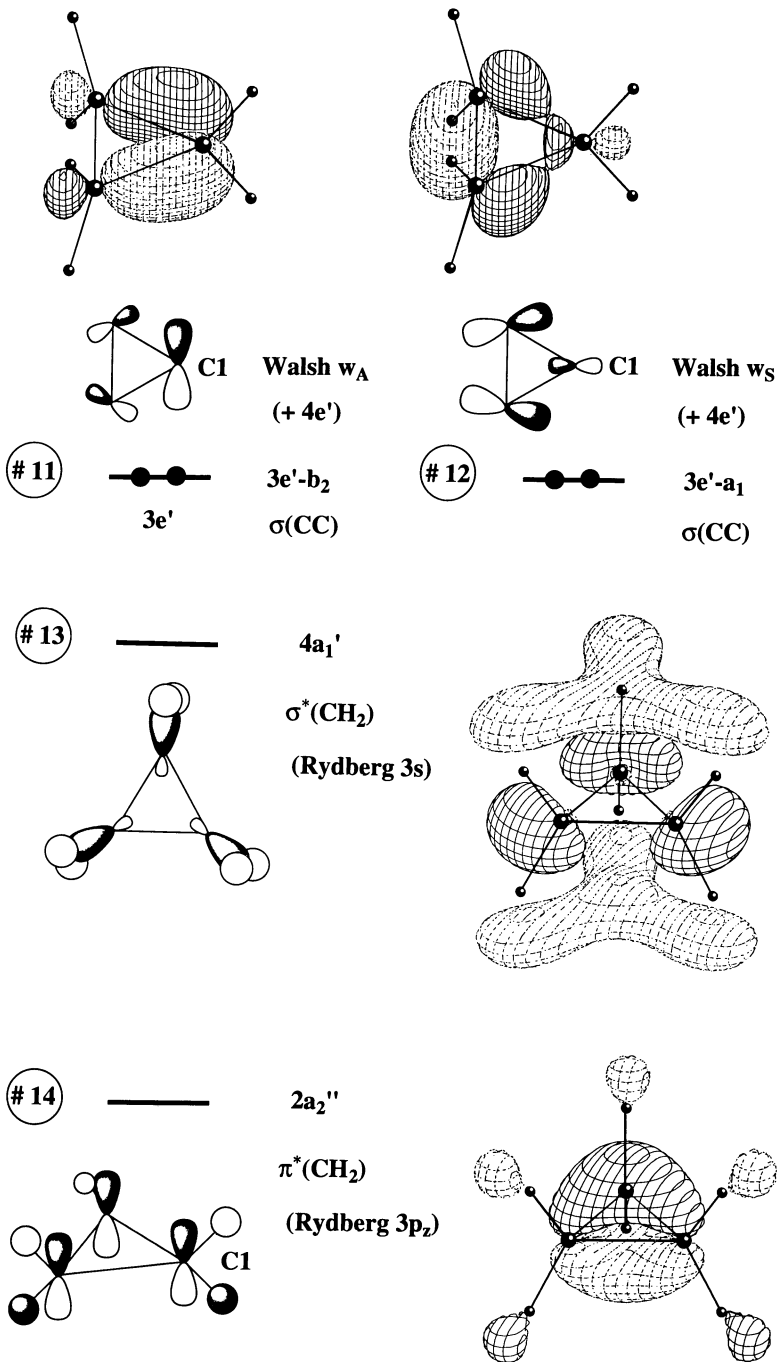


FIGURE 6. (continued)

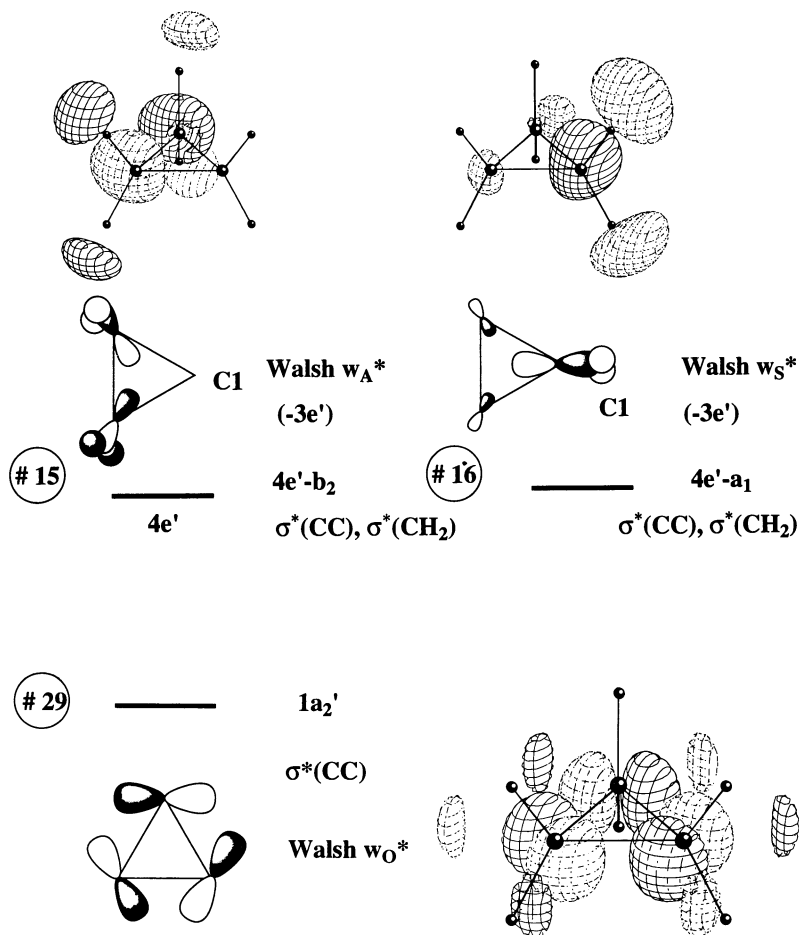


FIGURE 6. Hartree-Fock SCF orbitals of cyclopropane as obtained with a DZ + P basis set. The corresponding orbitals of the orbital interaction diagram shown in Figure 5 are given below or on the left side of each SCF MO. MOs are characterized with regard to their symmetry,  $\sigma/\pi$  character, their anti/bonding nature and possible Rydberg character (unoccupied MOs). For degenerate MOs, additional symmetry designations are given, which the MOs would obtain in case of a  $C_2$  distortion along the  $C_2$  axis that passes through C1. MOs are numbered including core orbitals  $1a_1'$  and  $1e'$ . Orbital mixing between  $3e'$  and  $4e'$  MOs is indicated. CC bonding and antibonding MOs that correspond to one of the refined Walsh orbitals are denoted by the appropriate symbol, namely  $w_O$ ,  $w_A$ ,  $w_S$ ,  $w_O^*$ ,  $w_A^*$  or  $w_S^*$

## B. Förster-Coulson-Moffitt Orbitals and Non-orthogonal Valence Bond Hybrid Orbitals

Coulson and Moffitt<sup>23</sup> established a bent bond model of **1** by elaborating ideas first proposed by Förster<sup>24</sup>. They determined  $sp^n$  (CC) and  $sp^m$  (CH) hybrid orbitals with optimal hybridization ratios  $n$  and  $m$  to describe bonding in **1**. Calculations showed that, for **1**, the p-character of the CC hybrid orbitals has to be increased from  $sp^3$  to  $sp^4$  while the s-

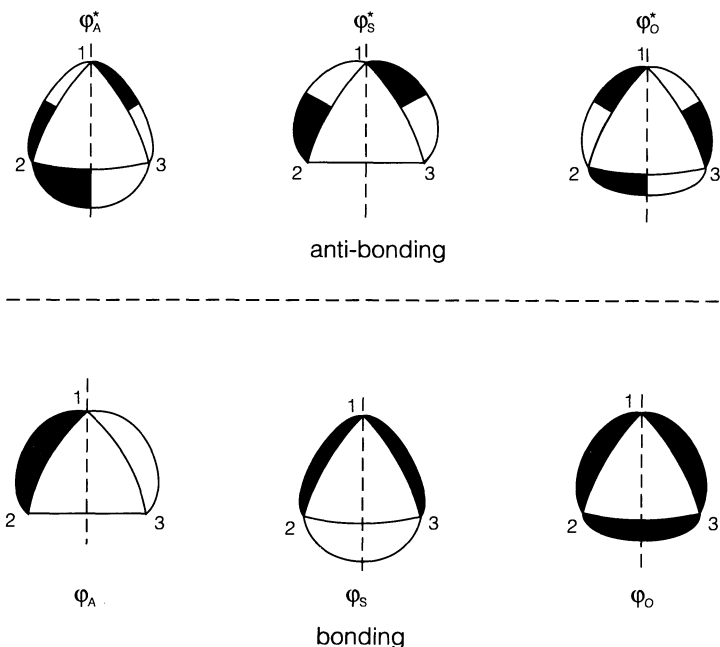


FIGURE 7. Förster–Coulson–Moffitt bent bond orbitals of cyclopropane. Reprinted from E. Honegger, E. Heilbronner and A. Schmelzer, *Nouv. J. Chim.*, **6**, 519 (1982) by permission of Gauthier-Villars Publishers

character of the CH hybrid orbitals increases from  $sp^3$  to  $sp^2$ . Bonding and antibonding CC bond orbitals obtained from these hybrid orbitals are shown in Figure 7.

The Förster–Coulson–Moffitt orbitals ( $\varphi_0$ ,  $\varphi_A$ ,  $\varphi_S$ ,  $\varphi_0^*$ ,  $\varphi_A^*$ ,  $\varphi_S^*$ ) reveal that the CC hybrid orbitals are considerably bent in an attempt to avoid the geometrical angle  $\alpha = 60^\circ$  and to come close to the strain-free tetrahedral angle. Bending of the hybrid orbitals can only be achieved by an increase of their p character. The corresponding orbital energies are increased and the CC bond is weakened. Hence, the Förster–Coulson–Moffitt orbitals suggest weakening of the CC bonds and a strained three-membered ring as a result of bond weakening.

The results of the Coulson–Moffitt model have been verified many times using different energy minimization criteria for obtaining the best hybridization ratios ( $n$  and  $m$ ) and determining angles between bent bond orbitals. Some results are summarized in Table 1<sup>7,23,31,45–47</sup>.

According to SCF calculations followed by a Boys localization<sup>48</sup>, the CC bonding hybrid orbitals deviate by  $28^\circ$  from the CC internuclear connection line, which leads to a interorbital angle of  $115^\circ$ , i.e.  $55^\circ$  larger than the geometrical angle  $\alpha = 60^\circ$ <sup>7</sup>. Wardeiner and coworkers<sup>46</sup> have used the  $^1J(\text{CH})$  coupling constant of **1** and the Müller–Pritchard equation<sup>49</sup> to derive an interorbital angle of  $103^\circ$ . Hence, the original description of CC bonding in **1** by Coulson and Moffitt is essentially confirmed and adds support to the usefulness of the Förster–Coulson–Moffitt bent bond orbitals.

Heilbronner and coworkers<sup>31</sup> have shown that for all practical purposes, Förster–Coulson–Moffitt orbitals can be used as representatives for the final SCF orbitals of **1** while this is only true for the refined Walsh orbitals  $w$  given in equations 1–4 rather than the original Walsh

TABLE 1. Hybridization and interorbital angles in cyclopropane using orthogonal hybrid orbitals

Author(s)	Year	$n$ in $sp^n$		$m$ in $sp^m$		Interorbital angle (deg)		Ref.
		CC	CH	CCC	HCH			
Coulson and Moffitt	1949	4.12	2.28	104	116	23		
Randic and Maksic	1965	4.91	2.02	102	120	45		
Newton	1977	3.38	1.86	115	117	7		
Honegger and coworkers	1982	3.21	1.94	117	116	31a		
Wardeiner and coworkers	1982	4.58	2.12	103	118	46a		
Inagaki and coworkers	1994	4.0	2.0			47		

orbitals  $\omega$ . The use of Förster–Coulson–Moffitt orbitals also helps to correct another common belief based on Walsh orbital descriptions, namely that the ability of the cyclopropyl group to conjugate with unsaturated groups results from the presence of tangential  $p_{ip}$ -orbitals. However, calculations by Heilbronner and coworkers<sup>31</sup> reveal that it is the orbital energy of the  $3e'$ -MOs well above those of other alkanes or cycloalkanes and close to that of the  $\pi$ -orbital of an alkene that leads to delocalization of cyclopropyl CC bonding electrons and the observed conjugative propensity.

Recently, two interesting VB investigations of **1** have been published, which provide insight into the nature of bond orbitals and bonding of **1** and some reference molecules<sup>50,51</sup>. Hamilton and Palke<sup>50</sup> applied a steepest-descent technique to obtain optimized hybrid orbitals and optimized overlap within a perfect-pairing VB approach. They used a DZ + P basis set of Slater-type orbitals (!) and the experimental geometry of **1**. Contrary to previous descriptions of **1** that used orthogonal hybrid orbitals and constraints on the composition (amount of s or p character on one centre is constant) and number of hybrids, the VB description leads to non-orthogonal hybrid orbitals and, accordingly, the hybridization ratios of CC and CH hybrid orbitals are not directly related. Eliminating the orthogonality constraint between CC and CH hybrid orbitals increases their s-character, which can only be analysed by comparing hybridization ratios for suitable reference molecules calculated with the same type of VB wave function.

TABLE 2. Hybridization and overlap values obtained with non-orthogonal hybrid orbitals within a valence bond calculation of cyclopropane<sup>a</sup>

Molecule	CC Bond		CH Bond	
	$sp^n$	overlap	$sp^m$	overlap
CH <sub>4</sub>			$sp^{1.514}$	0.831
H <sub>3</sub> C—CH <sub>3</sub>	$sp^{1.381}$	0.832	$sp^{1.524}$	0.829
H <sub>2</sub> C=CH <sub>2</sub> <sup>b</sup>	$sp^{1.370}$	0.823	$sp^{1.561}$	0.830
Cyclopropane	$sp^{1.706}$	0.827	$sp^{1.348}$	0.833

<sup>a</sup>From Reference 50.

<sup>b</sup>The ethene double bond is composed of two banana bonds, one above and one below the plane of the nuclei. Therefore, the CC overlap value has to be multiplied by a factor 2 to get the total CC bond overlap.

As can be seen from Table 2, the amount of s-character of the CH hybrid orbital of **1** is indeed increased relative to that of the CH hybrid orbitals of ethene, ethane and methane while at the same time the s-character of the CC hybrid orbitals is decreased. This seems to confirm predictions based on model calculations with orthogonal hybrid orbitals. However, closer inspection of the data in Table 2 reveals that s-character of the CH hybrid

orbitals does not parallel expected trends in CH bond strengths. For example, the s-character of the CH hybrid orbitals of ethene is lower than that of methane and ethane, while overlap values suggest similar values for the three molecules with **1** possessing a clearly larger CH overlap value (Table 2). This contradicts the well-documented fact that the CH bond in ethene is significantly stronger than the CH bonds of alkanes. Obviously, the general belief that the bond strength increases as the overlap of the two orbitals in a VB pair is not always confirmed by fully optimized VB calculations.

In this connection, a recent spin-coupled VB calculation of **1** by Karadakov, Gerratt, Cooper and Raimondi<sup>51</sup> is interesting. This approach removes the strong orthogonality constraint of GVB calculations and makes use of the whole spin space and not just of the perfect pairing spin function of other less general one-configuration approaches. In this way, the energy obtained with the single-configuration spin-coupled VB wave function comes in most cases close to that of its CASSCF counterpart. Calculations were done with a DZ+P basis of Gaussian functions for **1**, cyclobutane and propane at experimental geometries. The active space was limited to six, eight and four singly-occupied non-orthogonal CC hybrid orbitals corresponding to the fact that the three molecules contain three, four and two symmetry-equivalent CC bonds.

TABLE 3. Overlap values calculated using non-orthogonal hybrid orbitals within valence bond calculations of propane, cyclopropane and cyclobutane<sup>a</sup>

Overlap	Propane	Cyclopropane	Cyclobutane
Bonding overlap	0.817	0.803	0.798
Geminal overlap	0.290	0.340	0.309
Vicinal through-ring overlap	0.087	0.207	0.144
Vicinal $\pi$ -type overlap	—	0.049	0.124
1,3-Overlap	-0.092	—	-0.022 0.081

<sup>a</sup>From Reference 51. In cyclopropane, bonding overlap corresponds to overlap between hybrid orbitals 1 and 2, geminal overlap to overlap between 2 and 3, vicinal through-ring overlap to overlap between 1 and 3, vicinal  $\pi$ -type overlap between 1 and 4. Compare with Figure 17.

Karadakov and coworkers<sup>51</sup> have published overlap matrices for their optimized non-orthogonal CC hybrid orbitals that show some interesting trends in bonding and non-bonding hybrid orbital overlap (see Table 3). Although the authors claim that CC bonding is similar in **1** and cyclobutane as documented by calculated bonding overlap values (this argument is in itself very problematic, since on the same basis the Hamilton-Palke results would suggest the same CC bonding for ethane and **1**!), comparison of their overlap values reveals a striking difference between **1** on the one side and propane and cyclobutane on the other:

(1) Geminal overlap is 10–20% larger in **1** than in the two other compounds.  
 (2) Vicinal through-ring overlap is more than 40% larger for **1** than in the case of cyclobutane.

(3) Antibonding 1,3 overlap does not exist for **1**, but takes considerable values in propane and cyclobutane.

Nonbonding overlap is significantly larger for **1** and leads to a shift of electron density into the three-membered ring. This is one important aspect of the VB calculations of Karadakov and coworkers (not mentioned by the authors)<sup>51</sup>, which becomes obvious when looking at the VB hybrid orbitals depicted in Figure 8.

No matter whether calculated within the perfect pairing VB approach or by the spin-coupled VB approach, in both cases the CC hybrid orbital extends outside the three-membered ring as expected by the schematic representations in Figure 7, *but also inside*



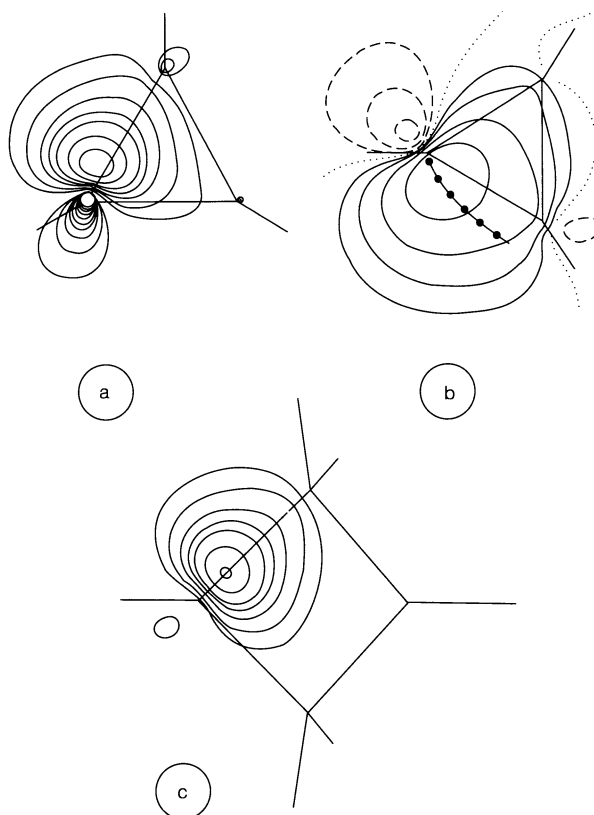


FIGURE 8. Calculated valence bond orbitals of cyclopropane and cyclobutane in the form of contour line diagrams plotted in the plane of the carbon rings. Because of the chosen topside view, only CC and one of the CH bonds of each  $\text{CH}_2$  group can be seen in the form of solid lines connecting atom positions. (a) Orbital density plot of one of the six symmetry-equivalent valence orbitals of cyclopropane obtained from spin-coupled valence bond calculations. (b) Orbital amplitude plot of one of the six symmetry-equivalent valence orbitals of cyclopropane obtained from perfect-pairing valence bond calculations. Solid lines denote positive, dashed lines negative and the dotted line the zero amplitude contour line. Orbital bending is indicated by  $\bullet\text{---}\bullet\text{---}\bullet$  where each point  $\bullet$  is given by the maximum orbital amplitude. (c) Orbital density plot of one of the eight symmetry-equivalent valence orbitals of cyclobutane obtained from spin-coupled valence bond calculations. Diagrams have been reconstructed according to calculations by (a,c) P. B. Karadakov, J. Gerratt, D. L. Cooper and M. Raimondi, *J. Am. Chem. Soc.*, **116**, 7714 (1994) and (b) J. G. Hamilton and W. E. Palke, *J. Am. Chem. Soc.*, **115**, 4159 (1994)

the ring covering the whole ring surface, which cannot be predicted from the pictures in Figure 7.

Hamilton and Palke<sup>50</sup> determined the interorbital angle between the CC hybrid orbitals to be  $123^\circ$  at the position of the C nucleus given by the direction of the maximum orbital amplitude (see  $\bullet\text{---}\bullet\text{---}\bullet$  line in Figure 8). With increasing distance from the nucleus the orbital

bends toward the internuclear connection line as reflected by a decrease of the interorbital angle to  $100^\circ$ . Bending of the orbitals will lead to strain and, since the bending of the CC hybrid orbitals for **1** is clearly larger than for the CC orbitals of cyclobutane (Figure 8), there should be higher strain in the case of **1** in line with common chemical thinking.

### C. SCF Orbitals, Orbital Energies and Ionization Potentials

In Figure 6 perspective drawings of Hartree–Fock SCF orbitals are given. They reveal that the construction of MOs from the basis orbitals shown in Figure 4 leads to a reasonable description of SCF MOs, but their exact form can only be obtained from appropriate mixing of Walsh orbitals of the same symmetry. Worthy of note is the difference in shape of the  $3e'$  HOMOs (#11 and #12) and the  $a_1'$   $\sigma$ -MOs ( $2a_1'$ ,  $3a_1'$ , #4 and #8) that is of relevance for a detailed description of the electronic structure and chemical bonding in **1**.

A complete set of orbital energies, including core orbitals and a large number of unoccupied orbitals, has been published by Segal and coworkers, who used a DZ basis augmented by ring-centred diffuse functions<sup>52</sup>. Valence shell orbital energies or ionization potentials, which can be related to orbital energies via the Koopmans theorem, have been published over the years by various authors<sup>39,52–59</sup>. Some of these data can be found in Ballard's review on the photoelectron spectroscopy of **1** and related three-membered rings<sup>17</sup>. Therefore, only a short summary of orbital energies, calculated ionization potentials and their comparison with experimental vertical ionization potentials of **1** is give in Table 4.

TABLE 4. Orbital energies and ionization potentials of cyclopropane<sup>a</sup>

Orbital		Ionization potential (eV)				
number	sym.	LCAO- $X\alpha$ Ref. 59	HAM/3 Ref. 56	<i>ab initio</i> Ref. 55	Green Ref. 55, 58	Exp Ref. 60
# 11,12	$3e'$	11.9	11.0	11.5	10.7	10.6
# 9, 10	$1e''$	13.1	13.3	13.9	13.0	13.0
# 8	$3a_1'$	16.0	15.4	17.0	15.7	15.7
# 7	$1a_2''$	17.1	16.7	18.3	16.8	16.7
# 5,6	$2e''$	19.1	20.1	22.9	19.9	19.5
# 4	$2a_1'$	27.3	26.1			26.3

<sup>a</sup>Direct calculation of the ionization potential by LCAO- $X\alpha$ , HAM/3 and Green's function techniques or via the Koopmans theorem by *ab initio* techniques.

All calculations confirm the sequence of orbitals given in Figure 6. In particular, they underline the magnitude of the lowest ionization potential (10.6 eV<sup>60</sup>), which according to the Koopmans theorem<sup>61</sup> gives a  $3e'$  orbitals energy similar to that of the ethene  $\pi$ -orbital (10.5 eV<sup>60</sup>). Probably, the most reliable calculations of the ionization of **1** are those by von Niessen and coworkers using Green's functions<sup>55,58</sup>. But also HAM/3 calculations by Fridh<sup>56</sup> and LCAO- $X\alpha$  calculations of ionization potentials by Alti and coworkers<sup>59</sup> are quite satisfactory (apart from the value of the first ionization potential). Hartree–Fock calculations of ionization potentials on the basis of the Koopmans theorem<sup>61</sup> depend on the basis set used, but are on the average 8% too large.

Wiberg and coworkers<sup>62</sup> have calculated the vertical and adiabatic ionization potential of **1** in a comparative study including fused cyclopropanes. Using MP4/6-31G(d) and spin contamination corrected UMP4/6-31G(d) energies calculated at MP2/6-31G(d) geometries of the parent compound and radical cation, they obtained an adiabatic ionization potential (relaxation of geometry of the radical cation) of 9.48 eV and a vertical ionization

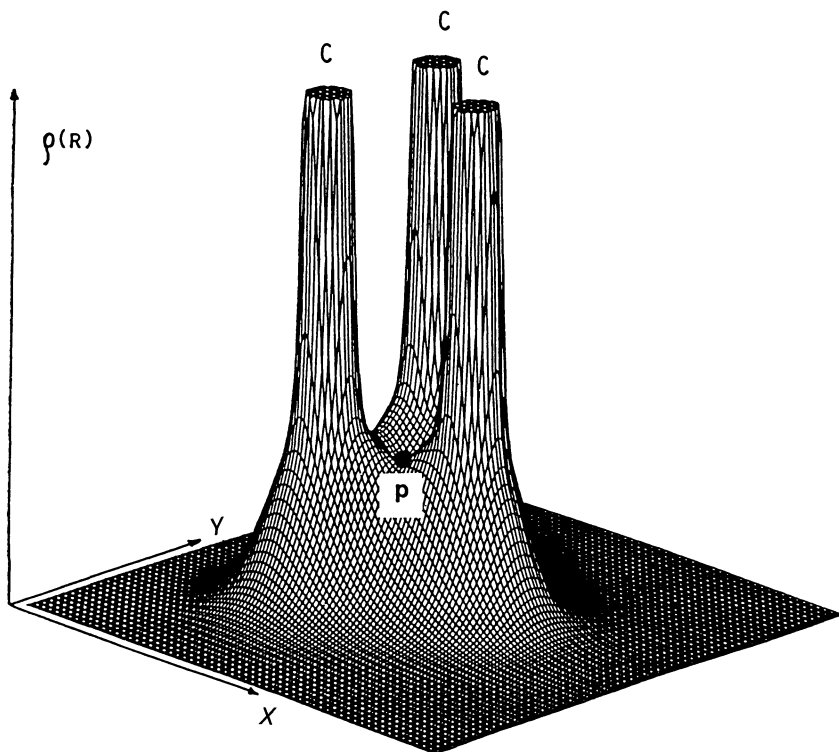


FIGURE 9. Perspective drawing of the calculated electron density distribution  $\rho(\mathbf{r})$  in the plane of the cyclopropane ring [HF/6-31 G(d,p) calculations]. Point **p** denotes the position of the bond critical point between two neighbouring C atoms. For better presentation, density values above  $14 \text{ e } \text{\AA}^{-3}$  are cut off

potential (geometry of parent molecule used for radical cation) of 10.43 eV, where the latter ionization potential has to be compared with an experimental value of 10.6 eV. Although there seems to be reasonable agreement between theory and experiment, calculational results are flawed by the fact that a transition state rather than the ground state of the cyclopropyl radical cation (see Section XI. C) was calculated<sup>62</sup>.

#### IV. ELECTRON DENSITY DISTRIBUTION AND CHEMICAL BONDING

Analysis of the total electron density distribution  $\rho(\mathbf{r})$  of a molecule is useful since  $\rho(\mathbf{r})$ , contrary to MOs and wave functions, is an observable quantity that can be determined both experimentally and theoretically<sup>63</sup>. As shown by Hohenberg and Kohn<sup>64</sup>, the energy of a molecule in a non-degenerate ground state is a function of  $\rho(\mathbf{r})$ . All physical and chemical properties of a molecule depend in some way on the electron density distribution. Accordingly, it is plausible that analysis of  $\rho(\mathbf{r})$  should lead to primary information of electronic structure and chemical bonding of **1**.

In Figure 9, a perspective drawing of the calculated HF/6-31G(d,p) electron density distribution  $\rho(\mathbf{r})$  in the plane of the C atoms of **1** is shown<sup>11</sup>. The electron density takes maxi-

mal values at the positions of the three nuclei and decreases exponentially in off-nucleus directions. This is typical of all molecular  $\rho(\mathbf{r})$ -distributions and obscures many details of the density distribution that relate to bonding, accumulation of density in the region of lone-pair electrons, holes in the valence shell in the direction of unoccupied orbitals or to other anisotropies of the electron density distribution at a bonded atom. There exist three major ways to unravel details of electronic structure and bonding from  $\rho(\mathbf{r})$ , namely (a) the analysis of difference electron density distributions  $\Delta\rho(\mathbf{r})$ , (b) the analysis of  $\rho(\mathbf{r})$  by the virial partitioning method and (c) analysis of  $\rho(\mathbf{r})$  via its Laplacian. All three methods have been used to investigate **1** and results of these investigations are summarized in Sections IV. A, IV. B and IV. C.

### A. Analysis of the Difference Electron Density Distribution

The difference density distribution is defined in equation 5<sup>65</sup>:

$$\Delta\rho(\mathbf{r}) = \rho[\text{molecule}] - \rho[\text{promolecule}] \quad (5)$$

where the promolecular density distribution is conventionally constructed by summing over spherically averaged atomic densities, with the atoms kept in the positions they adopt in the molecule. A positive  $\Delta\rho(\mathbf{r})$  in the internuclear region is generally considered to be indicative of covalent bonding.

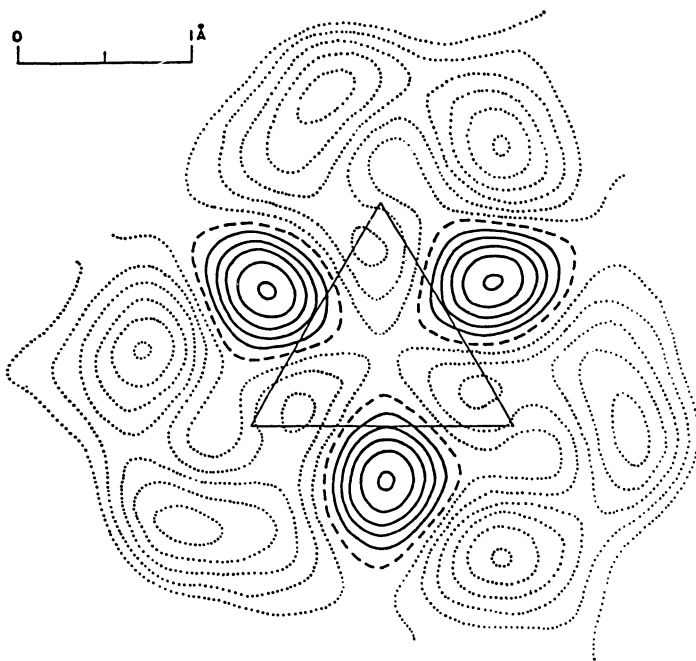
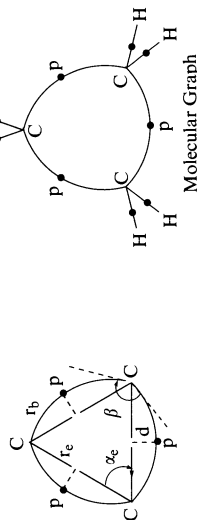


FIGURE 10. Contour line diagram of the difference electron density distribution in the ring plane of *cis,cis*-1,2,3-tricyanocyclopropane as obtained by X-ray diffractometric measurements. Solid lines are in the regions with positive difference densities, dotted lines in regions with negative difference densities. Dashed lines correspond to zero values. Reprinted from A. Hartman and F. L. Hirshfeld, *Acta Crystallogr.*, **20**, 80 (1966) by permission of the International Union of Crystallography

TABLE 5. Description of atoms in molecules and chemical bonds in terms of the properties of  $\rho(\mathbf{r})^a$ 

Chemical term	Term used in density analysis	Comment
Atom	Nucleus + basin $\Omega$	Basin filled by trajectories that terminate at the nucleus as the attractor of these trajectories
Atomic volume	Volume $V$ of basin	$\int_{\Omega} d\mathbf{r} = V$
Atomic charge	Atomic charge	$\int_{\Omega} \rho(\mathbf{r}) d\mathbf{r} = Q$
Atomic dipole moment	Atomic dipole moment	$\int_{\Omega} \rho(\mathbf{r}) \mathbf{r} d\mathbf{r} = \mu$ with $n = 1$
Atomic energy	Atomic energy	$\int_{\Omega} H(\mathbf{r}) d\mathbf{r} = E$
Interatomic surface	Zero-flux surface $S$	Internuclear surface through which the flux of $\nabla\rho(\mathbf{r})$ is zero (see equation 6)
Covalent bond	Bond path	Necessary condition: Existence of a MED path linking the bonded atoms Sufficient condition: Negative energy density $H(\mathbf{p})$ at the bond critical point $\mathbf{p}$
Bond energy	Bond critical point $\mathbf{p}$	Saddle point of $\rho(\mathbf{r})$
Bond energy BE	Bond energy BE	$BE(A, B) = \alpha(A, B) N(A, B) / R(A, B)^2$ with
Bond length $r_c$	Bond path length $r_b$	$N(A, B) = \mathbf{R}(A, B) \int_{\text{AB}} \rho(\mathbf{r}) \mathbf{n}_A(\mathbf{r})$
Bond angle $\alpha_c$	Interpath angle $\beta$	$r_b$ is larger than the geometrical distance $r_c$ for bent bonds
Bent bond character	Distance $d$	Angle between geminal bond paths; $\beta$ is larger than the geometrical angle $\alpha$ in strained rings
Bond order	Bond order $n$	Deviation $d$ of bond path from internuclear connection line
$\pi$ Character	(local property) Bond ellipticity Anisotropy of $\rho(\mathbf{p})$ (local property)	$\pi(AB) = \exp \{a [ \rho(\mathbf{p}) - b ] \}$ where $a$ and $b$ are determined from two suitable reference bonds AB with fixed bond order $n$ $\varepsilon = (\lambda_1/\lambda_2) - 1$ where $\lambda_1 \leq \lambda_2 \leq \lambda_3$ are the curvatures of $\rho(\mathbf{p})$ along the principal axes calculated from the Hessian of $\rho(\mathbf{p})$ ; $\lambda_1$ is called the hard curvature, $\lambda_2$ the soft curvature
Molecular geometry	Molecular graph	Network of bond paths plus bond critical points
Molecular structure	Molecular structure	Equivalent class of molecular graphs

<sup>a</sup>For an explanation of geometrical parameters and bond parameters in the case of cyclopropane, see below.

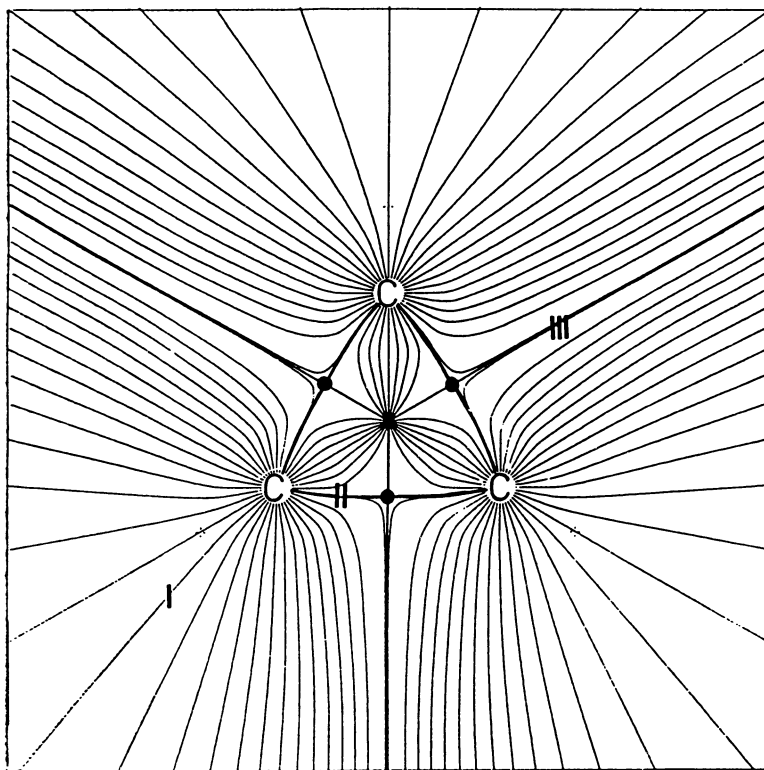


FIGURE 11. Gradient vector field of the HF/6-31 G(d,p) electron density distribution  $\rho(\mathbf{r})$  calculated for the plane of the cyclopropane ring. Bond critical points  $\mathbf{p}$  are denoted by dots. There are three different types of trajectories: type I trajectories start at infinity or the centre of the ring and end at a carbon nucleus; type II trajectories (heavy lines) define the bond path linking two neighbouring carbon atoms; type III trajectories form the three zero-flux surfaces between the C atoms (in the two-dimensional display only their traces can be seen). They terminate at the bond critical points

Distributions  $\Delta\rho(\mathbf{r})$  have been determined for various derivatives of **1** by both *ab initio* and X-ray diffraction studies<sup>66</sup>. In Figure 10, a contour line diagram of  $\Delta\rho(\mathbf{r})$  in the ring plane of *cis*, *cis*-1,2,3-tricyanocyclopropane is shown<sup>66a</sup>. Positive difference densities are found between the three C atoms, but the  $\Delta\rho(\mathbf{r})$  maxima are displayed up to 0.3 Å from the internuclear axis<sup>66</sup>. The displacement of the maxima is considered to indicate the bent bond character of the CC bonds of **1**.

## B. Analysis of the Electron Density Distribution

Since difference electron densities, deformation densities or valence electron densities are not observable quantities, and since the Hohenberg-Kohn theorem<sup>64</sup> applies only to the total electron density, much work has concentrated on the analysis of  $\rho(\mathbf{r})$ . The accepted analysis method today is the virial partitioning method by Bader and coworkers<sup>67</sup>, which is based on a quantum mechanically well-founded partitioning of the molecular

space into subspaces using  $\rho(\mathbf{r})$ . Since Bader could show (a) that these subspaces normally contain just one nucleus and (b) that the virial theorem applies to the subspaces, the subspaces are considered to be atomic subspaces and the partitioning of the molecular space into atomic subspaces is called the virial partitioning method. This method has been described in several review articles<sup>13,76</sup> and, therefore, only some essential terms of the method are summarized in Table 5.

The virial partitioning method is based on the calculation and analysis of the gradient vector field  $\nabla\rho(\mathbf{r})$  corresponding to the distribution  $\rho(\mathbf{r})$ <sup>67</sup>. Figure 11 shows the vector field  $\nabla\rho(\mathbf{r})$  calculated in the ring plane of **1**. One can distinguish three types of trajectories, indicated in Figure 11 by I, II and III. Type I trajectories start at infinity or at the ring centre and terminate at one of the three C nuclei of **1**, which are the (three-dimensional) attractors of type I trajectories. All type I trajectories that terminate at a particular C nucleus fill a subspace (basin) associated with this nucleus.

Type II trajectories start at a point  $\mathbf{p}$  in the internuclear region between two bonded atoms and end at one of the two nuclei in question. There are just two trajectories per bond, which together define a path of maximum electron density (MED path) that is visible in the perspective drawing of  $\rho(\mathbf{r})$  shown in Figure 9. Each lateral displacement from the MED path leads to a decrease of  $\rho(\mathbf{r})$ . The point  $\mathbf{p}$  corresponds to the minimum of  $\rho(\mathbf{r})$  along the path and to a saddle point of  $\rho(\mathbf{r})$  in three dimensions.

Saddle point  $\mathbf{p}$  is the sink of type III trajectories, i.e. it is the attractor of all trajectories in directions perpendicular to the MED path. Type III trajectories form a surface, which reaches from infinity (source of type III trajectories) to a line  $\mathbf{L}$  through the center of the ring and perpendicular to the ring plane. The flux of  $\nabla\rho(\mathbf{r})$  vanishes for all surface points (equation 6):

$$\nabla\rho(\mathbf{r}) \cdot \mathbf{n}(\mathbf{r}) = 0 \quad \mathbf{r} \in S \quad (6)$$

where  $\mathbf{n}$  is the unit vector normal to the surface  $S$ , which has been called the zero-flux surface<sup>67</sup>. There are three zero-flux surfaces in Figure 11, which meet at line  $\mathbf{I}$  and separate the three basins of the three C atoms of **1**. Other zero-flux surfaces are between C and H atoms of **1**. Hence, the zero-flux surfaces partition the molecular space into subspaces, each containing one atomic nucleus. Since there are just few exceptions to this observation, one has called the subspaces atomic basins and has considered them to represent the space of an atom in a molecule. Molecule **1** has nine of these atomic subspaces, three of which, namely those of the C atoms, can be recognized in Figure 11.

The three MED paths (type II trajectories) between the C atoms of **1** correspond to the three CC bonds. Since MED paths can also be found in the case of van der Waals interactions, Cremer and Kraka<sup>13,68,69</sup> suggested using the local energy density  $H(\mathbf{r})$  (equation 7):

$$H(\mathbf{r}) = G(\mathbf{r}) + V(\mathbf{r}) \quad (7)$$

[where  $G(\mathbf{r})$  is the local kinetic energy density and  $V(\mathbf{r})$  the local potential energy density] at the saddle point  $\mathbf{p}$  to distinguish between covalent bonds and closed-shell (van der Waals) interactions. It is of general understanding that the formation of a covalent bond is accompanied by delocalization of electrons, decrease in kinetic energy, orbital contraction and lowering of the potential energy<sup>70</sup>. If  $H(\mathbf{p}) < 0$ , then this will suggest a reduction of the kinetic energy density and a dominance of the potential energy density at the saddle point  $\mathbf{p}$  [ $V(\mathbf{p})$  is always  $< 0$  and  $G(\mathbf{p})$  is always  $> 0$ ]. Hence, accumulation of electron density in the bonding region at the point  $\mathbf{p}$  is stabilizing. On the other hand, if  $H(\mathbf{p}) \geq 0$ , then electron density at point  $\mathbf{p}$  will be destabilizing and indicates closed-shell interactions as for van der Waals interactions, ionic bonding or H-bonding. Therefore, Cremer and Kraka suggested that the existence of a MED path between two nuclei can be considered as the necessary condition and  $H(\mathbf{p}) < 0$  as the sufficient condition for covalent bonding<sup>13,68,69</sup>.

A clear definition of (covalent) bonding is essential for describing the strained CC bonds of **1**. Cremer and Kraka have shown in an electron density investigation of various three-membered rings that the CC bond paths are significantly bent (Table 6)<sup>9</sup>. The bond saddle point **p** is shifted by 0.06 Å from the midpoint of the internuclear connection line and the bond path length  $r_b(\text{CC})$  (1.506 Å, Table 6) is almost 0.01 Å longer than the internuclear distance  $r_e(\text{CC})$  (1.497 Å, Table 6). In addition, the interpath angle  $\beta(\text{CCC})$  is 79° due to the bending of the bonds. The deviation of  $\beta$  from a tetrahedral angle in **1** is less dramatic as suggested by the geometrical angle  $\alpha = 60^\circ$  and, therefore, it is physically more reasonable to use the interpath angle  $\beta(\text{CCC})$  rather than the geometrical angle  $\alpha(\text{CCC})$  to assess the ring strain of **1** (or other cycloalkanes)<sup>9-12</sup>.

TABLE 6. Description of cyclopropane and some related compounds in terms of the properties of the electron density distribution  $\rho(\mathbf{r})^a$

Property	Structural element	Cyclopropane	Aziridine	Oxirane	Cyclobutane
Distance $r_e$ (Å)	CC	1.497	1.470	1.453	1.544
Distance $d$ (Å)		0.060	0.080	0.094	0.038
Bond length $r_b$ (Å)		1.506	1.486	1.476	1.547
$\rho(\mathbf{p})$ ( $\text{e} \text{Å}^{-3}$ )		1.681	1.763	1.819	1.680
Bond order <sup>b</sup>		1.00	1.06	1.08	1.00
Ellipticity $\varepsilon(\mathbf{p})$		0.49	0.39	0.31	0.02
Distance $r_e$ (Å)	CX	1.497	1.449	1.401	1.544
Distance $d$ (Å)		0.060	0.043	0.004	0.038
Bond length $r_b$ (Å)		1.506	1.455	1.404	1.547
$\rho(\mathbf{p})$ ( $\text{e} \text{Å}^{-3}$ )		1.681	1.823	1.771	1.680
Bond order <sup>b</sup>		1.00	0.97	0.96	1.00
Ellipticity $\varepsilon(\mathbf{p})$		0.49	0.50	0.88	0.02
Geometrical angle $\alpha$	CXC	60	60.9	62.4	88.6
Bond angle $\beta$ (deg)		78.8	76.4	75.8	95.6
Geometrical angle $\alpha$	CCX	60	59.5	58.8	88.6
Bond angle $\beta$ (deg)		78.8	77.3	72.8	95.6
$\rho(\mathbf{c})$ ( $\text{e} \text{Å}^{-3}$ )	Ring	1.379	1.485	1.533	0.554
$\xi$ (%) <sup>c</sup>		82.0	83.1	85.8	32.9
Ellipticity $\varepsilon(\mathbf{c})^d$		0	0.445	0.094	0

<sup>a</sup> HF/6-31G(d) calculations from Reference 9. For an explanation of property terms, see Table 5 and text.

<sup>b</sup> All bond orders are normalized.

<sup>c</sup> Ratio  $[\rho(\mathbf{c})/\rho(\mathbf{p})_{\text{av}}] 100$  where  $\rho(\mathbf{p})_{\text{av}}$  is the average of all  $\rho(\mathbf{p})$  values.

<sup>d</sup> Ellipticity at the ring critical point **c**.

Bond order  $n$  and  $\pi$ -character  $\varepsilon$  can be extracted from the properties of  $\rho(\mathbf{r})$  at the bond critical point **p** (see Table 5). The calculated CC bond order of **1** ( $n = 1.00$ ), which is obtained from the electron density at the local point **p**, is not sensitive to the bending of the CC bond as has been pointed out by Cremer and Kraka<sup>11</sup>. This is in line with the observation made in VB calculations that the overlap between CC hybrid orbitals in **1** is similar to that of other cycloalkanes (see Table 3 and Section V. B)<sup>51</sup>.

More interesting is the calculated ellipticity  $\varepsilon$  of the CC bonds (Table 6), which is as high as that of the  $\pi$ -bond in ethene. However, contrary to ethene, the soft curvature of  $\rho(\mathbf{r})$  (Table 5) is in the plane of the carbon ring, i.e. the electron density extends from the bond critical point toward the centre of the ring as well as outside of the ring. This is in line with the orbital description of **1** and the expected  $\pi$ -character of its CC bonds substantiated in many experimental investigations. Investigation of  $\rho(\mathbf{r})$  of **1** reveals that *bending of a formal CC  $\sigma$  bond leads to an admixture of  $\pi$  character*.



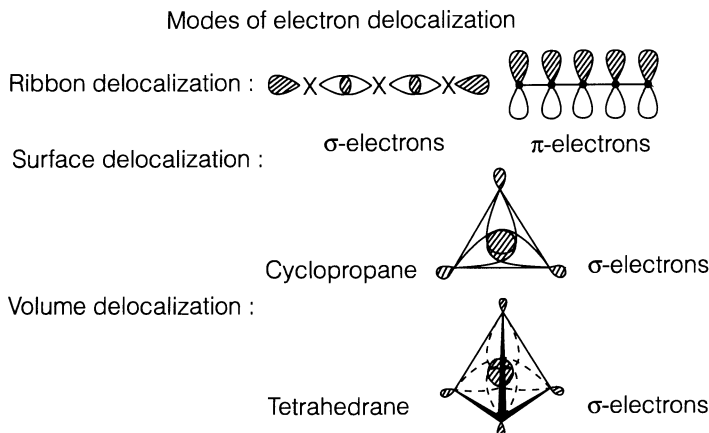
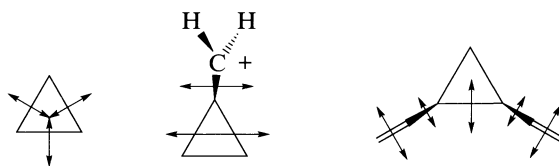


FIGURE 12. Possible modes of electron delocalization. Reprinted from D.Cremer *Tetrahedron*, **44**, 7427 (1988) with kind permission from Elsevier Science Ltd., The Boulevard, Langford Lane, Kidlington OX5 1GB, UK

Another characteristic property of the electron density of **1** is its relatively high value at the centre **c** of the ring (more than 80% of that at the CC bond critical point). Density is smeared out over the ring surface and concentrated at its centre because of the occupation of the  $w_0$ -orbital (MO #8,  $3a_1'$ , Figure 6), which has the character of a 'surface orbital'. Cremer and Kraka<sup>9, 11, 13</sup> have termed this phenomenon 'surface delocalization' of electrons, to be distinguished from ribbon delocalization and volume delocalization of electrons (Figure 12)<sup>12</sup>.

Surface delocalization is characterized by  $\xi$ , which is the percentage of negative charge at the ring critical point relative to that at the bond critical point. The value of  $\xi$  is 82% for **1**, but below 35% for ring molecules such as cyclobutane (Table 6) or benzene. For substituted **1**, interactions between ring and substituents influence the  $\pi$ -character of the CC bonds and surface delocalization. Depending on the nature of the substituent (see Section VI) the bond ellipticity of the vicinal CC bonds exceeds that of the distal CC bond or vice versa. For the same reason,  $\rho(\mathbf{c})$  at the ring critical point becomes anisotropic, i.e. the ellipticity at the ring critical point,  $\varepsilon(\mathbf{c})$ , becomes  $> 0$  because  $\lambda_1 \neq \lambda_2$  (for **1**,  $\lambda_1 = \lambda_2$ , Table 6). The soft curvature of the ring ellipticity  $\varepsilon(\mathbf{c})$  always points to the CC bond(s) with the largest  $\pi$ -character. Hence, a direction can be assigned to surface delocalization (indicated by a double-headed arrow) in substituted three-membered rings, which is the direction of the soft curvature of  $\varepsilon(\mathbf{c})$  (see Scheme 2)<sup>9</sup>.

Surface delocalization is not found for cyclobutane or larger cycloalkanes<sup>10</sup>. Furthermore, it does not appear for cyclotrisilane since in this case the overlap within the surface orbital is not sufficient to bring enough electron density into the centre of the ring<sup>71</sup>.



SCHEME 2

### C. Analysis of the Laplacian of the Electron Density Distribution

It is a disadvantage of the analysis of  $\rho(\mathbf{r})$  that many features of the orbital description of a molecule are not reflected by the properties of the electron density. However, this gap between orbital and  $\rho(\mathbf{r})$  description can be closed by investigating the Laplacian of  $\rho(\mathbf{r})$ ,  $\nabla^2\rho(\mathbf{r})$ <sup>72</sup>. The Laplacian of any scalar function is negative where the scalar function concentrates, and it is positive where the scalar function is depleted. This becomes obvious, when considering the second derivative of a general function  $f(x)$ :

$$\begin{aligned}\lim_{\Delta x \rightarrow 0} \{f(x) - 1/2[f(x - \Delta x) + f(x + \Delta x)]\} &= -1/2 \lim_{\Delta x \rightarrow 0} \{[f(x + \Delta x) - f(x)] - [f(x) - f(x - \Delta x)]\} \\ &= -1/2(d^2f/dx^2) dx^2\end{aligned}$$

If the second derivative, and hence the curvature of  $f$ , is negative at  $x$ , then  $f$  at  $x$  will be larger than the average of  $f$  at all neighbouring points, i.e.  $f$  concentrates at point  $x$ <sup>73</sup>. Therefore  $-\nabla^2\rho(\mathbf{r})$ , which is the second derivative of a function depending on three coordinates  $x$ ,  $y$  and  $z$ , has been called the Laplace concentration of the electron density distribution. Furthermore, the Laplacian of  $\rho(\mathbf{r})$  provides the link between electron density  $\rho(\mathbf{r})$  and energy density  $H(\mathbf{r})$  via a local virial theorem (equation 8)<sup>67</sup>,

$$(\hbar^2/4m) \nabla^2\rho(\mathbf{r}) = 2G(\mathbf{r}) + V(\mathbf{r}) = G(\mathbf{r}) + H(\mathbf{r}) \quad (8)$$

where  $G(\mathbf{r})$ ,  $V(\mathbf{r})$  and  $H(\mathbf{r})$  are kinetic, potential and total energy density distribution<sup>68, 69</sup>. Integration of the Laplacian over an atomic basin or the total molecular space leads to zero, i.e. the fluctuations in  $\nabla^2\rho(\mathbf{r})$  are such that local depletion of negative charge [ $\nabla^2\rho(\mathbf{r}) > 0$ ] and local concentration of negative charge [ $\nabla^2\rho(\mathbf{r}) < 0$ ] cancel each other, both for the atoms in a molecule as well for the molecule itself. Investigation of the Laplace concentration in the valence shell of an atom reveals maxima (lumps) and minima (holes) that can be associated with the amplitudes and the form of the HOMO and LUMO of this atom<sup>13, 72</sup>. This applies also to molecules and leads to a visualization of the frontier orbitals via the Laplace concentration of the electron density. Hence, the Laplacian  $\nabla^2\rho(\mathbf{r})$  bridges the gap between the orbital and the density description of the electronic structure of a molecule.

In Figure 13, the calculated Laplace concentration,  $-\nabla^2\rho(\mathbf{r})$ , of **1** is shown in the plane of the ring<sup>9-12</sup>. The position of the C nuclei can be easily recognized by the 1s concentration peaks. Inner shell and valence region are separated by a sphere of charge depletion. Laplace concentration in the valence shell of the C atoms is distorted in a way such that there are concentration lumps in the direction of each bond (two of which are not visible, since they are in the direction of the CH bonds and therefore outside the reference plane). The concentration lumps in the ring plane can be associated with the 3e' HOMOs (MOs #11, #12) of **1** while the arrangement of the holes at the C atoms resembles the shape of the 1a<sub>2</sub>' LUMO of the C<sub>3</sub> ring (lower-lying unoccupied MOs are of either  $\sigma^*(\text{CH}_2)$  or  $\pi^*(\text{CH}_2)$  character).

The contour line diagram of  $-\nabla^2\rho(\mathbf{r})$  reveals concentration of electronic charge (dashed contour lines) not only in the CC bonding regions, but also inside the ring, thus confirming surface delocalization of electrons. Surface delocalization of  $\sigma$ -electrons inside the ring implies that there is a relatively low kinetic energy density  $G(\mathbf{r})$  and a relatively large potential energy density  $|V(\mathbf{r})|$ . *Electrons stay longer inside the ring since they experience there the stabilizing attraction of three C nuclei.* The electrostatic potential of the three C nuclei is homomorphic with  $\rho(\mathbf{r})$ , which indicates that electron-nucleus attraction is supporting  $\sigma$ -electron delocalization inside the ring of **1**.

### D. Surface Delocalization, $\pi$ -Complexes and Bonding

Surface delocalization has been confirmed by various other authors. Coulson and Moffitt<sup>23</sup> were the first to note that there is a plateau of relatively high electron density

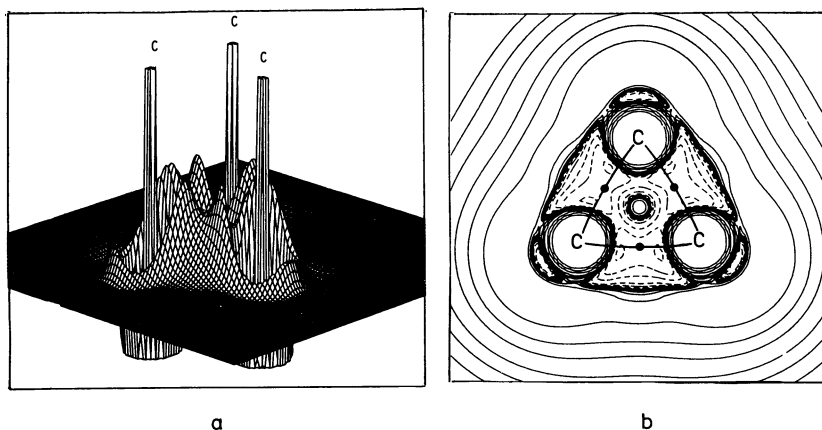


FIGURE 13. (a) Perspective drawing of the HF/6-31G(d,p) Laplace concentration  $-\nabla^2\rho(\mathbf{r})$  of cyclopropane depicted in the ring plane. Inner-shell concentrations are indicated by the atomic symbol C. For a better presentation values above and below a threshold are cut off. (b) contour line diagram of the Laplace concentration shown in (a). Bond paths are indicated by heavy solid lines and bond critical points by dots. Dashed lines are in regions where electronic charge is concentrated and solid lines in regions where charge is depleted. Inner-shell concentrations are not shown. Reprinted from D. Cremer *Tetrahedron*, **44**, 7427 (1988) with kind permission from Elsevier Science Ltd., The Boulevard, Langford Lane, Kidlington OX5 1GB, UK

inside the ring of **1**. Schwarz and coworkers<sup>74</sup> calculated that  $\rho(\mathbf{r})$  is increased by  $0.16 \text{ e \AA}^{-3}$  in the centre of the ring relative to a promolecular density formed by three spherical isolated atoms. These authors attributed the increase in density to surface delocalization of electrons, which leads to a decrease in their kinetic energy and a subsequent contraction of the carbon AOs. This in turn lowers the potential energy as well as the total energy, restores the virial relation and leads to CC bond shortening.

Ahrlrichs and Ehrhardt<sup>75</sup> calculated shared electron numbers for **1**. While bonding is normally reflected by two-centre contributions and negligible contributions from three and four-centre terms, a CCC shared electron number of 0.3 was calculated for **1**, which is indicative of significant three-centre bonding.

Recent VB calculations by Hamilton and Palke<sup>50</sup> reveal that optimized (non-orthogonal) CC hybrid orbitals for **1** cover the whole ring surface (see Section III. B, Figure 8) and take the character of surface orbitals that bring via six-fold overlap electron density into the surface of the ring, thus leading to surface delocalization of electrons and increased stability of the ring. For cyclobutane, hybrid orbitals are much more confined to the bonding region and therefore overlap inside the ring is much smaller<sup>51</sup>. In this case, it is not justified to speak about surface orbitals and surface delocalization of electrons (Figure 8).

Inagaki and coworkers<sup>47</sup> carried out a configuration analysis of the HF wave function of **1** (see also Section V. D). Using the coefficients for ground and excited configurations as a measure for electron delocalization, they found no indication of  $\sigma$ -electron delocalization in **1**. For ring molecules such as cyclobutane, they observed antibonding geminal electron delocalization that reduces the electron density inside the ring. But in the case of **1**, antibonding geminal electron delocalization is significantly lower than in other cycloalkanes. As a consequence, the electron density inside the  $C_3$  ring of **1** is higher than inside a  $C_4$  ring of cyclobutane in line with the calculated  $\rho(\mathbf{r})$ .

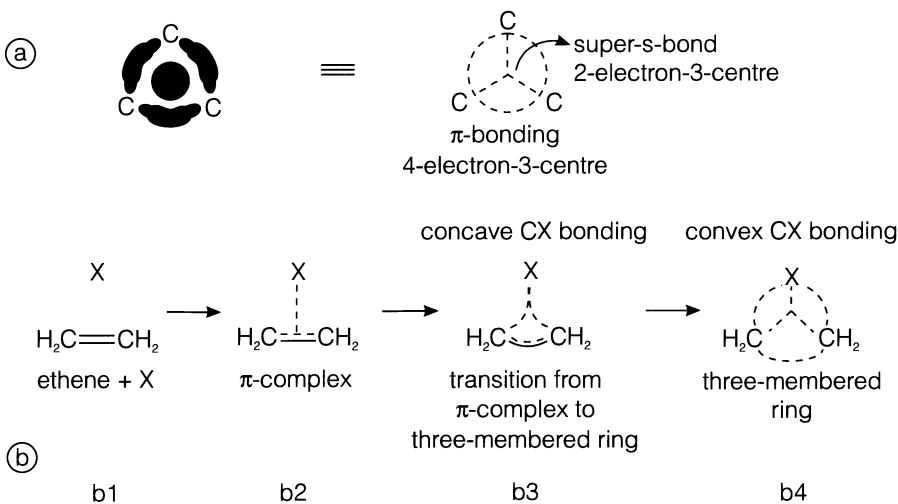


FIGURE 14. (a) Bonding in cyclopropane. On the left side the regions of relatively large internuclear electron density are indicated schematically. On the right side, 2-electron 3-centre bonding ('super- $\sigma$  bond') and peripheral 4-electron 3-centre bonding (' $\pi$ -bonds') are given by dashed lines. (b) Transition from ethene + X (b1) to a  $\pi$ -complex (b2, b3) and a three-membered ring (b3, b4)

Cremer<sup>12</sup> has pointed out that the term *delocalization* can be used in a quantum mechanical sense (delocalization of electrons in the space of two or more bonded atoms) and a heuristic sense (delocalization implies non-additivity of bond properties). The use of the term delocalization in the language of configuration (orbital) interactions (delocalization of electrons from occupied bond orbitals of the ground state configuration into antibonding orbitals of an excited configuration) does not coincide with these meanings. Clearly, the term surface delocalization has been based on the quantum mechanical meaning of electron delocalization, which can be translated to the language of configuration (orbital) interactions by describing **1** as a resonance hybrid of three  $\pi$ -complexes [delocalization of  $\text{CH}_2$  electrons into antibonding ( $\pi^*$ ) orbital of  $\text{CH}_2\text{CH}_2$ ], which implies that the reference function is that of the  $\pi$ -complex and not that of **1** (reference for benzene is cyclohexatriene and not benzene itself).

Surface delocalization can be considered as the result of occupying the  $3a_1'$  surface orbital (MO #8,  $w_0$ , Figure 6) in **1** and the  $\pi$ -character of the CC bonds as the result of occupying the two  $3e'$  HOMOs (MOs #11 and 12;  $w_A$  and  $w_S$ , Figure 6). Hence, bonding in **1** is exceptional since the C atoms are held together by (see Figure 14):

1. a central 2-electron 3-centre bond ('super- $\sigma$  bond') and
2. two peripheral 2-electron 3-centre bonds (' $\pi$ -bonds')<sup>12</sup>.

Hamilton and Palke<sup>50</sup> have critically considered the question of a 2-electron 3-centre bond. They compare CC hybrid orbitals calculated at the VB level (see Section III. B) with the orbitals representing the 2-electron 3-centre bonds in diborane,  $\text{B}_2\text{H}_6$ . Since the latter fully envelope the bridging H atoms and since this is not the case for the CC hybrid orbitals of **1**, Hamilton and Palke conclude that 2-electron 3-centre bonding does not play any role in **1**.

Since orbitals are not observable objects, it is clear that orbital sets related to each other by a unitary transformation, all will lead to valid descriptions of the electronic structure of the molecule although they may suggest very different orbital interactions leading to bond-

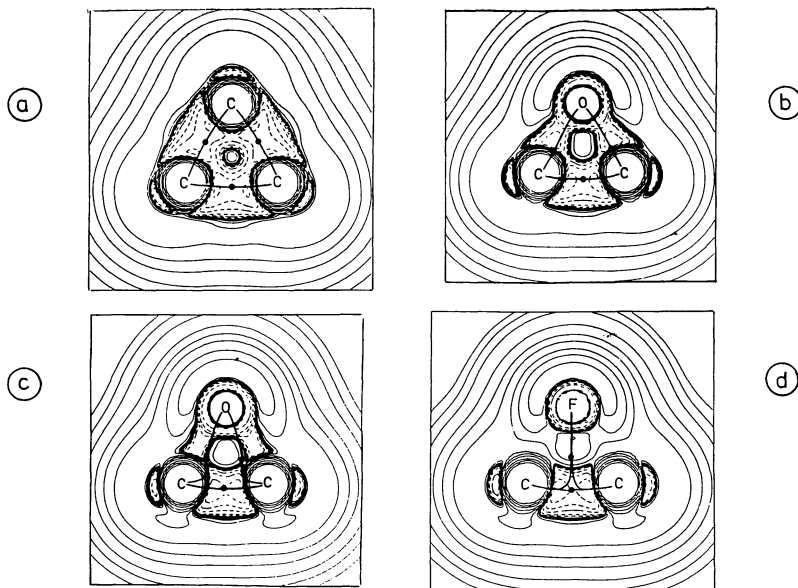


FIGURE 15. Molecular graphs and Laplace concentrations  $-\nabla^2\rho(\mathbf{r})$  of (a) cyclopropane, (b) oxirane, (c) protonated oxirane and (d) halogen-bridged fluororethyl cation. The reference plane contains the nuclei of the heavy atoms. Bond paths are indicated by heavy solid lines and bond critical points by dots. Dashed lines are in regions where electronic charge is concentrated [ $-\nabla^2\rho(\mathbf{r}) > 0$ ] and solid lines in regions where charge is depleted ( $-\nabla^2\rho(\mathbf{r}) < 0$ ). Inner-shell concentrations are not shown. [HF/6-31G(d) calculations from Reference 9]. Reprinted with permission from D. Cremer and E. Kraka, *J. Am. Chem. Soc.*, **107**, 3800 (1985). Copyright (1985) American Chemical Society

ing. Using delocalized MOs, surface delocalization seems to be best explained by a 2-electron 3-centre bond caused by the occupation of the  $3a_1'$  MO (MO#8, Figure 6). However, a description of CC bonding in **1** by hybrid orbitals optimized at the VB level of theory<sup>51</sup> suggests that the extension of the CC hybrid orbitals over the ring surface and their mutual overlap inside the ring (Section III. B, Table 3) leads to a transfer of electron density into the ring and to surface delocalization of electrons. Hence, both orbital descriptions lead to the same result. It is a matter of taste and suitability which orbital description is preferred and which bond description is considered to be more useful.

Dewar<sup>34, 36, 43</sup> was the first to point out a relationship between three-membered rings and  $\pi$ -complexes. His idea was later ventilated by a number of other authors<sup>35, 37-45</sup>. Cremer and Kraka<sup>9</sup> demonstrated, on the basis of electron density studies, that there is a continuous transition from three-membered rings to  $\pi$ -complexes depending on the electronegativity of the constituent atoms (see Figures 14 and 15). Molecule **1** is a three-membered ring with convex (outwardly) bent ring bonds. But if a  $\text{CH}_2$  group in **1** is replaced by a more electronegative group X such as, e.g., O,  $\text{OH}^+$  or  $\text{F}^+$  (Figure 15b, c, d), then the CX bonds will be gradually bent inwardly toward the centre of the ring (concave bent bonds, Figure 15). For  $\text{X} = \text{F}^+$ , concave bending of the CX bond paths is so strong that the two paths coincide largely and form the T-structure of a  $\pi$ -complex (Figures 14 and 15d). Cremer and Kraka<sup>9, 13</sup> explained the relationship between three-membered rings and  $\pi$ -complexes by an orbital model, in which the orbitals of the apex group X interact in two ways (interactions 1 and 2) with the orbitals of a basal group  $\text{A}=\text{A}$  (Figure 16).

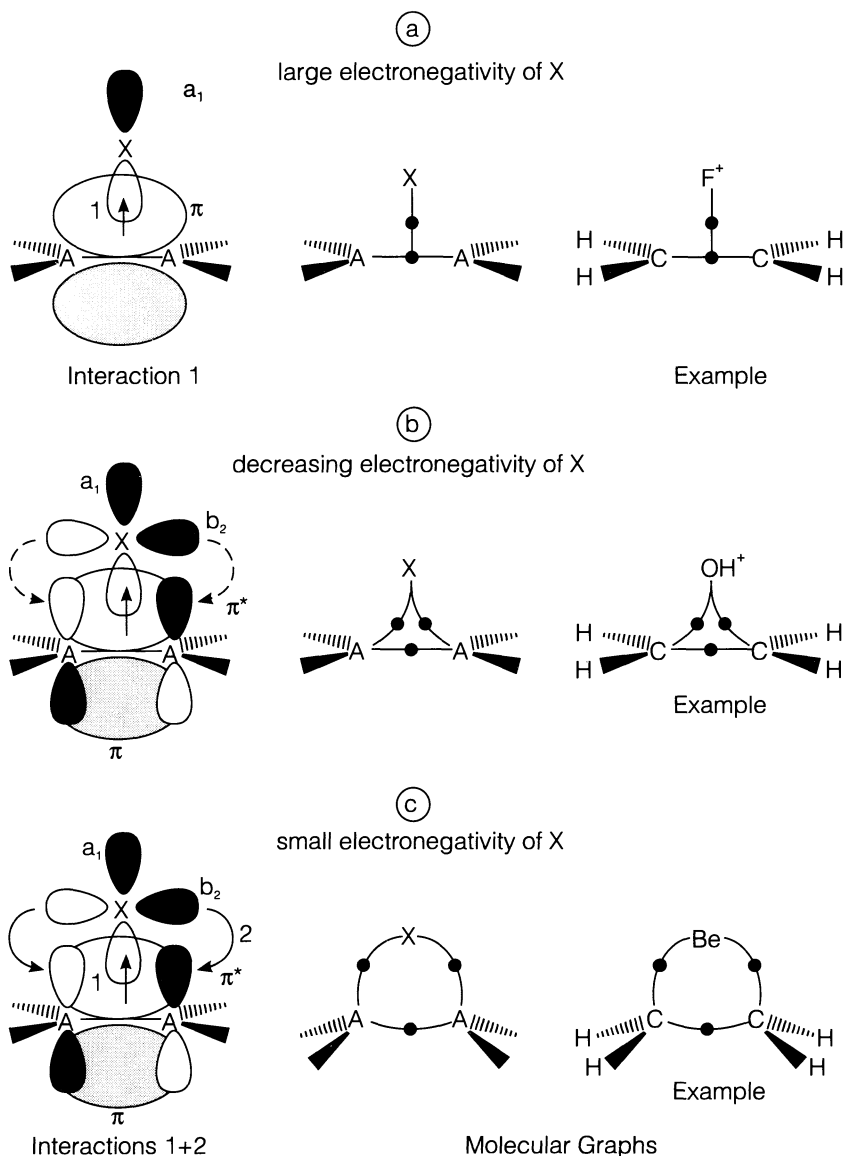


FIGURE 16. MO description of donor–acceptor interactions between the basal group  $A_2H_4$  ( $A = C, Si$  etc.) and the apex group  $X$ . The relevant orbitals ( $a_1$  and  $b_2$  symmetry) are shown on the left side and the corresponding molecular graphs together with an appropriate example on the right side of each diagram. The direction of charge transfer caused by orbital interactions 1 and 2 is indicated by arrows (dashed arrows indicate reduced charge transfer). Top:  $\pi$ -Complex. Middle: Three-membered ring with concave bent bonds. Bottom: Three-membered ring with convex bent bonds. The electronegativity of  $X$  decreases from top to bottom

Interaction 1: The basal group A=A donates electrons from a  $\pi$  MO into a suitable low lying  $a_1$  MO ( $C_{2v}$  symmetry assumed) thus establishing a build-up of electron density in the centre of the ring.

Interaction 2: Back donation from a relatively high-lying  $b_2$  MO into the  $\pi^*$ MO of A=A leads to an accumulation of electron density in the periphery of the ring, which determines the bending of bond paths.

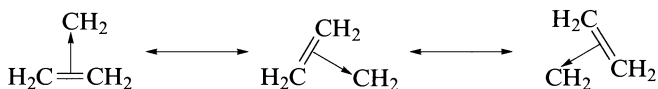
Three different cases can be considered<sup>9, 13, 71</sup>:

(a) If interactions 1 and 2 are of comparable magnitude, then a three-membered ring with convex bent bonds will be formed (Figure 16c, example: **1** in Figure 15a).

(b) If interaction 2 is reduced because of the electronegativity of X (reduced donor capacity of X), a three-membered ring with concave bent bonds results (Figure 16b, example: X = OH<sup>+</sup>, Figure 15c).

(c) If back donation is totally suppressed because of the large electronegativity difference between X and A, then there is just interaction 1, which leads to the T-structure of a  $\pi$ -complex, i.e. X is bound to the bond critical point of A=A (Figure 16a, example: X = F<sup>+</sup>, Figure 15d).

According to the relationship between three-membered rings and  $\pi$ -complexes, cyclopropane can be considered as a resonance hybrid of three equivalent methylene-ethene  $\pi$ -complexes<sup>12, 13</sup>. Of course, such  $\pi$ -complexes do not exist but this is also true in the case of the two cyclohexatriene resonance structures normally used to present benzene. Spin-coupled valence bond calculations of Karadakov and coworkers<sup>51</sup> reveal that there is a small but significant contribution of 3.7% to the electronic structure of **1** resulting from  $\pi$ -complex structures (see Section V. E). This indicates that the  $\pi$ -complex description of **1** is not totally unreasonable and, although seldom used, helps to unravel some of the peculiarities of bonding in **1**:



(a) There are different types of CC interactions in **1**. The orbital interaction 1 leads to a three-centre two-electron bond and surface delocalization. Orbital interaction 2 is responsible for the two peripheral 2-electron 3-centre bonds (' $\pi$ -bonds').

(b) The  $\pi$ -complex description explains the  $\pi$ -character of the CC bonds.

(c) It further suggests increased s-character in the CH bonds and a concomitant strengthening of the CH bonds, which is experimentally confirmed.

(d) In a methylene, ethene  $\pi$ -complex typical CC distances are 2 Å and 1.34 Å, respectively. The CC bonds of **1** should be between these two values (because of resonance) and not necessarily identical with those of normal CC bonds.

Resonance between three  $\pi$ -complex structures might lead to stabilization of **1** in the sense of  $\pi$ -aromatic stabilization involving the six CC bond electrons. Therefore, Dewar<sup>8</sup> has discussed the stability of **1** in terms of a  $\sigma$ -aromatic stabilization (Section V). However, spin-coupled valence bond theory clearly shows that **1** cannot be considered as the  $\sigma$ -aromatic analogue to  $\pi$ -aromatic benzene<sup>51</sup>. The  $\pi$ -complex description of **1** is a (very formal) model description, which should be discarded as soon as it leads to conflicting descriptions of the properties of **1**. This will be discussed in Section V.

## V. ENERGY AND STABILITY

Several authors have pointed out that the conventional strain energy (CSE) of **1** (27.5 kcal mol<sup>-1</sup>) is about of the same magnitude as that of cyclobutane (26.5 kcal mol<sup>-1</sup>) and there-

fore **1** must be stabilized in some way relative to cyclobutane<sup>8,9,76</sup>. In the last 15 years a number of investigations by Dewar<sup>8</sup>, Cremer<sup>9-13</sup>, Schleyer<sup>76</sup>, Allen<sup>32</sup>, Wiberg<sup>14,77-79</sup>, Inagaki<sup>47,80</sup> and other authors<sup>81-83</sup> have been published to pin down the electronic causes for the unusual strain energy of **1**. These studies have also helped to clarify the concept of ring strain in general and the strain of three-membered rings in particular<sup>5,11-13</sup>. Since little of this work is covered in the previous review by Wiberg<sup>14</sup>, we will summarize here the most important results of investigations concerning stability and strain of **1**.

The CSE of **1** is determined by comparison with the energy of a suitable reference compound. Theoretically, this has been done by defining homodesmotic reactions such as those in equations 9 and 10<sup>84</sup>:



which are formal reactions and for which the reaction energy can be easily determined by *ab initio* calculations. Alternatively, CSE values can be obtained by the traditional group equivalent method that has been transferred to *ab initio* theory by Wiberg<sup>85</sup> and by Ibrahim and Schleyer<sup>86</sup>. Applications of these approaches to **1** and other cycloalkanes in order to calculate CSE values have been amply discussed in previous reviews on strained hydrocarbons<sup>5,11,14,77</sup> and need not to be described here.

Four different ways have been pursued to rationalize the CSE of **1** with the help of electronic structure calculations.

(1) Dissection of the energy into atomic energies with the help of the virial partitioning method.

(2) Dissection of the energy into bond energies.

(3) Dissection of the energy into strain contributions in a molecular mechanics related fashion.

(4) Dissection of the molecular wave function by a configuration analysis.

Each of these approaches leads to a different description of strain and stability of **1** and therefore the question is whether the various rationalizations of strain and stability are compatible.

## A. Analysis of Ring Strain in Terms of Atomic Energies

Cremer and Gauss<sup>10</sup> were the first to show that the strain energy of **1** can be derived from atomic energies obtained by the virial partitioning method. These authors calculated charges and energy of the CH<sub>2</sub> group in **1**, cyclobutane and propane at the HF/6-31G(d,p) level of theory. The 6-31G(d,p) basis set was chosen because it contains polarization functions for both C and H atoms and, accordingly, guarantees a balanced description of geometry, CH bond polarity and charge distribution. For all molecules, the H atoms were found to be negatively charged, suggesting a larger electronegativity for H than for C (see also Section VIII). However, the difference in electronegativities between H and C was reduced when going from propane to cyclobutane and **1**, i.e. with increasing strain the electronegativity of the C atom increases (Table 7). This leads to two opposing effects:

(1) Increasing strain diminishes atomic volume  $V_\Omega$  (Table 5) and atomic charge  $Q_\Omega$  of the H atoms and, as a consequence, the H atoms are destabilized, i.e. their energy becomes more positive.

(2) At the same time, the C atoms accumulate more electronic charge in their atomic basin and therefore their energy becomes more negative, indicating stabilization of the atoms.

The total effect on the energy of a CH<sub>2</sub> group in case of increased strain, namely the destabilization of two H atoms and the stabilization of a C atom, is destabilizing, as can be seen when using an appropriate CH<sub>2</sub> reference group such as, e.g., the CH<sub>2</sub> group of cyclo-



TABLE 7. Atomic energies and atomic charges of cyclopropane, cyclobutane and propane as calculated by the virial partitioning method<sup>a</sup>

Property	Atom/group	Cyclopropane	Cyclobutane	Propane	Reference CH <sub>2</sub> (cyclohexane)
Energy	C	-37.7126	-37.6896	-37.6378	
	H	-0.6552	-0.6687 (eq) -0.6691 (ax)	-0.6738	
Rel. energy	CH <sub>2</sub>	-39.0230	-39.0274	-38.9854	-39.0379
	CH <sub>2</sub>	9.3	6.6	32.9	0
Strain energy		27.9	26.4	-	0
Charge	C	105.6	171.9	222.9	
	H	-52.8	-87.0 (eq) -84.9 (ax)	-92.2	
	CH <sub>2</sub>	0	0	38.5	0

<sup>a</sup> From Reference 10. Absolute energies in hartree, relative energies and strain energies in kcal mol<sup>-1</sup>, charges in melectron according to HF/6-31G(d,p) calculations. The reference group —CH<sub>2</sub>— has properties almost identical with those of the CH<sub>2</sub> group of cyclohexane.

hexane. Cremer and Gauss<sup>10</sup> pointed out that the CH<sub>2</sub> group of propane is not suitable as a reference group since it is positively charged (Table 7), contrary to the CH<sub>2</sub> groups in cycloalkanes such as **1** or cyclohexane. The positive charge results from the larger group electronegativity of CH<sub>3</sub> (three electronegative H atoms) compared to CH<sub>2</sub> (two H atoms) and can only be balanced by filling up the atomic basins of the CH<sub>2</sub> group of propane by negative charge until electroneutrality is reached. This corresponds to an adjustment of the charge of the two CH<sub>3</sub> groups in propane to that of the CH<sub>3</sub> groups in ethane. A new hypothetical CH<sub>2</sub> reference group is derived that comprises the total subspace of the CH<sub>2</sub> group and a part of the subspaces of the two adjacent C atoms, which is indicated by the notation —CH<sub>2</sub>—. Its energy is equal to  $E(\text{CH}_2, \text{propane}) + 2 \{E(\text{CH}_3, \text{propane}) - E(\text{CH}_3, \text{ethane})\}$ , i.e. ethane is used to get the appropriate reference group. This is identical to the way of getting homodesmotic strain energies from the formal reaction 9 (*vide infra*) or to directly using a 'diagonal reference state'<sup>5c</sup> such as the CH<sub>2</sub> group in cyclohexane, which has almost the same properties as the group —CH<sub>2</sub>—. (Using cyclohexane as a diagonal reference state would have been easier, but was not feasible because of computational reasons.)

Cremer and Gauss<sup>10</sup> could obtain in this way the CSEs of **1**, cyclobutane and other small cycloalkanes. Later, their work was extended to other strained hydrocarbons by using the same approach but smaller basis sets<sup>78, 79</sup>. A puzzling result of these investigations is the fact that ring strain seems to be a result of destabilization of the H atoms, which in turn is a result of a charge transfer from H to C caused by the increased electronegativity of C. This, of course, can be connected with hybridization models of Coulson and Moffitt<sup>23</sup> and others<sup>7, 45-47, 50</sup>. An increase in angle strain leads to increased p-character of the hybrid orbitals that constitute the CC bonds. The hybrid orbitals for the CH bonds obtain more s-character, i.e. the electronegativity of the C atom increases and C attracts negative charge from the H atoms with increasing angle strain. This is exactly reflected by the atomic charges and energies calculated with the virial partitioning method. Hence, the dissection of the molecular energy into atomic energies leads to a description of ring strain, which is consistent with other interpretations, but it does not explain the similarity in the CSEs of **1** and cyclobutane.

## B. Analysis of Ring Strain in Terms of Bond Energies

Bond energies are not observable quantities and therefore they can only be calculated on the basis of a suitable model. Several attempts have been made on the basis of the max-

imum overlap model<sup>45</sup> or semiempirical calculations<sup>87</sup> to rationalize the stability of **1** in terms of CC bond weakening (because of angle strain) slightly compensated by simultaneous CH bond strengthening because of the higher s-character of the hybrid orbitals forming the CH bonds. Cremer and Gauss<sup>10</sup> have used the virial partitioning method to calculate CC and CH bond energies from first principles. Virial partitioning of the electron density distribution  $\rho(\mathbf{r})$  is based on the zero-flux surfaces  $S(A,B)$  (see equation 6 and Table 5) that separate the atomic basins of bonded atoms A and B in a molecule. The bond energy  $BE(A,B)$  should be proportional to the electron density  $N(A,B)$  in the surface  $S(A,B)$  and the forces exerted on this density. For non-polar and weakly polar bonds, the second factor can be covered by a proportionality constant  $\alpha(A,B)$  so that the bond energy is given by equation 11<sup>88</sup>:

$$BE(A,B) = \alpha(A,B) N(A,B)/R(A,B)^2 \quad (11)$$

where  $N(A,B)$  is determined by equation 12:

$$N(A,B) = \mathbf{R}(A,B) \oint_{AB} dS(\mathbf{r}) \rho(\mathbf{r}) \mathbf{n}_A(\mathbf{r}) \quad (12)$$

where  $\mathbf{R}(A,B)$  is the vector from the nucleus of A to the nucleus of B, and  $\mathbf{n}_A$  is a unit vector normal to the surface, outwardly directed from A.

TABLE 8. Bond energies and strain energies of cyclopropane, cyclobutane and propane as calculated by the virial partitioning method<sup>a</sup>

Property	Bond group	Cyclopropane	Cyclobutane	Propane
Bond energy	C—C	71.0	73.9	81.9
	C—H	106.6	105.9	105.5
Strain energy	C—C	32.7	32.0	0
Stabilization energy <sup>b</sup>	C—H	-6.6	-3.2	0
Error in atomization energy		1.4	-3.1	0.6
Total strain energy		27.5	25.7	0

<sup>a</sup> From Reference 10. Bond and strain energies in kcal mol<sup>-1</sup> according to HF/6-31G(d,p) calculations. The strain energy is derived from the difference in CC bond energies and CH stabilization energies corrected for errors in the theoretical atomization energies.

<sup>b</sup> Stabilization due to hybridization effects in CH bonding.

In Table 8, HF/6-31G(d,p) bond energies for **1**, cyclobutane and propane are given, which indicate a decrease in  $BE(CC)$  from 82 to 71 kcal mol<sup>-1</sup> when going from propane to **1**, thus leading to a strain energy of 34 kcal mol<sup>-1</sup> (including small corrections in calculated atomization energies<sup>10</sup>). The strain energy of the ring is slightly reduced by an increase of the CH bond energy from 105.5 in propane (*sec*-CH bond) to 106.6 kcal mol<sup>-1</sup> in **1** (increased s-character of CH hybrid orbitals). Hence, the final strain energy (27.5 kcal mol<sup>-1</sup>, Table 8) is in good agreement with the accepted CSE of **1**. For cyclobutane, the corresponding values are 73.9 kcal mol<sup>-1</sup> ( $BE(CC)$ ), 105.9 ( $BE(CH)$ ) and 26 kcal mol<sup>-1</sup> (final SE, Table 8). Hence, the SE of **1** results from CC bond destabilization caused by angle bending and the concomitant increase of p-character in the hybrid orbitals forming the CC bonds<sup>10</sup>.

The difference in the values of the CC bond energies for **1** and cyclobutane does not contradict observations made for bond orders and overlap values, namely that

- bond orders  $n$  for **1** and cyclobutane are identical ( $n = 1.00$ , Table 6<sup>9,10</sup>), and
- CC bonding overlap for **1** and cyclobutane as calculated at the VB level of theory is almost identical (Table 3)<sup>51</sup>.

Both bond order  $n$  and CC bonding overlap  $S$  are local quantities<sup>11</sup>. The bond order is derived from the value of  $\rho(\mathbf{r})$  at position  $\mathbf{p}$  and  $S$  contains just the CC hybrid orbital over-

lap. Bond energies by definition are global rather than local quantities because they are derived by appropriate dissection of atomization energies and, accordingly, contain all bonding and non-bonding interactions between two atoms. If one wants to estimate bond energies from overlap values, one has to consider both bonding and non-bonding overlap (see Table 3). In addition, one has to include effects such as bond bending and bond polarity, where the former determines hybridization and electronegativity of the atoms forming the bond and the latter is a result of the electronegativity difference between the atoms of a bond. In the case of **1**, the bond energy should be given by a relationship such as equation 13:

$$\text{BE}(\text{CC}) = a I_{\text{C}} S(\text{CC}) + b \quad (13)$$

where  $a$  and  $b$  are constants,  $S(\text{CC})$  is the CC overlap and  $I_{\text{C}}$  the ionization potential of a C atom in the  $\text{C}_3$  ring. Equation 11 is exactly of the form of equation 13 with  $\alpha(\text{A,B})$  taking the part of  $I$  and  $N(\text{A,B})$  the part of  $S$ .

Neither bond order or CC overlap values alone can lead to an estimate of the CC bond energy and, in this respect, the observation that both **1** and cyclobutane possess similar CC bonding overlap<sup>51</sup> does not say anything with regard to the CC bond strength.

As in the case of the calculation of *in situ* atomic energies, it is possible to give a reasonable explanation for the strain of **1** by comparing calculated bond energies, but it is not possible to explain the similar stability of **1** and cyclobutane on this basis. For example, it is not clear why the CC bonds in **1** and cyclobutane have comparable strengths. It has been suggested by Schleyer<sup>76</sup> that CH bond strengthening in **1** is much larger than that of the *sec*-CH bond in propane. For example, the CH bond dissociation enthalpy DH of **1** (106.3 kcal mol<sup>-1</sup>) is 11.2 kcal mol<sup>-1</sup> higher than the one for the secondary CH bond of propane (95.1 kcal mol<sup>-1</sup>)<sup>89</sup>. However, DH values do not necessarily reflect the magnitude of bond energies since they depend on the stability of both reactant and product. In this way, the large DH(CH) value of **1** may just reflect the increase in ring strain when the cyclopropyl radical is formed.

### C. Dissection of the Molecular Energy into Strain Contributions

According to the classical definition of ring strain introduced by Baeyer at the end of the last century<sup>90</sup>, a three-membered ring should be much more strained than a four-membered ring. Its bond angles  $\alpha$  deviate from the standard, strain-free CCC angle (109.5°) by  $\Delta\alpha = 49.5^\circ$  while those of the planar four-membered ring deviate by just 19.5°. According to Hooke's law, the Baeyer strain energy (angle bending strain energy) as given in equation 14:

$$\Delta E(\text{Baeyer}) = n(k_{\alpha}/2)(\Delta\alpha)^2 \quad (14)$$

(where  $n$  is the size of the ring and  $k_{\alpha}$  is the CCC bending force constant) should be 173 kcal mol<sup>-1</sup> for **1** and 36 kcal mol<sup>-1</sup> for cyclobutane if  $k_{\alpha}(\text{CCC}) = 1.071$  mdyne Å rad<sup>-2</sup> of propane<sup>91</sup> is used as an appropriate bending force constant.

Cremer and Gauss<sup>10</sup> have pointed out that it is unrealistic to use geometrical angles  $\alpha$  and the bending force constant of propane to calculate the Baeyer strain energy of **1**. These authors chose the CC bond path length  $r_b$  (1.506 Å compared to  $r_c = 1.497$  Å, Table 6) and the interpath angles  $\beta(\text{CCC})$  (79° compared to  $\alpha_c = 60^\circ$ , Table 6) rather than the geometrical parameters to get realistic stretching and angle strain energies. Furthermore, they pointed out that the bending force constant of propane depends on 1,3-non-bonded interactions, which are totally missing in **1**. In molecular mechanics, this problem is solved by considering the bending force constant  $k$  as an adjustable parameter that takes values between 0.45 and 0.8 mdyne Å rad<sup>-2</sup> to reproduce measured molecular properties<sup>92</sup>. Cremer and Gauss<sup>10</sup> determined  $k(\text{CCC}) = 0.583$  mdyne Å rad<sup>-2</sup> using the strain energy of cyclobutane in the absence of 1,3-CC non-bonded repulsion (Dunitz-Schomaker strain energy)<sup>93</sup>.

Table 9. Dissection of the strain energy of cyclopropane<sup>a</sup>

Strain	Cyclopropane	Cyclobutane	Reference	Comment	Method <sup>Ref</sup>
Stretching	0.5	1.0	ethane	$k_r(\text{CC}) = 4.57 \text{ mdyn } \text{Å}^{-1}$	exp <sup>91</sup> exp <sup>91</sup> HF/6-31G(d,p) <sup>10</sup> HF/6-31G(d,p) <sup>10</sup>
				$k_r(\text{CH}) = 4.88 \text{ mdyn } \text{Å}^{-1}$	
				$r(\text{CC}) = 1.5268 \text{ Å}$	
				$r(\text{CC}) = 1.0858 \text{ Å}$	
<i>Note:</i> Bond path lengths $r_b$ are used for bent bonds					
Baeyer (angle bending)	46.3	13.0	propane	$k_b(\text{CCC}) = 0.583 \text{ mdyn } \text{Å} \text{ rad}^{-2}$	exp <sup>91</sup> exp <sup>91</sup>
				$k_x(\text{CCH}) = 0.656 \text{ mdyn } \text{Å} \text{ rad}^{-2}$	
				$k_x(\text{HCH}) = 0.550 \text{ mdyn } \text{Å} \text{ rad}^{-2}$	
				$\alpha = 109.5^\circ$	
<i>Note:</i> Bond path angles $\beta$ are used for bent bonds. According to Hooke's law, the Baeyer strain energy is $41.3 \text{ kcal mol}^{-1}$ , anharmonicity effects lead to another $5 \text{ kcal mol}^{-1}$					
Pitzer (bond eclipsing) Dunitz-Schomaker (non-bonded interactions)	4.0	3.9	ethane	$V_3 = 3.0$	HF/6-31G(d,p) <sup>10</sup> CNDO/2 <sup>93</sup>
				$\tau = 60^\circ$	
				cyclobutane	
<i>Note:</i> Results scaled as a function of $k_b(\text{CCC})$ to reproduce CSE and inversion barrier of cyclobutane					
Total	50.8	29.9			
CH strengthening	-6.4	-2.8	from <i>ab initio</i> bond energies		HF/6-31G(d,p) <sup>10</sup>
$\sigma$ Delocalization	-16.4	0	<i>Note:</i> Rehybridization leads to higher s-character Difference between CSE and $\Delta E = 50.8 - 6.4 = 44.4 \text{ kcal mol}^{-1}$		
CSE	28.0	27.1	Conventional Strain Energy		

<sup>a</sup> All energy values in  $\text{kcal mol}^{-1}$

Table 9 shows the various strain energies calculated for **1** and cyclobutane by Cremer and Gauss<sup>10</sup>. The Baeyer strain energy of **1** is 46 kcal mol<sup>-1</sup>, including an estimated 5 kcal mol<sup>-1</sup> from anharmonicity effects, while the Baeyer strain energy of cyclobutane is just 13 kcal mol<sup>-1</sup>. However, the four-membered ring is destabilized by 12 kcal mol<sup>-1</sup> because of 1,3-CC repulsion (Dunitz–Schomaker strain). Stretching strain and Pitzer strain add together just 4–5 kcal mol<sup>-1</sup> to the total strain energy, which is 51 kcal mol<sup>-1</sup> in the case of **1** and 30 kcal mol<sup>-1</sup> for cyclobutane. These values are in line with an expected increase of the strain energy with decreasing ring size. However, they must be corrected for stabilizing effects, namely

(a) CH bond strengthening as a result of increased s-character of the hybrid orbitals forming the CH bond orbitals, and

(b) surface delocalization of  $\sigma$ -electrons<sup>9</sup>.

If one takes the bond strengthening effects calculated with equations 11 and 12 (see Table 8), then surface delocalization of  $\sigma$ -electrons must add about 16 kcal mol<sup>-1</sup> to the stability of **1** to lead to a CSE of 28 kcal mol<sup>-1</sup><sup>10</sup>.

## D. Dissection of the Molecular Wave Function

While the three approaches discussed above lead to a quantitative reproduction of the SE of **1**, a dissection of the HF wave function suggested by Inagaki and coworkers<sup>47, 80</sup> provides qualitative arguments for a rationalization of strain and stability of **1**. The method is based on a configuration analysis of the HF wave function,  $\Psi_{\text{HF}}$  according to equation 15:

$$\Psi_{\text{HF}} = C_G \Phi_G + \sum C_T \Phi_T \quad (15)$$

where  $\Phi_G$  is the ground state configuration and  $\Phi_T$  are singly excited configurations. The ground configuration is made up from localized bond orbitals each of which is a linear combination of hybrid atomic orbitals located at bonded atoms. Optimal hybrid atomic orbitals (with regard to the s/p ratio) are determined by maximizing the coefficient  $C_G$  of the ground state configuration<sup>47, 80</sup>.

The admixture of singly-excited configurations  $\Phi_T$  to  $\Phi_G$  to represent the HF wave function indicates electron transfer from bonding to antibonding orbitals and, accordingly, can be interpreted in terms of electron delocalization, which can be measured by the ratio  $C_T/C_G$ . Alternatively, one can define interbond populations by equation 16<sup>47, 80</sup>:

$$\text{IBP}_{ij} = 2\sum_p n_p c_{pi} c_{pj} s_{ij} \quad (16)$$

where  $n_p$  is the occupation number of the  $p$ th MO,  $c_{pi}$  the expansion coefficient of the  $i$ th bond orbital for the  $p$ th MO and  $s_{ij}$  the overlap between bond orbitals  $i$  and  $j$ . The method of configuration analysis leads to

(a) the percentage of s-character of the hybrid orbitals to describe the electronegativity of atoms forming the ring;

(b) atomic bond populations and overlap of hybrid orbitals to describe the strength of bonds;

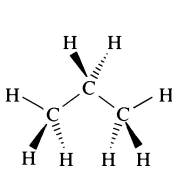
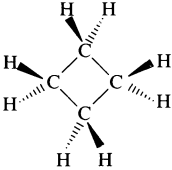
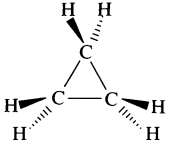
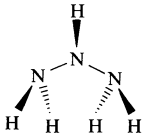
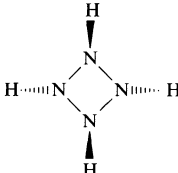
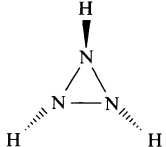
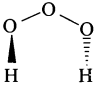
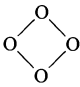
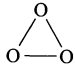
(c) overlap repulsion indices  $\text{IBP}_{\sigma\sigma}$  between geminal bonding orbitals to describe angle strain upon bond angle deformation and

(d) interbond population  $\text{IBP}_{\sigma\sigma^*}$  between bonding and antibonding orbitals to describe delocalization effects.

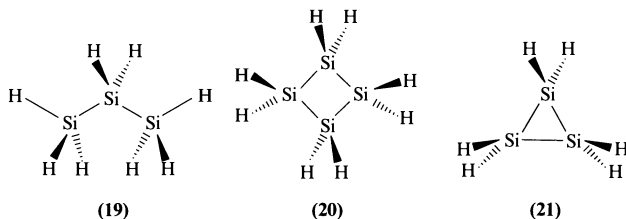
In Table 10, results of the configuration analysis of HF/6-31G(d) wave functions of several three-membered rings are shown. Data indicate that<sup>47</sup>:

(1) The s-character (p-character) of the hybrid orbitals forming the ring bonds decreases (increases) when going from the acyclic reference compound to the four- and then to the three-membered ring or when going to a system with more electronegative heavy atoms.

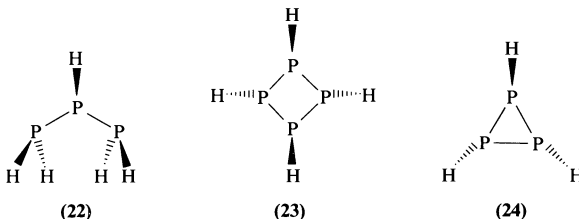
TABLE 10. Conventional strain energies (CSE), hybridizations, s-character, overlap values, overlap repulsions and geminal delocalizations of propane, cyclobutane, cyclopropane and their heterologues with X = NH, O, SiH<sub>2</sub>, PH, S from Reference 47<sup>a</sup>

Parameter	Acyclic compound	Four-membered ring	Three-membered ring
			
	(11)	(12)	(1)
CSE		26.6	28.7
sp <sup>n</sup> (CC) [s-character in%]	sp <sup>2.9</sup> [26]	sp <sup>3.2</sup> [24]	sp <sup>4.0</sup> [20]
sp <sup>m</sup> (CH) [s-character in%]	sp <sup>3.1</sup> [24]	sp <sup>2.8</sup> [26]	sp <sup>2.3</sup> [30]
S(CC)	0.61	0.58	0.56
S(CH)	0.65	0.66	0.67
IBPσσ	-0.021	-0.046	-0.132
IBPσσ*	-0.011	-0.017	-0.003
			
	(13)	(14)	(15)
CSE		33.4	31.8
sp <sup>n</sup> (NN) [s-character in%]	sp <sup>3.3</sup> [23]	sp <sup>4.8</sup> [17]	sp <sup>7.2</sup> [12]
S(NN)	0.57	0.52	0.48
S(NH)	0.64; 0.64	0.63	0.60; 0.63
IBPσσ	-0.010	-0.033	-0.095
IBPσσ*	-0.014	-0.022	-0.004
			
	(16)	(17)	(18)
CSE		57.0	38.7
sp <sup>n</sup> (OO) [s-character in%]	sp <sup>6.7</sup> [13]	sp <sup>8.6</sup> [10]	sp <sup>11.9</sup> [8]
sp <sup>m</sup> (lp) [s-character in%]	sp <sup>1.7</sup> [37]	sp <sup>1.5</sup> [40]	sp <sup>1.4</sup> [42]
S(OO)	0.42	0.39	0.37
IBPσσ	-0.006	-0.018	-0.061
IBPσσ*	-0.007	-0.011	0.004

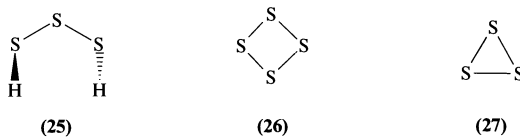
Parameter	Acyclic compound	Four-membered ring	Three-membered ring
-----------	------------------	--------------------	---------------------



CSE		16.6	38.8
$sp^n(\text{SiSi})$ [s-character in%]	$sp^{2.9}$ [26]	$sp^{3.4}$ [23]	$sp^{3.6}$ [22]
$sp^m(\text{SiH})$ [s-character in%]	$sp^{3.1}$ [24]	$sp^{2.7}$ [27]	$sp^{2.5}$ [28]
$S(\text{SiSi})$	0.48	0.45	0.44
$S(\text{SiH})$	0.37	0.36	0.35
$\text{IBP}\sigma\sigma$	-0.004	-0.024	-0.087
$\text{IBP}\sigma\sigma^*$	-0.005	-0.012	-0.021



CSE		9.5	11.2
$sp^n(\text{PP})$ [s-character in%]	$sp^{7.2}$ [12]	$sp^{9.6}$ [9]	$sp^{14.3}$ [6]
$S(\text{PP})$	0.41	0.39	0.36
$S(\text{PH})$	0.56	0.56	0.56
$\text{IBP}\sigma\sigma$	-0.002	-0.013	-0.058
$\text{IBP}\sigma\sigma^*$	-0.004	-0.007	-0.002



CSE		39.6	28.9
$sp^n(\text{SS})$ [s-character in%]	$sp^{9.6}$ [9]	$sp^{12.6}$ [7]	$sp^{16.3}$ [6]
$sp^m(\text{lp})$ [s-character in%]	$sp^{1.5}$ [40]	$sp^{1.3}$ [44]	$sp^{1.3}$ [44]
$S(\text{SS})$	0.40	0.37	0.36
$\text{IBP}\sigma\sigma$	-0.0021	-0.013	-0.055
$\text{IBP}\sigma\sigma^*$	-0.003	-0.006	-0.002

<sup>a</sup> Conventional strain energies (CSE) in kcal mol<sup>-1</sup> from HF/6-31G(d) calculations. Hybridization ratios  $n$  and  $m$ , overlap  $S$ , and interbond population values from a configuration analysis<sup>47</sup>.

(2) With increasing p-character, bond populations and the overlap between hybrid orbitals forming the bond orbital decrease. (We note that calculations based on non-

orthogonal hybrid orbitals might lead to different trends in orbital overlap<sup>51</sup>.) This indicates bond weakening in the order: open-chain compound < four-membered ring < three-membered ring.

(3) Destabilizing (antibonding) overlap repulsions between geminal bonds increase (i.e.  $IBP_{\sigma\sigma}$  becomes more negative) in the order: open-chain compound < four-membered ring < three-membered ring.

(4) Bonds XH become stronger as indicated by overlap and bond populations (hybrid orbitals of ring atoms forming the bonds possess more s-character) in the order: open-chain compound < four-membered ring < three-membered ring. However, in the case of ring atoms with lone-pair orbitals, the increase in s-character is observed only for the lone-pair orbitals and the peripheral ring bonds become actually weaker rather than stronger.

(5) Geminal delocalization measured by the interbond populations  $IBP_{\sigma\sigma^*}$  is destabilizing (antibonding) in most cases. For Si compounds, the destabilizing character of geminal delocalization increases from the open-chain compound to the four-membered and the three-membered ring. This means that geminal delocalization and overlap repulsion both lead to a decrease of the electron density between geminal bonds and that depression of electron density increases with increasing angle strain. However, if the p-character of the hybrid orbitals forming the ring increases because of an increase in electronegativity of the ring atoms X, then geminal delocalization in three-membered rings will become less antibonding [e.g. X = C (**1**), N (**15**)] or even bonding [e.g. X = O (**18**)].

While observations (1)–(4) are in line with other descriptions of the strain in **1** or three-membered rings, geminal delocalization seems to play a decisive role with regard to the relative stability of three-membered versus four-membered ring. Bonding geminal delocalization leads to a build-up of electron density inside the ring and surface delocalization. An increase of geminal delocalization (surface delocalization) reduces angle strain and leads to higher stability of the ring. This can be found in the series **1** (X = C), **15** (X = N), **18** (X = O) as well as in the series **21** (X = Si), **24** (X = P), **27** (X = S) where, for the hetero atom rings, the CSE is smaller in the three- than in the four-membered rings. Hence, the strain energy of **18** is 39 kcal mol<sup>-1</sup> compared to 57 kcal mol<sup>-1</sup> in the case of **17**. In this way, **1** is not so peculiar with regard to its stability as one might think.

In summary, the configuration analysis explains the peculiar stability of **1** and confirms the existence of surface delocalization in **1**. This leads to extra-stabilization of the ring and a reduction in the ring strain, so that it becomes comparable to that of cyclobutane. The configuration analysis can provide only trends but no energy data that lead to a dissection of the total strain energy. Accordingly neither interbond populations nor delocalization indices correlate with calculated strain energies.

## E. Strain Energy, $\sigma$ -Aromaticity and Surface Delocalization

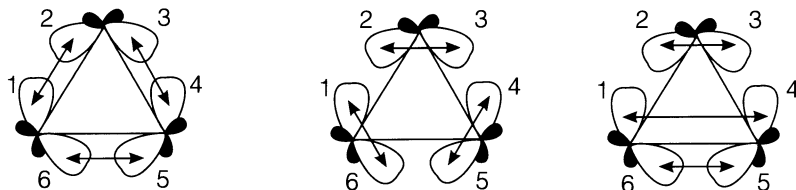
Dewar<sup>8</sup> has pointed out that there is an analogy between the =HC—CH= group of a conjugated cyclopolyene and the —CH<sub>2</sub>— group of a cycloalkane. He has argued that **1** and benzene are isoconjugate. While benzene is stabilized by a system of six delocalized  $\pi$ -electrons leading to  $\pi$ -aromaticity, **1** is stabilized by a sextet of delocalized  $\sigma$ -electrons leading to  $\sigma$ -aromaticity. Dewar<sup>8</sup> has related known properties of **1**, such as

- (1) its surprisingly low strain energy,
- (2) its relatively short CC bond lengths,
- (3) its relatively high CC bond strengths,
- (4) upfield shifts of its <sup>1</sup>H (1 ppm) and <sup>13</sup>C (20 ppm) NMR signals compared to those of other alkanes,
- (5) its electronic interactions with substituents and
- (6) its ability to enhance conjugation in homoaromatic systems

to a possible  $\sigma$ -aromatic stabilization. He estimated that the  $\sigma$ -aromatic stabilization energy might be as large as 55 kcal mol<sup>-1</sup>. Schleyer<sup>76</sup> and, independently, Grev and



cyclopropane:

classical (bond coupling) structure  
96.2%geminal coupling structure  
0.1% $\pi$ -complex structures  
3.7%

40.3%

40.3%

19.4%

benzene:

Kekule' structures

Dewar structures

FIGURE 17. Schematic representation of the symmetry-unique spin-coupling patterns in cyclopropane (above) and benzene (below). In the case of cyclopropane, carbon hybrid orbitals and, in the case of benzene, carbon  $p\pi$  orbitals are shown. For each structure, Gallup–Norbeck occupation numbers as determined by spin-coupled valence bond theory are given. All data from Reference 51

Schaefer<sup>94</sup> have criticized the concept of  $\sigma$ -aromaticity. Schleyer in particular noted that CH bond strengthening in **1** and 1,3-CC non-bonded repulsion in cyclobutane could easily explain the similarity in strain energies of the three- and four-membered rings. Karadakov and coworkers<sup>51</sup>, who carried out a spin-coupled VB calculation of **1**, found no indication that more than one spin-coupling pattern plays any significant role in the description of the electronic structure of **1** (see Figure 17). Two resonance structures with equally large weight as in the case of benzene (40.3%, Figure 17) do not exist in the case of **1** and therefore the authors reject the possibility of  $\sigma$ -aromaticity.

It is interesting to note that the spin coupling patterns that correspond to a  $\pi$ -complex (1–4, 2–3, 5–6 and two equivalent patterns obtained by cyclic permutation, see Figure 17) contribute to the wave function by 3.7%, which is not large but suggests that the resonance description of **1** in terms of ethene–methylene  $\pi$ -complexes is not totally wrong and may become more important for reacting **1** or other three-membered rings.

Cremer<sup>12</sup> has summarized the pros and cons for invoking the term  $\sigma$ -aromaticity. His major conclusion was that all the peculiar properties of **1** can be rationalized in terms of surface delocalization of  $\sigma$ -electrons *without invoking  $\sigma$ -aromaticity*. This is of advantage since surface delocalization is based on an experimental fact, namely the observed increase in electron density inside the ring. Surface delocalization adds to the stability of **1** and lowers the strain energy. It is, however, a question as to how the energy of **1** is dissected and whether the stabilization energy resulting from surface delocalization is 16 kcal mol<sup>-1</sup> or some other value<sup>10</sup>.

## VI. GEOMETRY

Investigation of the geometry of **1**, related three-membered rings and substituted **1** has been a major research goal of structural chemists for decades<sup>5, 26, 27, 32, 33, 71, 83, 94–125</sup> since these

primary information on the electronic structure of **1**, its ability to conjugated groups and its interactions with substituents in general. In addition, three-membered rings has been the testing ground for various theoretical substituent interactions with regard to their usefulness, limitations and view of this massive work, it is surprising that even today the exact  $r_e$  geometry of cyclopropane is a matter of controversy and that not all geometries of substituted **1** are well

### of Cyclopropane

Experimental geometries of **1** are summarized in Table 11<sup>10, 62, 126-133</sup>. There are several experimental investigations that derived the  $r_e$  (equilibrium) geometry from measured

equilibrium geometry of cyclopropane<sup>a</sup>

	$r$ (CC) (Å)	$r$ (CH) (Å)	$\alpha$ (HCH) (deg)	Ref.
	1.515	1.071	114.5	131
	1.503	1.072	113.7	128
	1.519	1.073	113.8	129
	1.497	1.076	114.0	128
)	1.497	1.076	114.1	10
1p]	1.503	1.078	114.4	132
2p]	1.499	1.072	114.4	132
2p]	1.497	1.073	114.4	133
)	1.502	1.084	114.2	62
2s1p]	1.513	1.083	115.1	130
3s2p]	1.507	1.076	115.2	133
2p1d/2s1p]	1.510	1.080	114.7	130
5s3p2d/3s2p]	1.514	1.079	115.1	133
3p2d/3s2p]	1.514	1.079	115.0	133
fraction)	1.5127 (12)	1.0840 (20)	114.5 (9)	126
	1.5157 (23)	1.0797 (34)	115.47 (38)	127
	1.501 (5)	1.084 (5)	114.5 (9)	126
	1.5101 (23)	1.0742 (29)	115.85 (33)	127

<sup>a</sup> experimentally based geometries, uncertainties are given in parentheses.

of **1**<sup>126, 127</sup>. Endo, Chang and Hirota<sup>127</sup> measured the microwave spectrum and determined its rotational and centrifugal distortion constants. Using these data and the published rotational constants for **1** ( $B_0$ ,  $C_0$ ) and **1-d<sub>6</sub>** ( $B_0$ ), these authors determined the  $r_e$  structures in good agreement with previously published  $r_e$  and  $r_z$  structures. Endo, Chang and Hirota derived an  $r_e$  geometry of **1** utilizing reported rotational constants and considering just the CC and CH third-order anharmonicity-justifiable parameters. This  $r_e$  geometry (Table 11) differs considerably from the  $r_e$  geometry published earlier by Yamamoto, Nakata, Fukuyama and Kuchitsu<sup>126</sup>, who performed a joint analysis of electron diffraction intensities and spectroscopic data and determined rotational constants for vibrationally excited states. Kuchitsu and co-workers determined the HCH angle ( $\alpha_z$ (HCH)) and used effective CC and CH stretching anharmonicity constants derived from the rotational constants for the  $\nu_{11}$  vibrational state<sup>126</sup>. The  $r_e$  geometries differ by 0.01 Å and 1.3° with regard to C—C (C—H) bond lengths respectively, which is well outside the error bars given in the two investigations (Table 11)<sup>126, 127</sup>. Considering the fact that  $r_e$  geometrical parameters of small molecules can be determined with a precision of 0.001 Å (0.5°) or better<sup>134</sup>, the deviation of the two geometries suggests that at least one of the published  $r_e$  geometries is seriously in error.

*Ab initio* geometries of **1** (Table 11) vary over a relatively large region<sup>10, 33, 62, 128–133</sup>. CC bond lengths from 1.497 to 1.519 Å, CH bond lengths from 1.072 to 1.084 Å and HCH angles from 113.5 to 115.2°. Considering, however, the known trends of calculated equilibrium geometries as dependent on method and basis set, it is rather straightforward to suggest the most likely  $r_e$  geometry of **1**<sup>135</sup>.

At the HF level of theory, the largest basis set leads to the shortest CC and CH bond lengths and the largest HCH angle. In general, bond lengths decrease with increasing basis set, which has to do with the redistribution of electron density in a molecule upon basis set enlargement. Since an electron ‘sees’ only the average field of all other electrons at the HF level, electronic charge can accumulate close to the nuclei to increase stabilizing electron–nucleus attractions. The more basis functions are available to describe the area around the nuclei, the more electrons are packed close to the nuclei, thus effectively shielding the nuclei with regard to each other. As a consequence, nuclear repulsion is reduced and internuclear distances are decreased. Short bond distances will lead to an increase in non-bonded repulsion of partially positive H atoms and thereby cause an enlargement of the HCH angles. Since HF/large basis set calculations will underestimate bond distances, HF is not the appropriate method for high-accuracy determinations of  $r_e$  geometries. Of course, it may be the case that HF/small or medium basis set calculations accidentally lead to accurate  $r_e$  geometries because of a fortuitous cancellation of basis set and correlation errors.

As can be seen from Table 11, inclusion of electron correlation leads to an increase of both CC and CH bond lengths. This is due to the fact that correlated movements of the electrons exclude clustering of electrons in the vicinity of the nuclei. Instead, electrons have to spread out in the molecule to avoid close contacts and destabilizing Coulomb repulsion. The nuclei become deshielded, nuclear repulsion is increased and, hence, bond distances become longer for correlation corrected *ab initio* methods. These effects are the larger the more correlation effects are included into the *ab initio* method. For example, MP2 covers just pair correlation effects, which is sufficient to get useful descriptions of  $r_e$  geometries for singly bonded molecules. However, in the case of molecules with multiple bonds, triple and quadruple excitations have to be included to obtain reliable  $r_e$  geometries. This suggests the use of methods such as MP4<sup>136</sup> or CCSD(T)<sup>137</sup>, where the latter method is correct to fourth-order perturbation theory but contains in addition infinite-order effects resulting from S, D and T excitations<sup>138</sup>.

Calculated CC bond distances of **1** obtained with various basis sets at the MP2 level<sup>136</sup> range from 1.502 to 1.513 Å. Both MP4/TZ + 2P and CCSD(T)/TZ + 2P calculations<sup>133</sup> suggest an even longer CC bond length of 1.514 Å, which is close to the experimentally based value of Endo and coworkers<sup>127</sup>. In view of the fact that the CC bonds of **1** possess considerable  $\pi$ -character, the inclusion of T excitations seems to be necessary and suggests higher reliability to MP4 and CCSD(T) (rather than MP2) results, which clearly support the  $r_e$  geometry predicted by Endo and coworkers<sup>127</sup>.

The geometrical parameters of **1** are characteristically different from those of other alkanes (Table 12)<sup>10, 62, 139–143</sup>. Compared to propane, both CC and CH bonds are shorter (0.02 and 0.01 Å, respectively) and HCH angles are larger (8°). Differences between the geometrical parameters of **1** and cyclobutane are similarly large or, as in the case of the CC bond (1.510 vs 1.548 Å, Tables 11 and 12), even larger. These characteristic differences are a result of the peculiar electronic structure of **1** (see Section III–V), which lend the molecule similarity to an alkene. This is confirmed by comparing the geometrical parameters of **1** and ethene: CH bond lengths and HCH angles have indeed similar values (Tables 11 and 12) while the CC bond of **1** is closer to that of an alkane than to that of an alkene.

If the cyclopropane ring is fused with another cyclopropane ring, thus leading to bicyclo[1.1.0]butane, all CC bonds become shorter but, in particular, the bridge bond C1C3, which decreases to 1.47 Å according to theory (Table 12)<sup>62, 141</sup>. The experimental value is longer (1.50 Å) and also suggests  $r(\text{C1C3}) > r(\text{C1C2})$ <sup>142</sup>, which may be doubted in view of the increase in  $\pi$ -character of the bridge bond (see Section XII. A). If three cyclopropane

TABLE 12. Geometries of propane, ethene, cyclobutane and some fused cyclopropanes<sup>a</sup>

Molecule	Parameter	Method			Reference		
		HF 4-31G	HF 6-31G(d) <sup>b</sup>	MP2 6-31G(d)	Exp.	Theor	Exp
Propane	CC	1.530	1.528	1.526	1.526	10	139
	<i>sec</i> -CH	1.085	1.088	1.096	1.092		
	CH <sub>i</sub>	1.083	1.086	1.094	1.096		
	CH <sub>o</sub>	1.084	1.088	1.095	1.096		
	CCC	112.6	112.8	112.4	112.7		
	CCH <sub>i</sub>	110.9	111.1	111.5			
	CCH <sub>o</sub>	111.3	111.1	110.8			
	H <sub>i</sub> CH <sub>o</sub>	107.4	107.8	106.3			
	H <sub>o</sub> CH <sub>o</sub>	107.8	107.6	107.9			
H <sub>s</sub> CH <sub>s</sub>	106.4	106.3	106.3	106.3			
Ethene	CC	1.315	1.317	1.335	1.339	10,	139
	CH	1.073	1.076	1.085	1.085	115	
	HCH	116.1	116.4	116.5	117.8		
Cyclobutane	CC	1.554	1.547	1.543	1.548	10	140
	CH	1.081	1.085	1.094	1.092		
	CCC	89.3	89.0	87.9	87.2		
	HCH	108.5	108.3	108.8			
	Puckering angle		15.0	30.8	25		
Bicyclo[1.1.0]butane	C1C2	1.502	1.489	1.492	1.489	62,	142
	C1C3	1.478	1.466	1.469	1.497	128	
	C1H	1.062	1.070	1.080	1.071		
	C2H <sub>eq</sub>	1.074	1.078	1.088	1.093		
	C2H <sub>ax</sub>	1.076	1.083	1.092	1.093		
	C1C2C3	59.0	58.9	60.2	60.0		
	C2C1C4	97.6	97.9		98.3		
	C3C1H	133.4	132.1	128.1	128.4		
	C1C2H <sub>eq</sub>	117.3	117.5	117.0			
	C1C2H <sub>ax</sub>	119.4	119.5	119.2			
	HC2H	113.9	114.0	114.1	115.6		
	Puckering angle		120.9	122.4	122.7		
[1.1.1]Propellane	C1C2	1.528	1.502	1.514	1.525	62,	143
	C1C3	1.600	1.543	1.592	1.596	128	
	C2H	1.070	1.075	1.088	1.106		
	HCH	114.7	114.5	114.9	116.0		

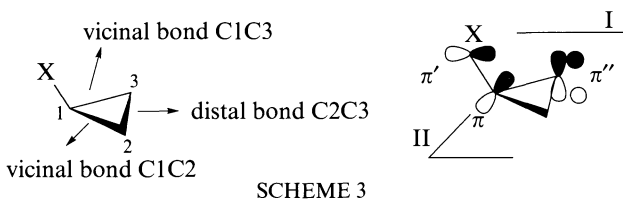
<sup>a</sup> Bond distances in Å, angles in deg. Subscripts s, i, o, ax, and eq denote secondary, in-plane and out-of-plane H atoms in case of propane and axial and equatorial H atoms in case of cyclobutane and bicyclobutane.

<sup>b</sup> Some geometries have been calculated at the HF/6-31G(d,p) level.

rings are fused to lead to [1.1.1]propellane, the bond C1C3 will become longer (1.60 Å, Table 12), which has been traced to an unusual type of bonding (see Section XII. B)<sup>32, 62, 141, 143</sup>

## B. Substituent Effects on the Geometry of the Cyclopropyl Group

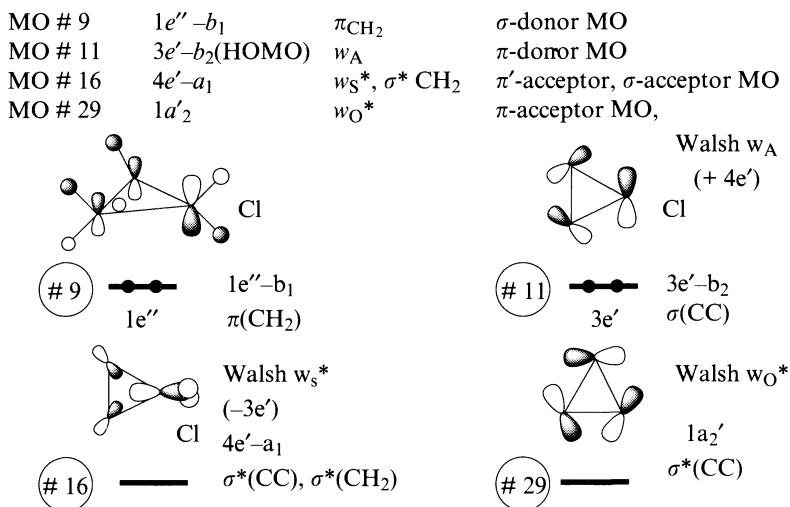
The influence of substituents on the bond lengths of **1** has received considerable attention in the past decades<sup>26, 27, 33, 95-123</sup>. Because of the peculiar electronic structure of **1**, substituent



effects on its geometry are more pronounced than in the case of other alkanes. Depending on the nature of substituents, both C1C2 (vicinal) and C2C3 (distal) bond lengths (Scheme 3) deviate from the CC bond lengths in **1**. Changes in vicinal and distal bond lengths usually have opposite sign, i.e. if C1C2 is elongated, C2C3 is shortened and *vice versa*. Allen and coworkers<sup>99</sup> have collected experimental geometries on substituted **1** and have analysed changes in geometry in a systematic way. These data are complemented by a considerable number of calculated equilibrium geometries of substituted cyclopropanes (Table 13), which are discussed in the following. Two alternative models have been developed to rationalize substituent effects on the geometry of **1**: (a) an MO model<sup>33</sup> and (b) an electron density model<sup>97</sup>.

### 1. The molecular orbital description

Clark and coworkers<sup>33</sup> have distinguished between four different classes of substituents, namely  $\pi$ -acceptor,  $\pi$ -donor,  $\sigma$ -acceptor and  $\sigma$ -donor substituents. This classification is based on possible 2-electron–2-orbital interactions involving substituent and cyclopropane MOs. Prerequisites for these interactions are comparable orbital energies for substituent and ring and a sufficiently large primary overlap between the orbitals involved. The latter requirement implies a large amplitude of the interacting cyclopropane orbital at C1, which is the location of the substituent X (compare with Scheme 3). This excludes all MOs of **1**, but those in Scheme 4, where degenerate MOs are characterized by symmetry notations they would obtain in (distorted)  $C_{2v}$ -symmetrical **I** (distortion along the  $C_2$  axis that passes through C1) and the MO ordering obtained with a large basis set (Figure 6) is used rather



SCHEME 4

TABLE 13. Distortion of the cyclopropane ring upon substitution at C1 by substituent X. Predictions by the molecular orbital (MO) and electron density (ED) model<sup>u,v,33,97</sup>

X	Conformation	Method/basis	C1C2		CX	Change of		MO model <sup>33</sup>			Prediction by			Reliability	
			vicinal	distal		C1C2	C2C3	MO model <sup>33</sup>			ED model <sup>97</sup>			MO	ED
							Type	C1C2	C2C3	Type	C1C2	C2C3	Type	C1C2	C2C3
Li		HF/6-31G(d) <sup>98</sup>	1.521	1.491		1	s	$\sigma$ -donor	1	s	$\sigma$ -repeller	1	s	yes	yes
		HF/4-31G <sup>33</sup>	1.533	1.500	1.963										
		HF/6-31G(d) <sup>98</sup>	1.522	1.484		1	s	$\sigma$ -donor	1	s	$\sigma$ -repeller	1	s	yes	yes
		HF/4-31G <sup>33</sup>	1.531	1.490	1.678										
BH <sub>2</sub>		HF/6-31G(d) <sup>98</sup>	1.527	1.473		1	s	$\pi$ -acceptor	1	s	$\pi$ -attractor	1	s	yes	yes
	bisected		1.503	1.499		1	s	$\sigma$ -donor	1	s	$\sigma$ -repeller	1	s	yes	yes
	perpend.		1.536	1.478	1.534										
	bisected		1.510	1.505	1.561										
CH <sub>2</sub> <sup>+</sup>		MP2/6-31G(d) <sup>111</sup>	1.645	1.414	1.356	1	s	$\pi$ -acceptor	1	s	$\pi$ -attractor	1	s	yes	yes
	bisected		1.647	1.415	1.351										
	bisected		1.524	1.530		s	1	$\pi$ -donor	1	1	$\pi$ -repeller	s	1	no	yes
	staggered		1.497	1.501		s	1	$\sigma$ -donor	1	s	$\sigma$ -repeller	1	s	no	no
CH <sub>2</sub>		HF/DZ <sup>96</sup>	1.524	1.530											
		HF/6-31G(d) <sup>98</sup>	1.497	1.501											
			1.503	1.506	1.510										
			1.503	1.501	1.519	1	s	$\sigma$ -donor	1	s	$\sigma$ -repeller	1	s	yes	yes
CH <sub>3</sub>		HF/4-31G <sup>33</sup>	1.503	1.506	1.510										
			1.514	1.514	1.513										
		MW <sup>116</sup>	1.509	1.509	1.517										
		ED <sup>17</sup>	1.525	1.505	1.435	1	s	$\pi$ -acceptor	1	s	$\pi$ -attractor	1	s	yes	yes
CN		HF/4-21G <sup>102</sup>	1.528	1.500											
		MW <sup>101</sup>	1.511	1.497	1.476	1	s	$\pi$ -acceptor	1	s	$\pi$ -attractor	1	s	yes	yes
		HF/6-31G(d) <sup>115</sup>	1.522	1.510	1.482	1	s	$\pi$ -acceptor	1	s	$\pi$ -attractor	1	s	yes	yes
		HF/4-21G <sup>102a</sup>	1.522	1.510	1.482	1	s	$\pi$ -donor	1	1	$\pi$ -attractor	1	1	yes	yes
COF		ED <sup>18</sup>	1.522	1.508	1.491	1	s	$\pi$ -acceptor	1	s	$\pi$ -attractor	1	s	yes	yes
			1.522	1.522	1.475										
		HF/6-31G(d) <sup>98</sup>	1.494	1.500		s	1	$\sigma$ -acceptor	s	1	$\sigma$ -attractor	s	1	yes	yes
CH <sub>2</sub> =CH															
NH <sub>2</sub>															



than that resulting from minimal basis set calculations (see Reference 33). However, this does not affect the discussion of substituent–ring interactions. The  $\pi$  MOs of substituent X and ring are classified as shown in Scheme 3<sup>33,96</sup>. The symmetry plane of a  $C_s$  symmetrical X-1 (plane I in Scheme 3) is the nodal plane for  $\pi$  MOs while  $\pi'$  MOs are lying in this plane and  $\pi''$  MOs are perpendicular to the ring plane (plane II in Scheme 3).

Depopulation or population of MOs #9, 11 and 16, but not the  $1a'_2$  MO 29, leads to opposing changes in vicinal and distal bond lengths. Accordingly, one can expect characteristic changes in the geometry of **1** upon substitution by a  $\pi/\sigma$ -acceptor/donor substituent (Table 14).

TABLE 14. Substituent effects on the geometry of cyclopropane as a function of interactions between substituent and cyclopropane MOs<sup>a,33</sup>

Substituent type	MO of cyclopropane involved	Change in vicinal bonds C1C2	Change in distal bond C2C3	Favoured substituent conformation
$\pi$ -Acceptor	$3e'-b_2$ ( $w_A$ ), #11 $\pi$ -type	longer	shorter	bisected
$\pi$ -Donor	$4e'-a_1$ ( $w_S^*$ ), #16 $\pi'$ -type	longer	shorter	perpendicular
$\sigma$ -Acceptor	$1e''-b_1$ ( $\pi_{CH}$ ), #9	shorter	longer	
$\sigma$ -Donor	$4e'-a_1$ ( $w_S^*$ ), #16	longer	shorter	

<sup>a</sup> Compare with Schemes 3 and 4. See also Figure 6.

The effect of  $\pi$ -acceptors, first treated by Hoffmann<sup>26</sup> and, independently, by Günther<sup>27</sup>, involves an interaction between HOMO  $3e'-b_2$  (#11, refined Walsh orbital  $w_A$ ), which is C1C2 bonding and C2C3 antibonding, with a vacant p or  $\pi^*$  orbital of substituent X and a subsequent depopulation of the C2C3 antibonding Walsh orbital  $w_A$  (Figure 6), thus leading to lengthening of the vicinal and shortening of the distal bond. This implies for substituents such as  $CH_2^+$  or  $BH_2$  a bisected rather than a perpendicular conformation in order to guarantee sufficient  $\pi$ ,  $\pi$  overlap.

$\pi$ -Donor substituents will transfer charge via an occupied  $\pi$  orbital into the  $1a'_2$  (MO #29,  $w_O^*$ ) orbital, but this will lead to lengthening of all CC bonds of **1**<sup>27</sup>. The interaction of a  $\pi'$ -donor MO of the substituent with the  $4e'-a_1$  MO (#16,  $w_S^*$ ) of **1** should be equally strong or even stronger because of the lower orbital energy of the latter. Charge transfer into  $4e'-a_1$  leads to lengthening of the vicinal bonds and shortening of the distal bond.

$\sigma$ -Acceptor substituents withdraw electron density from the  $1e''-b_1$  of **1** (MO #9). This results in lengthening of the distal and shortening of vicinal CC bonds, which is just opposite to the effects of  $\pi$ -acceptor substituents. Since the  $1e''-b_1$  MO is a  $\pi''$  MO with  $\pi_{CH}$  bonding character, the effect on the CC bonds can be considered to be indirect.

The  $4e'-a_1$  MO#16 of **1** can interact both with a  $\pi$ - and a  $\sigma$ -donor substituent. Hence,  $\sigma$ -donor substituents have the same effects as  $\pi$ -donor substituents, namely a lengthening of vicinal and a shortening of the distal CC bond of **1**.

## 2. The electron density description

Cremer and Kraka<sup>97</sup> based their model on a 'principal of avoidance<sup>97</sup> of geminal and vicinal charge concentrations', which they derived from the analysis of the Laplace concentration,  $-\nabla^2\rho(\mathbf{r})$ , in the valence shell of bonded atoms. As noted in Section IV. C, the Laplacian of  $\rho(\mathbf{r})$  reflects the shell structure of an atom. Upon bond formation, the 'valence



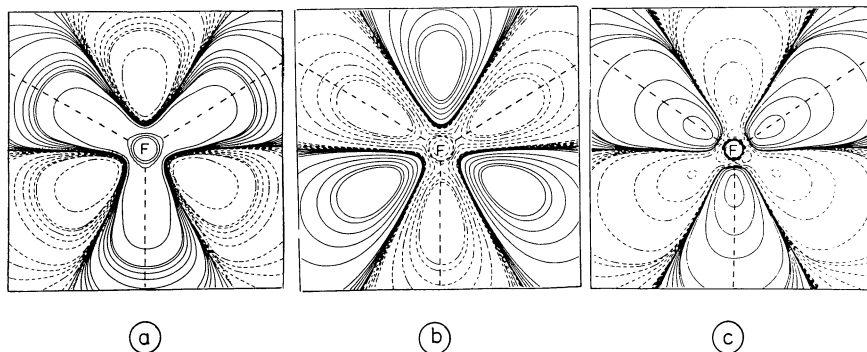


FIGURE 18. Concentration of electron density in the lone-pair regions of F in  $\text{CH}_3\text{F}$ . Contour-line diagrams have been drawn with regard to the plane that contains the F nucleus and is perpendicular to the CF bond axis. Positions of the methyl CH bonds are given by (heavy) dashed lines. (a) Energy density  $H(\mathbf{r})$ . (b) Electron density  $\rho(\mathbf{r})$ . (c) Laplace concentration  $-\nabla^2\rho(\mathbf{r})$ . In order to amplify effects, difference maps are used, i.e.  $H(\mathbf{r})$ ,  $\rho(\mathbf{r})$  and  $\nabla^2\rho(\mathbf{r})$  are plotted with regard to  $\text{CH}_3\text{F}$  with the methyl group rotated by  $60^\circ$  as reference. Dashed lines indicate areas with larger stabilizing energy density (lower electron density, larger concentration) and solid lines areas with lower stabilizing energy density (larger electron density, smaller charge concentration). (HF/6-31 G(d) calculations from Reference 97.) Reprinted with permission from D. Cremer and E. Kraka, *J. Am. Chem. Soc.*, **107**, 3811 (1985). Copyright (1985) American Chemical Society

shell' is distorted in the way that maxima (lumps) appear in the direction of the bonds with adjacent atoms. Since all changes in the Laplacian of  $\rho(\mathbf{r})$  have to cancel within the boundaries of an atom (no matter whether isolated or bonded), the formation of concentration lumps implies the formation of concentration minima (holes) of  $-\nabla^2\rho(\mathbf{r})$  in other regions of the valence sphere. Cremer and Kraka observed that the pattern of lumps and holes in the valence sphere of bonded atoms shows some regularities that are best described as the result of an avoidance of geminal and vicinal concentration lumps. For example, the electron concentration of an F atom of  $\text{F}_2$  will be cylindrical if viewed along the bond axis. However, if one F atom is replaced by a methyl group as in  $\text{CH}_3\text{F}$ , then the Laplace concentration  $-\nabla^2\rho(\mathbf{r})$  will become larger (smaller) in the regions that are staggered (eclipsed) with regard to the CH bonds. There is a preference for staggering of non-bonded charge concentrations (see Figure 18), which has also been founded for other molecules<sup>97</sup>.

Substituents distort the pattern of concentration lumps and holes in the valence shell of an atom by either pulling bonded ( $\sigma$ -) or non-bonded ( $\pi$ -) lumps in the direction of the substituent ( $\sigma/\pi$ -attractors) or pushing them closer to the atom in question ( $\sigma/\pi$ -repellers). Accordingly, the substituents of **1** can be classified by their  $\sigma$ -attractor,  $\sigma$ -repeller,  $\pi$ -attractor or  $\pi$ -repeller ability. Typical distortions caused by these substituents in the valence shell of the three C atoms are shown in Figure 19.

$\sigma$ -Attractors (Figure 19a) distort the valence sphere of the adjacent C1 atom by extending it on the frontside and compressing it on the backside. The C1 nucleus is better shielded in the direction of C2 and C3 and, as a consequence, the vicinal bonds become shorter, which, in turn, leads to a lengthening of the distal bond.  $\sigma$ -Repellers have the reverse effect (Figure 19b). Holes or charge concentrations in the  $\pi$ -region of a  $\pi$ -attractor/repeller substituent draw charge concentration at the C1 atom out of or into the direction of the vicinal bonds, which results in bond lengthening (Figure 19c) or bond shortening (Figure 19d). On this basis, the substituent effects summarized in Table 15 can be predicted (Figure 19).

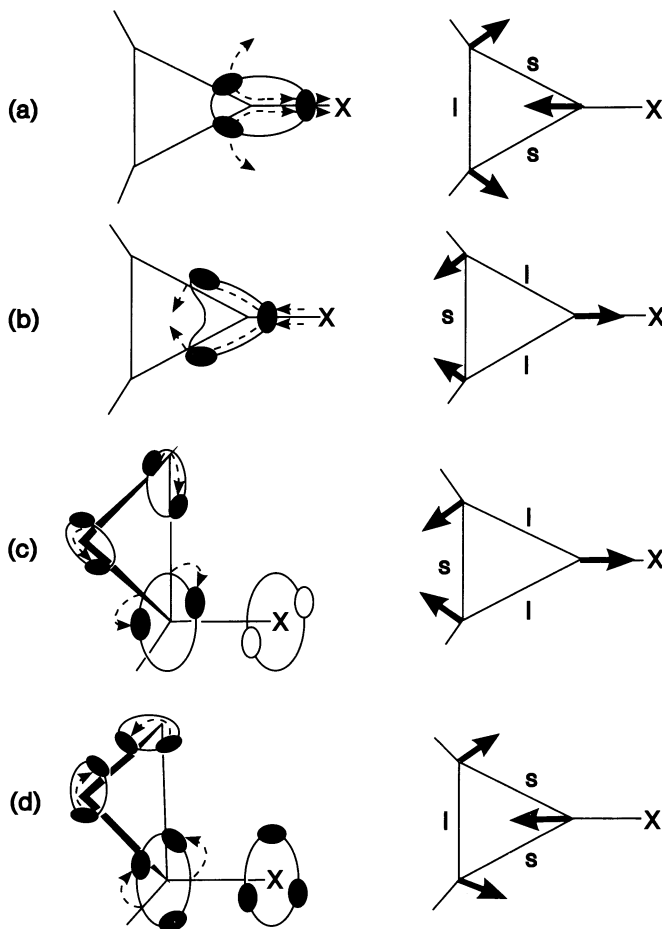


FIGURE 19. Schematic representation of distortions of the valence sphere of three-membered ring atoms upon C1 substitution by a substituent X with (a)  $\sigma$ -attractor, (b)  $\sigma$ -repeller, (c)  $\pi$ -attractor and (d)  $\pi$ -repeller ability. Distorted valence spheres are indicated by (large) ellipses or circles. Small ellipses depict locations in the valence sphere or the bond region with charge compression (solid) or charge expansion (open). Dashed arrows indicate the direction of distortions of the valence spheres. The nuclei of the three-membered ring move into the areas with charge compression as indicated by the heavy arrows in the diagrams on the right side. The corresponding bond length changes are denoted by s (short) and l (long). Reprinted with permission from D. Cremer and E. Kraka, *J. Am. Chem. Soc.*, **107**, 3811 (1985). Copyright (1985) American Chemical Society

In Table 13, calculated and measured geometry data of substituted cyclopropanes are compared with predictions of the MO model of Clark and coworkers (Table 14)<sup>33</sup> and those of the electron density model by Cremer and Kraka (Table 15)<sup>97</sup>. From the comparison, it becomes clear that both models lead to similar predictions, but differ with regard to some

TABLE 15. Substituent effects on the geometry of cyclopropane according to the electron density (ED) model of Cremer and Kraka<sup>a,97</sup>

Type of substituent	Change in vicinal bonds C1C2 and C1C3	Change in distal bond C2C3
$\sigma$ -Attractor	shorter	longer
$\sigma$ -Repeller	longer	shorter
$\pi$ -Attractor		
bisected	longer	shorter
perpendicular	(longer)	(shorter)
$\pi$ -Repeller	shorter	longer

<sup>a</sup> Compare with Figure 19.

important details. It seems that the MO model cannot be applied in some cases without additional assumptions (see next Section).

### 3. Substituted cyclopropanes

*Cyclopropyl carbanyl cation*<sup>111</sup>. The most dramatic example for a  $\pi$ -acceptor/ $\pi$ -attractor substituent effect is provided by the cyclopropyl carbanyl cation. In its bisected conformation, the vicinal CC bonds are considerably longer (1.65 Å) and the distal CC bond considerably shorter (1.41 Å) than the bonds in **1** (Table 13). The CH<sub>2</sub><sup>+</sup> group stabilizes **1** considerably more in the bisected form than in the perpendicular form (13 kcal mol<sup>-1</sup>). Since the CC<sup>+</sup> bond possesses partial double bond character, it is shorter (1.35–1.36 Å, Table 13) than a normal CC<sup>+</sup> bond (1.51 Å).

*Cyclopropylborane*<sup>33,98</sup>. A strong  $\pi$ -acceptor ( $\pi$ -attractor) effect is also found for the BH<sub>2</sub> substituent that, according to HF calculations, prefers by 7 kcal mol<sup>-1</sup> the bisected over the perpendicular conformation (Table 16, NMR measurements suggest a similar energy difference<sup>119</sup>). In the former conformation, the vicinal bonds are elongated to 1.53 Å while the distal bond is shortened to 1.47 Å (Table 13). Compared to the CH<sub>2</sub><sup>+</sup> group, substituent–ring interactions are weaker because of a longer C1–X distance (smaller overlap) and a larger energy difference between donor and acceptor orbital. In the perpendicular conformation, the  $\pi$ -acceptor effect is turned off thus leading to changes in the geometry of **1** that identify BH<sub>2</sub> as a  $\sigma$ -donor ( $\sigma$ -repeller) substituent.

*Cyanocyclopropane*<sup>97, 101, 102</sup> and *isocyanocyclopropane*<sup>114, 122</sup>. According to Skancke and Boggs<sup>102a</sup>, the CN group is a  $\pi$ -acceptor that leads to lengthening of vicinal and shortening of distal CC bond. A similar effect could also be expected for the isocyano group, and CC bond lengths (lengthening of vicinal, shortening of distal bond) in accordance with this have been measured spectroscopically<sup>122</sup>. On the other hand, HF/6-31G(d) calculations by Reynders and Schrupf<sup>114</sup> suggest the reverse CC bond length pattern for isocyanocyclopropane. Calculation of Davidson–Roby populations<sup>144</sup> indicates a  $\sigma$ -acceptor nature of the NC substituent in agreement with calculated ring bond lengths. In view of the difficulties of getting multiple bonds correctly described<sup>135</sup>, further calculations have to clarify the true nature of the isocyano substituent.

*Nitrocyclopropane*. Skancke<sup>113</sup> reported that in the bisected conformer of nitrocyclopropane, the vicinal bonds are longer and the distal bond is shorter than the CC bonds of **1**. This is a result of charge transfer from the  $w_A$  orbital of **1** to the empty  $p\pi$  orbital of the nitro group. Rotation of the nitro group leads to an energy increase by 3.2–4.7 kcal mol<sup>-1</sup><sup>145,146</sup>. At the same time, the vicinal bond lengths are decreased while the distal bond length is increased. Skancke explained these changes by interactions between the symmet-

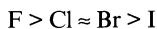
TABLE 16. Energy differences  $\Delta E$  (kcal mol<sup>-1</sup>) between the different rotamers of mono-substituted cyclopropanes calculated at the Hartree-Fock level with various basis sets

Substituent	Conformation <sup>a</sup>	Basis set	$\Delta E$	Reference
BH <sub>2</sub>	bisected	6-31G(d,p)	0.0	98 (see also 33)
	perpendicular		7.2	
CH <sub>3</sub>	staggered	6-31G(d,p)	0.0	98
	eclipsed		2.9	
NH <sub>2</sub>	180°	6-31G(d,p)	0.0	98
	43°		2.6	
	0°		3.0	
	106°		4.9	
OH	72°	6-31G(d,p)	0.0	98
	180°		2.5	
	163°		2.5	
	0°		2.7	
SiH <sub>3</sub>	staggered	6-31G(d,p)	0.0	98
	eclipsed		1.7	
GeH <sub>3</sub>	staggered	3-21G(d)	0.0	123
	eclipsed		1.4	
PH <sub>2</sub>	180°	6-31G(d,p)	0.0	98
	48°		1.5	
	0°		2.7	
	108°		3.6	
SH	75°	6-31G(d,p)	0.0	98
	180°		2.8	
	156°		2.8	
	0°		3.6	
NO <sub>2</sub>	staggered	4-21G	0.0	113
	eclipsed		6.6	
CH <sub>2</sub> SH	<i>gauche</i>	3-21G(d)	0.0	148
	<i>anti</i>		3.3	
COF	0°	6-31G(d)	0.0	115
	90°		6.1	
	180°		0.1	
	270°		6.0	

<sup>a</sup> H—C—X—H torsional angles for OH and SH are given. For NH<sub>2</sub> or PH<sub>2</sub>, H—C—X—lp torsional angles are given, where lp is the lone pair, which is assumed to be *anti* to the bisector N(HH) and P(HH). For CH<sub>2</sub>SH and COF, the conformation is determined by the torsion angles H—S—C—C and H—C—C—F, respectively.

ric Walsh MO  $w_5$  and the empty  $p\pi$  orbital of the nitro group. However, this interpretation does not consider the fact that the amplitude of  $w_5$  is rather low at C1 and therefore overlap between the interacting orbitals is relatively small. It is more reasonable to consider the NO<sub>2</sub> group in the perpendicular conformation as a  $\sigma$ -acceptor or  $\sigma$ -attractor that leads to the observed changes in the CC bonds by interaction with the  $1e''-b_1$  MO #9 of **1**.

*Halocyclopropanes*<sup>33, 96-98, 112</sup>. According to Clark and coworkers,<sup>33</sup> F acts predominantly as  $\sigma$ -acceptor. If  $\pi$ -donor ability is invoked for F, then controversial geometry effects are predicted by the MO model. Predictions by the electron density model of Cremer and Kraka<sup>97</sup> are consistent, no matter whether  $\sigma$ -attractor or  $\pi$ -repeller ability of F is considered (Table 13). The other halogens are also  $\sigma$ -attractors/ $\pi$ -repellers but their effects on the geometry of **1** decrease in the order



Substitution by two F atoms<sup>97, 105, 131</sup> at C1 reduces vicinal bond lengths by 0.02 Å (1.465 Å, HF/4-31G) and increases the distal bond length by 0.04 Å (1.532 Å), thus indicating additivity for the two F effects.

*Cyclopropanol and cyclopropanethiol*<sup>33, 97, 98</sup>. Calculated geometry changes of **1** upon substitution by an OH or SH group (*anti* conformation) can only be explained by the MO model by assuming  $\sigma$ -acceptor character for the substituent. Again, the electron density model leads to prediction of the correct geometry changes, no matter whether a  $\sigma$ -attractor or  $\pi$ -repeller nature of the OH (SH) substituent is assumed. In the most stable conformation, OH and SH groups are in a *gauche* position (dihedral angle 72° and 75°, respectively; Table 16). The rotational barriers will be 2.7 kcal mol<sup>-1</sup> (OH) and 3.6 kcal mol<sup>-1</sup> (SH group) if rotation proceeds via the *syn* form, but 2.5 and 2.8 kcal mol<sup>-1</sup>, respectively, if rotation proceeds via the *anti* form.

*Cyclopropylamine*<sup>33, 98, 106</sup> and *cyclopropylphosphine*<sup>98</sup>. The NH<sub>2</sub> and PH<sub>2</sub> groups both prefer an *anti* conformation. Calculated changes in vicinal and distal bond length can only be explained on the basis of the MO model of Clark and coworkers<sup>33</sup> if one assumes a dominant  $\sigma$ -acceptor nature for NH<sub>2</sub> and  $\sigma$ -donor nature for PH<sub>2</sub>. Again, the electron density model does also allow  $\pi$ -repeller ability for the NH<sub>2</sub> group. The calculated rotational barriers of NH<sub>2</sub> and PH<sub>2</sub> are 4.9 and 3.6 kcal mol<sup>-1</sup> (Table 16)<sup>98</sup>.

*Methyl*-,<sup>33, 97, 98</sup> *silyl*-,<sup>98, 119</sup> and *germylcyclopropane*<sup>123</sup>. Although changes in the geometry of **1** caused by a methyl group are small, they represent a critical test for the applicability of MO<sup>33</sup> and the ED model<sup>97</sup>. Changes obtained for the staggered conformation of the methyl group suggest  $\sigma$ -acceptor ability for the substituent. However, this prediction is in conflict with the known large electronegativity of the C atoms in the three-membered ring, which forces a methyl group to act as a  $\sigma$ -donor rather than a  $\sigma$ -acceptor. Hyperconjugative interactions between substituent and ring could also lead to a  $\pi$ -donor/acceptor character of the methyl group. However, none of these possibilities leads to the observed pattern of vicinal and distal bond length changes (see Table 13). The electron density model suggests both  $\sigma$ -repeller and  $\pi$ -repeller character for methyl with a preponderance of the latter. In the eclipsed conformation, the  $\sigma$ -repeller ( $\sigma$ -donor) nature of the substituent prevails.

The silyl and germyl groups are  $\sigma$ -donors and  $\pi$ -acceptors<sup>123</sup>. Calculated CC distances in silyl-<sup>98, 119</sup> and germyl cyclopropane<sup>123</sup> suggest that the  $\pi$ -acceptor character is significantly more pronounced for a silyl than a germyl substituent.

*Vinylcyclopropane*<sup>102a</sup>. The vinyl group can act both as  $\pi$ -donor and  $\pi$ -acceptor. This is indicated by lengthening of all ring bonds, where the vicinal bonds become longer than the distal bond. The same bond length pattern is obtained by considering the  $\pi$ -attractor propensity of the vinyl group on the basis of the electron density model<sup>97</sup>.

*Lithiocyclopropane*<sup>33, 98</sup>. Lithium is a  $\sigma$ -donor according to the MO interpretation<sup>33</sup> and a  $\sigma$ -repeller according to the electron density description<sup>97</sup>. Both models predict a lengthening of the vicinal and a shortening of the distal CC bond, which is confirmed by *ab initio* calculations (Table 13).

*Cyclopropylmethylene anion and cyclopropyl oxide anion*<sup>96</sup>. Clearly, CH<sub>2</sub><sup>-</sup> (in its bisected conformation) and O<sup>-</sup> are  $\pi$ -donor substituents that would lead to a lengthening of all ring bonds ( $\pi$ -donor effect) with the vicinal bonds becoming longer than the distal bond ( $\pi$ -donor effect, see Scheme 3) according to the MO model. However, the reverse geometry effect (vicinal CC bonds shorter than distal CC bond) is calculated. This geometry change is correctly predicted by the electron density model of Cremer and Kraka<sup>97</sup> on the basis of the  $\pi$ -repeller nature of CH<sub>2</sub><sup>-</sup> and O<sup>-</sup>. In the latter case, the resulting geometry effect is enhanced by the  $\sigma$ -attractor nature of the substituent.

*Summary*. The electron density model of substituent–ring interactions functions better than the MO model, which is not surprising since the electron density covers all MO effects while any MO model will simplify orbital interactions by selecting just a few important

ones. This, of course, leads to incorrect descriptions in cases where many orbital interactions contribute to observed properties.

With the aid of virial partitioning of the electron density it has been shown that the cyclopropyl group is more electronegative than the 2-propyl group<sup>97</sup>. This is in line with hybridization models and the analysis of isodesmic reactions. Clark and coworkers<sup>33</sup> characterize the cyclopropyl group in the following way:

$\sigma$ -acceptor ability: methyl > cyclopropyl > 2-propyl  
 $\sigma$ -donor ability: methyl > 2-propyl > cyclopropyl

If the cyclopropyl group is compared with a 2-propyl group, then electropositive substituents ( $\sigma$ -donor substituents such as Li) stabilize the ring while strongly electronegative groups such as F, OH, etc. destabilize the ring.

Cyclopropyl is a fairly strong  $\pi$ -donor and therefore it is stabilized by  $\pi$ -acceptor substituents, which implies that the interacting  $\pi$  orbitals overlap sufficiently. Cyclopropyl can also act as a  $\pi'$ -acceptor provided it interacts with a strong donor that possesses high-lying occupied  $\pi'$ -donor orbitals (Scheme 3). In exceptional cases such as X = CH<sub>2</sub><sup>-</sup>, cyclopropyl turns out as a  $\pi$ -acceptor that accepts charge in its  $1a_2'$  MO.

### C. Rationalization of the Geometry of Three-membered Rings

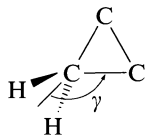
The analysis of the geometry and electronic structure of the cyclopropyl group has led to a better understanding of three-membered ring geometries in general. Several comparisons of the geometry of **1** with that of heterocyclopropanes have been made utilizing *ab initio* and experimental data<sup>6,9,27,32,43,47,71,76,94,124,125,130,147-153</sup>. It turns out that there are some simple trends in the geometry of three-membered rings as shown in Table 17<sup>9,32,147</sup>.

TABLE 17. Effect of a hetero atom on the geometry of cyclopropane. Transition from a three-membered ring to a  $\pi$ -complex<sup>a</sup>

Parameter	Basal group H <sub>2</sub> C=CH <sub>2</sub> + Apex group X			
X =	BH <sup>151</sup>	CH <sub>2</sub> <sup>97</sup>	NH <sup>97</sup>	O <sup>97</sup>
CC	1.544	1.498	1.470	1.453
XC	1.534	1.498	1.449	1.401
$\gamma$	145.5	150	162.5	158.5
X =	AlH <sup>149</sup>	SiH <sub>2</sub> <sup>124</sup>	PH <sup>124</sup>	S <sup>124</sup>
CC	1.600	1.553	1.492	1.473
XC	1.904	1.855	1.853	1.811
$\gamma$	135.2	141.2	148.3	151.6
X =	NH <sub>2</sub> <sup>+97</sup>	OH <sup>+97</sup>	F <sup>+97</sup>	H <sup>+97</sup>
CC	1.488	1.446	1.445	1.371
XC	1.460	1.498	1.533	1.306
$\gamma$	160.0	165.5	171.3	178.3

<sup>a</sup> Distances in Å, CC(HH) angle  $\gamma$  in deg. HF/6-31 G(d) or HF/DZ + P calculations as given in References 97, 124, 149 and 151.

With increasing electronegativity of group (atom) X, both the CC and the CX bond length decrease and the (HH)CC angle  $\gamma$  increases until it becomes finally close to 180°. Changes in the CX bond lengths just reflect the decrease in the covalent radius of the heavy

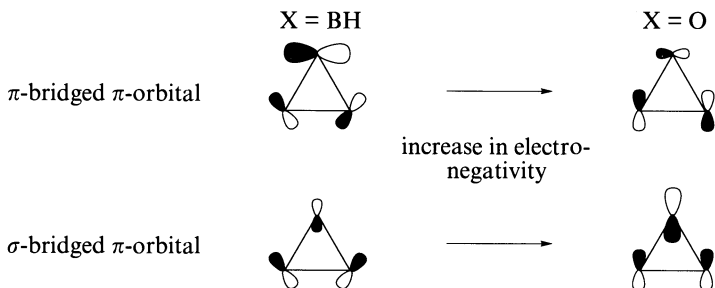


atom of X as this becomes more electronegative. With increasing electronegativity of X, there is a transition from three-membered rings to  $\pi$ -complexes that leads to a gradual conversion of the basal  $\text{CH}_2\text{CH}_2$  group of the ring into an ethene fragment only loosely bound to the apex group X. This transition has been made visible and rationalized by electron density studies<sup>9, 13</sup> (see Section IV. D, Figures 14 and 15) and orbital considerations<sup>13, 32, 43, 71</sup> (Figure 16 in Section IV. D). Hence for X = BH,  $\text{CH}_2$ , NH and O, the increase in electronegativity reduces back donation via a  $b_2$ -symmetrical orbital of X to the  $\pi^*$  MO of the ethene unit. Since  $\pi$ -back donation is primarily responsible for distortions of the ethene unit (CC bond lengthening; pyramidalization of the  $\text{CH}_2$  groups and deviation from planarity), a reduction in  $\pi$ -back donation has the CC bond length and the (HH)CC angle approaching the values of ethene.

Similar trends can also be observed for X =  $\text{AlH}^+$ <sup>149</sup>,  $\text{SiH}_2$ <sup>32b, 47, 124</sup>,  $\text{PH}^+$ <sup>47, 124</sup> and  $\text{S}^+$ <sup>47, 124</sup> where, however, CC bond shortening and the increase in  $\gamma$  are somewhat smaller because of the decrease in electronegativity when going up in the columns of the periodic table.

Since  $\pi$ -back donation requires CX bonding overlap in the  $\pi$ -bridged  $\pi$ -orbital (MO #11,  $w_A$ , Figure 6) of the three-membered ring and since this will be reduced with increasing electronegativity of X, one should expect that a decrease in back donation might lead to a weakening of bonds CX and, hence, to a weakening of the stability of the three-membered ring (see Scheme 5). Accordingly, one could expect that heterocyclopropanes of the second row will be more stable than their analogues from the first row of the periodic table. Allen<sup>32</sup> has pointed out that this is not the case because three-membered ring bonding is also supported by CX bonding overlap in the  $\sigma$ -bridged  $\pi$ -orbital. This orbital, however, becomes more bonding in the way the  $\text{CH}_2\text{CH}_2$  unit approaches ethene. Accordingly, the  $\sigma$ -bridged  $\pi$ -orbital can partially compensate a loss in bonding overlap and retain the stability of three-membered rings, such as aziridine or oxirane similar to that of **1**<sup>32</sup>. The  $\sigma$ -bridged  $\pi$ -orbital is also responsible for transferring electron density into the surface of the ring and adding in this way to surface delocalization, which is a stabilizing factor of the three-membered ring<sup>9, 13, 32, 71</sup>.

The situation changes, however, if the electronegativity of the group X increases drastically as in the series X =  $\text{NH}_2^+$ ,  $\text{OH}^+$ ,  $\text{F}^+$ <sup>9</sup>.  $\pi$ -Back donation is stepwise decreased to zero and  $\pi$ -complexes are formed. This has been demonstrated via the electron density analysis, which reveals that convex bent bonds change into concave (inwardly curved) bent



SCHEME 5

bonds ( $X = OH^+$ ) and, finally, collapse to one bond path that connects  $X$  and the midpoint of the  $CH_2CH_2$  unit, thus yielding the T structure of a  $\pi$ -complex<sup>9</sup>. In these cases, interactions between  $X$  and  $CH_2CH_2$  become so weak that the  $CX$  distance increases rather than decreases with the electronegativity of the heavy atom of  $X$ .

The  $\sigma$ -donation  $\pi$ -back donation model has been used to explain bonding in a large variety of three-membered rings with different apex group  $X$  (atoms from the first, second and third rows in the periodic table) and different basal groups ( $H_2CCH_2$ ,  $BHBH$ ,  $OO$ ,  $HCCH$ ,  $NN$ ,  $H_2SiSiH_2$ ,  $H_2GeGeH_2$ , etc.)<sup>9, 32, 43, 47, 71, 94, 124, 148-152</sup>.

## VII. VIBRATIONAL SPECTRA

High-resolution infrared spectra<sup>154, 155</sup>, reliable experimentally based force fields and a detailed normal coordinate analysis<sup>156, 157</sup> have been available for **1** for a relatively long time. The high symmetry ( $D_{3h}$ ) of **1** facilitates an analysis of its 14 fundamental vibrations (derived from 21 non-redundant coordinates), which transform as three  $a_1'$ , one  $a_2'$ , one  $a_1''$ , two  $a_2''$ , four  $e'$  and three  $e''$  and which can be described by using symmetry coordinates such as bond stretching,  $CH_2$  angle deformation,  $CH_2$  wagging,  $CH_2$  rocking or  $CH_2$  twisting motion (see Table 18 and Figure 20).

*Ab initio* investigations of the vibrational spectra of **1**<sup>129, 130, 158, 159</sup> have been exclusively based on the harmonic approximation, and therefore they were primarily concerned to find

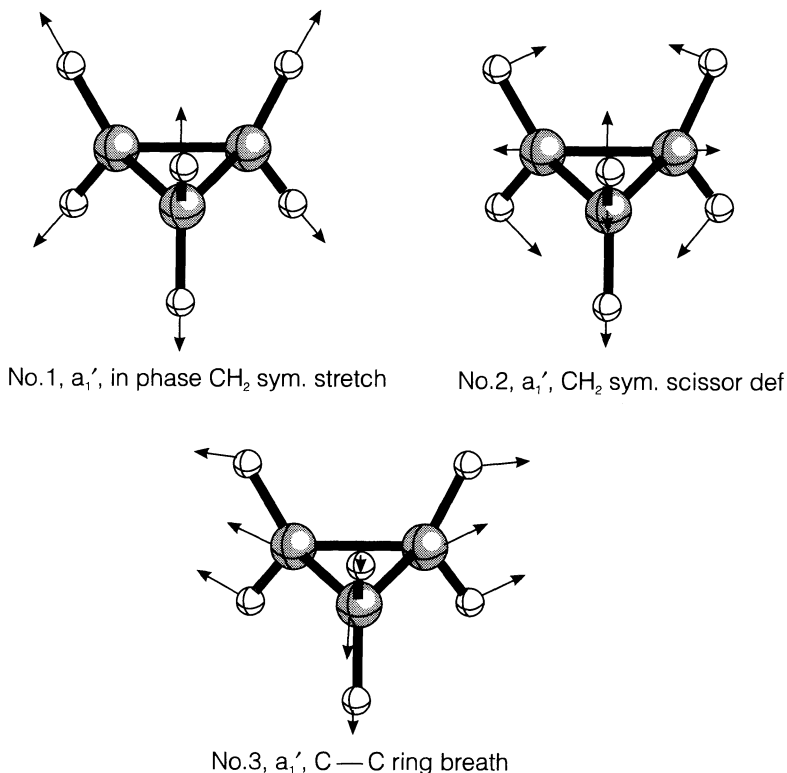
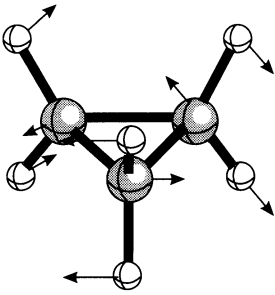
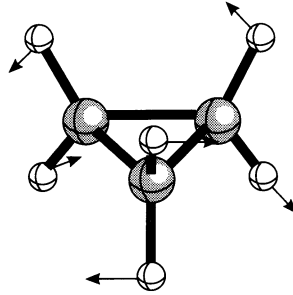


FIGURE 20. (Caption on page 100)

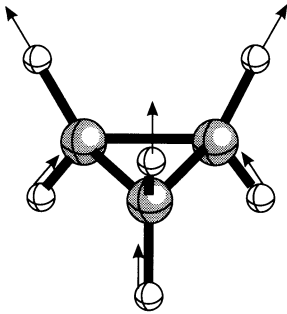




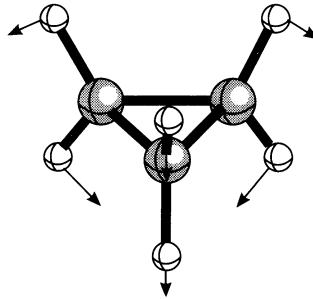
No. 4,  $a_2'$ ,  $\text{CH}_2$  wag



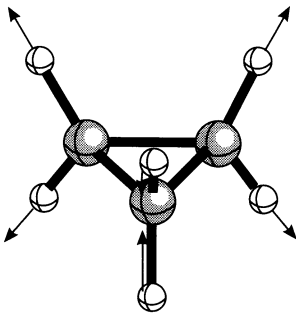
No. 5,  $a_1''$ ,  $\text{CH}_2$  twist



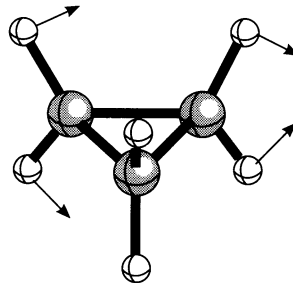
No. 6,  $a_2''$ , in phase  $\text{CH}_2$  asym. stretch



No. 7,  $a_2''$ ,  $\text{CH}_2$  rock



No. 8,  $e'$ , out of phase  $\text{CH}_2$  sym. stretch



No. 9,  $e'$ ,  $\text{CH}_2$  asym scissor def

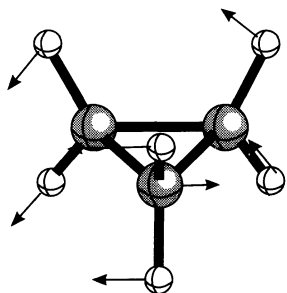
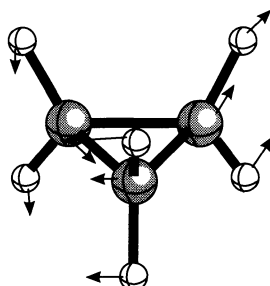
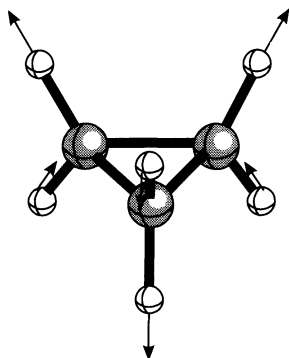
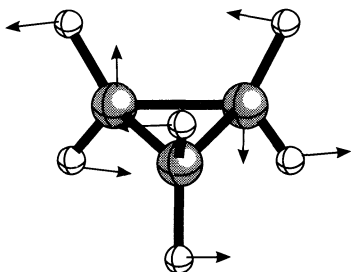
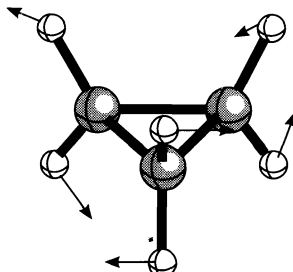
No. 10,  $e'$ ,  $\text{CH}_2$  wagNo. 11,  $e'$ , C—C ring defNo. 12,  $e''$ , out of phase  $\text{CH}_2$  asym. stretchNo. 13,  $e''$ ,  $\text{CH}_2$  rock +  $\text{CH}_2$  twistNo. 14,  $e''$ ,  $\text{CH}_2$  twist +  $\text{CH}_2$  rock

FIGURE 20. Vibrational modes of cyclopropane as obtained at the HF/6-31G(d,p) level of theory. Arrows indicate the direction and amplitude of each atomic motion. Symmetry assignments and a characterization of each mode is also given in line with the notations used in Table 18

TABLE 18. Comparison of observed fundamental vibrational frequencies ( $\nu_j$ ) and calculated harmonic frequencies ( $\omega_j$ ) (in  $\text{cm}^{-1}$ ) for cyclopropane

#	Sym	Characterization	Exp. <sup>a</sup>		<i>Ab initio</i>					
			HF/DZ <sup>b</sup>		HF/6-31 G(d) <sup>c</sup>		HF/TZ + 2P <sup>d</sup>		MP2/DZ + P <sup>e</sup>	
			unscaled	scaled	unscaled	scaled	unscaled	scaled	unscaled	scaled
1	$a_1'$	in-phase CH <sub>2</sub> symmetric stretch	3038	3340	3300	3130	3219	3239	3077	
2		CH <sub>2</sub> scissoring deformation	1479	1660	1667	1570	1657	1575	1496	
3		C—C ring breathing	1188	1288	1299	1238	1269	1244	1182	
4	$a_2'$	CH <sub>2</sub> wag	1070	1266	1220	1158	1212	1098	1043	
5	$a_1''$	CH <sub>2</sub> twist	1126	1260	1261	1197	1256	1188	1129	
6	$a_2''$	in-phase CH <sub>2</sub> asymmetric stretch	3102	3438	3385	3211	3377	3352	3184	
7		CH <sub>2</sub> rock	854	930	920	873	917	890	846	
8	$e'$	out-of-phase CH <sub>2</sub> symmetric stretch	3024	3320	3286	3117	3278	3229	3067	
9		CH <sub>2</sub> scissoring deformation	1438	1618	1602	1515	1599	1515	1439	
10		CH <sub>2</sub> wag	1028	1204	1187	1113	1171	1098	1043	
11		C—C ring deformation	868	931	959	911	931	918	872	
12	$e''$	out-of-phase CH <sub>2</sub> asymmetric stretch	3082	3416	3363	3189	3082	3335	3168	
13		CH <sub>2</sub> rock + CH <sub>2</sub> twist	1188	1328	1323	1271	1320	1239	1177	
14		CH <sub>2</sub> twist + CH <sub>2</sub> rock	739	832	802	744	739	773	734	

<sup>a</sup> From Reference 157.<sup>b</sup> From Reference 129, calculated with a (9s5p/4s) [4s2p/2s] basis set.<sup>c</sup> From Reference 158. In this work, frequencies were calculated by numerical differences, which leads to small inaccuracies.

Values have been corrected by using analytical second derivatives. Scaled values were obtained by scaling the diagonal force constants.

<sup>d</sup> From Reference 132, calculated with a (9s5p2d/4s2p) [4s2p2d/4s2p] basis set.<sup>e</sup> From Reference 130, calculated with a (9s5p1d/4s1p) [4s2p1d/2s1p] basis set. The calculated frequencies were scaled by 0.95 in this work.

out about the differences between calculated and experimental vibrational frequencies (force constants). Force constants and vibrational frequencies of **1** have been calculated at the HF<sup>129, 130, 158, 159</sup> and MP2<sup>130</sup> level of theory using minimal (STO-3G)<sup>158</sup>, DZ<sup>129, 158</sup>, DZ + P<sup>130, 158</sup> and TZ + 2P basis sets<sup>159</sup>. HF/STO-3G frequencies are too large by 20–30%<sup>158</sup>, HF/DZ frequencies by 10–20%<sup>129</sup> while inclusion of polarization functions into a split valence or DZ basis set reduces the deviation to 10–15%<sup>158</sup>. The MP2/DZ + P frequencies agree with the measured ones within 5–10%<sup>130</sup>. The largest discrepancies between calculated harmonic ( $\omega_i$ ) and experimentally observed frequencies ( $\nu_i$ ) are found for the stretching motions, for which anharmonic effects are considerable.

These discrepancies result (a) from the harmonic approximation used in all calculations [ $\omega_i$  (theory) >  $\nu_i$  (exp)], (b) the known deficiencies of minimal and DZ basis sets to describe three-membered rings [polarization functions are needed to describe small CCC bond angles:  $\omega_i(\text{DZ} + \text{P}) > \omega_i(\text{DZ}) > \omega_i(\text{minimal basis})$ ] and (c) the need of electron correlated wave functions to correctly describe the curvature of the potential energy surface at a minimum energy point [ $\omega_i(\text{SCF}) > \omega_i(\text{MP2})$ ]. Because of these relationships, one can expect that

$$\omega_i(\text{SCF}) > \omega_i(\text{MP2}) > \nu_i(\text{exp})$$

holds at least for the stretching frequencies, but in the case of **1** this is also true for all other frequencies (Table 18)<sup>130</sup>. By appropriate scaling of calculated frequencies for force constants [scaling factors<sup>160</sup>: 0.87 (HF) to 0.93 (MP2); the best scaling factor for the MP2 frequencies of Table 18 is 0.95], predicted frequencies of **1** are within 1–3% of experimental values (Table 18)<sup>158</sup>.

For CH stretching modes and CH<sub>2</sub> deformation modes, all calculations lead to the ordering of frequencies observed experimentally (Table 18). The correct assignment of vibrational frequencies in the mid-frequency region (1100–1300 cm<sup>-1</sup>) is ring stretch ( $\nu_3$ , 1188 cm<sup>-1</sup>), CH<sub>2</sub> twist ( $\nu_5$ , 1126 cm<sup>-1</sup>) and CH<sub>2</sub> wag ( $\nu_4$ , 1070 cm<sup>-1</sup>), which is correctly reproduced by using polarization functions but not by DZ basis sets, thus underlining the necessity of augmented basis sets.

Recently, attempts have been made to attain electronic structure information on **1** by analysing its normal modes in terms of 'internal modes' that are largely localized in molecular fragments which, in turn, can be characterized by a single internal parameter such as a bond length (diatomic fragments), bond angles (triatomic fragment) or dihedral angles (tetraatomic fragments)<sup>161–163</sup>. In this way, each 'internal mode' corresponds to an internal geometry parameter, which can be used for the normal-mode analysis. Normally, the description of molecular vibrations is carried out in terms of normal coordinates, which are in most cases linear combinations of several internal parameters. This has to do with the fact that vibrational motions described by normal coordinates are symmetry-adapted, i.e. each normal mode of the molecule transforms as one of the irreducible representations of the molecular point group<sup>164</sup>. Accordingly, a specific internal coordinate will contribute to several normal modes and each normal mode is delocalized in a similar way as canonical MOs are delocalized.

Boatz and Gordon<sup>161</sup> and, recently, Konkoli, Larsson and Cremer<sup>162, 163</sup> have worked out methods for assigning vibrational frequencies to individual internal coordinate motions. These procedures can be considered in many ways as being similar to the calculation of localized MOs from canonical SCF MOs. They yield, in the case of the Boatz–Gordon method, 'intrinsic frequencies'<sup>161</sup>, which in their nature are averaged frequencies without an associated mode and which have the disadvantage of depending on a careful construction of the molecular geometry from non-redundant and (in case of symmetry) redundant internal coordinates. The method by Konkoli and coworkers leads to 'adiabatic motions' and 'adiabatic frequencies' that do not depend on redundant parameters<sup>162, 163</sup>.

Analysis of the vibrational normal modes obtained at the HF/6-31G(d,p) level of theory in terms of adiabatic modes provides the basis for a quantitative dissection of the

TABLE 19. Analysis of the normal modes of cyclopropane using, as 'internal parameter' modes, adiabatic modes from Reference 163<sup>a</sup>

#	Sym	Freq.	Characterization	Number of internal parameters
1	$a_1'$	3300	CH stretch (96%)	CH: (6 × 16%)
2		1667	CH <sub>2</sub> scissoring def (81%) + CC stretch (18%)	CH <sub>2</sub> : (3 × 27%) + CC (3 × 6%)
3		1299	CC stretch (90%)	CC stretch: (3 × 30%)
4	$a_2'$	1220	CH <sub>2</sub> wag (99%)	CH <sub>2</sub> wag (3 × 33%)
5	$a_1''$	1261	CH <sub>2</sub> twist (99%)	CH <sub>2</sub> twist (3 × 33%)
6	$a_2''$	3385	CH <sub>2</sub> stretch (100%)	CH stretch (6 × 16.7%)
7		920	CH <sub>2</sub> rock (99%)	CH <sub>2</sub> rock (3 × 33%)
8	$e'$	3286	CH stretch (100%)	CH stretch (4 × 25%)
		3286	CH stretch (66%)	CH stretch (2 × 33%)
9		1602	CH <sub>2</sub> def (98%)	CH <sub>2</sub> def (66% + 17% + 16%)
		1602	CH <sub>2</sub> def (98%)	CH <sub>2</sub> def (2 × 49%)
10		1187	CH <sub>2</sub> wag (86%) + CC stretch (9%)	CH <sub>2</sub> wag (48% + 38%) + CC (9%)
		1187	CH <sub>2</sub> wag (86%) + CC stretch (14%)	CH <sub>2</sub> wag (57 + 9 + 20%) + CC stretch (8 + 6%)
11		959	CC stretch (88%)	CC stretch (64% + 24%)
		959	CC stretch (96%)	CC stretch (55 + 41%)
12	$e''$	3363	CH stretch (98%)	CH stretch (2 × 25% + 2 × 24%)
		3363	CH stretch (66%)	CH stretch (2 × 33%)
13		1323	CH <sub>2</sub> rock (34%) + CH <sub>2</sub> twist (49%)	CH <sub>2</sub> rock (34%) + CH <sub>2</sub> twist (25 + 24%)
		1323	CH <sub>2</sub> rock (51%) + CH <sub>2</sub> twist (33%)	CH <sub>2</sub> rock (26 + 25%) + CH <sub>2</sub> twist (33%)
14		802	CH <sub>2</sub> twist (56%) + CH <sub>2</sub> rock (30%)	CH <sub>2</sub> twist (2 × 28%) + CH <sub>2</sub> rock (30%)
		802	CH <sub>2</sub> rock (44%) + CH <sub>2</sub> twist (37%)	CH <sub>2</sub> rock (2 × 22%) + CH <sub>2</sub> twist (37%)

<sup>a</sup> All frequencies in cm<sup>-1</sup>. HF/6-31G(d,p) calculations. Each normal mode is dissected into internal parameter associated vibrations according to Reference 162. Compare with Figure 20.

former as shown in Table 19<sup>163</sup>. The dissection is based on a comparison of normal-mode vectors and adiabatic vectors through force constants, and therefore it is similar to an analysis in terms of potential energy contributions<sup>164</sup> but has several advantages with regard to the latter analysis<sup>162</sup>.

The normal modes of **1** (Figure 20) are easy to identify because most of them involve motions associated with the same type of internal parameter, e.g. all six CH bond lengths (mode 1) or all three CH<sub>2</sub> twisting parameters (mode 5). Strong coupling between different types of internal parameters can only be found for modes 2, 10, 13 and 14 (Table 19). In the first two cases, CC stretching motions are mixed in, which is obvious from the pictorial representations in Figure 20. However, these representations are sometimes misleading as can be seen from mode 3. According to the pictorial representation, one might expect that the ring breathing motion is connected with a CH scissoring or CH stretching motion, but the adiabatic analysis shows that mode 3 does not involve CH<sub>2</sub> scissoring or CH stretching. (The arrows at the H atoms result from the movement of the C atoms.) Modes 13 and 14 are a result of strong coupling between adiabatic CH<sub>2</sub> rocking and CH<sub>2</sub> twisting motions that is described quantitatively in the adiabatic mode analysis (Table 19).

Adiabatic frequencies of **1** are compared in Table 20 with those of some other hydrocarbons<sup>163</sup>. The adiabatic CC frequency is about 80 and the adiabatic CH stretching frequency about 100 cm<sup>-1</sup> larger than the corresponding values for cyclohexane. Compared to ethene, adiabatic CH stretching frequencies are almost identical, which is in line with the high dissociation energy of the CH bond of **1** (see Section V. E)<sup>89</sup>. The same observation has been made by McKean using isolated CH frequencies obtained by appropriate deuteration of **1**<sup>165</sup>.

TABLE 20. Adiabatic internal frequencies of cyclopropane and some simple hydrocarbons from Reference 163<sup>a</sup>

Molecule	CC stretch	CH stretch	HCH def	CH <sub>2</sub> twist	CH <sub>2</sub> rock	CH <sub>2</sub> wag
Ethene	1798	3344	1626		1121	
Cyclopropane	1169	3328	1614	1072	1017	1196
Cyclobutane	1114	3222 (ax) 3233 (eq)	1621	1201	927	1368
Cyclohexane	1132	3172 (ax) 3200 (eq)	1621	1286	1012	1416
Propane	1143	3192	1623	1293	984	1427

<sup>a</sup> All frequencies in cm<sup>-1</sup>. HF/6-31G(d,p) calculations.

Since adiabatic frequencies provide direct information on the curvature of the potential energy surface and since the curvature is related to the dissociation energy (a large  $D_e$  should lead to a large positive curvature), adiabatic frequencies can be correlated with dissociation energies (but not bond energies, which are just averages over dissociation energies). Therefore, a suggested increase in the CC dissociation energy (the activation energy of CC bond breakage for **1** is 61.0 compared to 62.5 kcal mol<sup>-1</sup> for cyclobutane<sup>166</sup>) is not necessarily a contradiction with regard to the relatively small CC bond energies calculated for **1** (Section V. B and Table 8).

With the development of analytical energy derivative methods<sup>135, 167</sup>, the calculation of vibrational frequencies (second derivatives of the energy with regard to atomic coordinates) and infrared absorption intensities (derivatives of the energy with regard to components of electronic field and atomic coordinates, i.e. dipole moment derivatives) both at the HF and correlation corrected levels has become routine<sup>168</sup>. There are six (two  $a_2''$  + four  $e'$ )

infrared active vibrational modes, which is confirmed by theory (Table 21)<sup>163</sup>. The intensity pattern agrees well with experimental infrared data, but a direct comparison between calculated and measured absolute infrared intensities<sup>157</sup> has not been carried out so far.

TABLE 21. Integrated infrared intensities and calculated infrared intensities of cyclopropane

#	Sym	Experiment		HF/6-31G(d,p)		Characterization according to Exp.
		Freq (cm <sup>-1</sup> )	IR intensity <sup>157</sup> (cm <sup>2</sup> m mol <sup>-1</sup> )	Freq (cm <sup>-1</sup> )	IR intensity <sup>173</sup> (km mol <sup>-1</sup> )	
6	$a_2''$	3102	0.974	3385	54.6	strong
7		854	0.058	919	0.03	very weak
8	$e'$	3024	1.274	3286	73.2	strong
9		1438	0.126	1602	0.4	weak
10		1028	1.976	1187	8.0	strong
11		868	3.584	959	49.5	very strong

There is considerable interest by experimentalists in infrared intensities, because these can be used to describe electronic charge reorganizations in vibrating molecules<sup>169</sup>. For this purpose, atomic polar tensors<sup>170</sup> and various effective charges<sup>157, 169</sup> have been derived, which are related directly to dipole moment derivatives. Effective charges can be compared to calculated atomic charges (see Section VIII).

Several features of the vibrational spectrum of **1** are characteristic also for its heterocyclic analogues, such as oxirane and aziridine. Komornicki and coworkers<sup>158</sup> showed that the three ring molecules have six types of internal coordinates in common (CH stretch, CH<sub>2</sub> deformation, CH<sub>2</sub> twist, CH<sub>2</sub> rock, CH<sub>2</sub> wag and ring motions; see Figure 20). The experimental order for the CH stretching motions of **1** is  $\nu_6$  ( $a_2''$ , 3102 cm<sup>-1</sup>),  $\nu_{12}$  ( $e''$ , 3082 cm<sup>-1</sup>),  $\nu_1$  ( $a_1'$ , 3038 cm<sup>-1</sup>) and  $\nu_8$  ( $e'$ , 3024 cm<sup>-1</sup>); see Table 18. This order is maintained for all three molecules. In addition, the mode with the highest symmetry leads to the highest frequency.

Kaupert, Heydtmann and Thiel<sup>112</sup> calculated the vibrational spectrum of monohalogenated **1** at the HF level using the 6-31G(d) basis set and effective core potentials with DZ + P basis sets for Cl, Br and I. Reduction from  $D_{3h}$  to  $C_s$  symmetry leads to considerable coupling between modes (exceptions: C—H stretching and CH<sub>2</sub>-deformation modes) of **1**. Vibrational frequencies that are influenced by the halogen substituent are shifted to lower values with increasing mass of the halogen.

Marstokk and Møllendal<sup>171</sup> investigated the equilibrium conformation and the rotational potential of cyclopropanemethanethiol using microwave and vibrational spectroscopy in connection with *ab initio* calculations. They found a heavy-atom *gauche* conformation with the thiol H atom residing over a vicinal CC bond of the ring to be most stable. Comparison of experimental and theoretical vibrational spectra suggested the existence of a weak hydrogen bond involving the SH group and the 'quasi- $\pi$ ' bond of the cyclopropane ring.

An investigation of the vibrational spectrum of cyclopropylcarbonyl fluoride was carried out by Durig and coworkers using HF/3-21G theory<sup>115</sup>. The authors could assign all frequencies of *cis* and *trans* conformations and analyse normal modes in terms of potential energy contributions using appropriate symmetry coordinates. The calculated conformational stability and rotational barriers [HF/6-31G(d) and HF/3-21G] were compared with results obtained from the far-infrared spectrum.

Vibrational circular dichroism (VCD) reflects the stereochemistry of a chiral molecule<sup>172</sup>. According to Stephens<sup>173</sup>, analysis and prediction of VCD spectra can be carried

out on the basis of calculated vibrational rotational strengths  $R_i$ , which depend on dipole strengths (determined by atomic polar tensors  $\mathbf{P}_{\alpha\beta}^{\lambda}$ ; see equation 17) and tensors  $\mathbf{I}_{\alpha\beta}^{\lambda}$  (equation 18) that describe changes of the molecular wave function upon changes in atomic coordinates and magnetic field components:

$$\mathbf{P}_{\alpha\beta}^{\lambda} = [(\partial\mu_{\text{el}})_{\beta}/\partial x_{\lambda\alpha}]_{\mathbf{R}_e} \quad (\alpha, \beta = x, y, z) \quad (17)$$

$$\mathbf{I}_{\alpha\beta}^{\lambda} = \langle (\partial\psi_G(\mathbf{R}\mathbf{z})/\partial x_{\lambda\alpha})_{\mathbf{R}_e} | (\partial\psi_G(\mathbf{R}_e, H_{\beta})/\partial H_{\beta}) \rangle_{H_{\beta}=0} \quad (18)$$

where  $\mu_{\text{el}}$  is the electric dipole moment of the ground state,  $\partial x_{\lambda\alpha}$  the Cartesian displacement coordinate from  $\mathbf{R}_e$  of nucleus  $\lambda$ ,  $\mathbf{R}_e$  the equilibrium geometry,  $\psi_G(\mathbf{R})$  the electronic wave function of the ground state, and  $\psi_G(\mathbf{R}_e, H_{\beta})$  is the wave function in the presence of a magnetic field perturbation. Using these definitions, Jalkanen and coworkers<sup>174</sup> investigated the VCD spectrum of *trans*-1(*S*),2(*S*)-dicyanocyclopropane at the HF/4-31G level. Frequencies, relative absorption intensities and VCD intensities were in reasonable agreement with experimental values.

Lazzeretti and coworkers<sup>175</sup> calculated nuclear electric and electromagnetic shielding tensors for **1** and oxirane. These properties are related to atomic polar tensors and atomic axial tensors used by infrared and VCD spectroscopists. The authors demonstrated that they could obtain fairly accurate sum rules for atomic polar tensors and atomic axial tensors with relatively little computational effort.

### VIII. ONE-ELECTRON PROPERTIES

Although **1** is one of the best investigated molecules, there is, apart from data concerning its electron density distribution, very little information available on its one-electron properties. In principle, accurate data could be obtained by correlation-corrected *ab initio* methods, but almost nothing has been done in this direction, which of course has to do with the fact that experimental data on one-electron properties of **1** are also rare, and therefore, it is difficult to assess the accuracy and usefulness of calculated one-electron properties such as higher multipole moments, electric field gradients, etc.

The most important one-electron property of **1** is its electron density distribution  $\rho(\mathbf{r})$ , which has been discussed in Section IV. Apart from X-ray and neutron diffraction studies, information on  $\rho(\mathbf{r})$  is also obtained from experimentally based atomic charges and measured multipole moments of a molecule. Zerbi and coworkers<sup>169</sup> use integrated infrared-absorption intensities (Section VII) to derive atomic densities. Since infrared intensities result from changes in the molecular dipole moment upon activating vibrational modes, one can express the total dipole moment as a sum of bond dipole moments, and hence dipole moment derivatives in terms of bond dipole moment derivatives. In this way, it is possible to evaluate from infrared intensities bond dipole moments and, with known bond lengths  $r$ , effective atomic charges  $q$  from bond dipole moments  $\mu(\text{Bond}) = qr$ . In Table 22, experimentally based atomic charges are compared with calculated atomic charges for small hydrocarbons with different hybridizations. It is well known that the electronegativity of a C atom increases with increasing s-character, which is nicely reflected by the virial charges. In addition, virial charges suggest similar hybridizations for **1** and ethene as far as the CH hybrid orbitals are concerned.

The H charges derived from infrared intensities seem to confirm the increase in the electronegativity of the C atom with increasing s-character. However, the corresponding C charges reveal that the electronegativity change from ethene to acetylene is not correctly described and that a large electronegativity difference between **1** and ethene is predicted. Mulliken charges also fail to reproduce the increase in the C electronegativity when going from ethene to acetylene. They suggest similarity between ethene and **1**, flawed however by the fact that Mulliken charges suggest larger electronegativity (s-character) for C in **1**.



TABLE 22. Experimentally derived and calculated atomic densities [electron]

Molecule	Infrared intensities <sup>a</sup>		Mulliken <sup>b</sup>		Virial partitioning <sup>c</sup>	
	C	H	C	H	C	H
CH <sub>4</sub>	-0.260	0.065	-0.472	0.118	0.244	-0.061
H <sub>3</sub> C—CH <sub>3</sub>	-0.135	0.045	-0.335	0.112	0.237	-0.079
Cyclopropane	-0.170	0.085	-0.261	0.130	0.104	-0.052
H <sub>2</sub> C=CH <sub>2</sub>	-0.268	0.134	-0.254	0.127	0.082	-0.041
HC≡CH	-0.208	0.208	-0.233	0.233	-0.121	0.121

<sup>a</sup> Derived from infrared intensities (Reference 169). Carbon charges were determined from H charges by symmetry arguments.

<sup>b</sup> HF/6-31G(d,p) calculations. This work.

<sup>c</sup> HF/6-31G(d,p)//HF/6-31G(d) calculations (Reference 79).

Hence, neither experimentally based charges nor Mulliken charges provide a consistent picture and, in addition, they show little resemblance (apart from the sign of  $q$ ) contrary to what has been claimed previously<sup>169</sup>.

Virial charges<sup>67</sup> have been criticized because (a) they show little similarity to Mulliken charges, (b) they are often very large and (c) they lead to bond polarities in contradiction to established chemical thinking. For example, virial charges suggest a C<sup>+</sup>—H<sup>-</sup> bond polarity while Mulliken charges and intensity-based charges predict C<sup>-</sup>—H<sup>+</sup> bond polarity. This seems to result from the basically different definition of atomic charges used by various authors. For example, experimental atomic charges represent effective quantities derived to fit both molecular dipole moment and infrared intensities; i.e. *they absorb the effects of (true) atomic charges and atomic dipole moments, where the latter result from the anisotropy of the electron density at an atom*. In the virial partitioning method, atomic charges and atomic dipole moments (multipole moments) are calculated separately and their values may cancel largely in the expression for the molecular dipole moment<sup>67</sup>. Hence, effective atomic charges and true atomic charges can differ considerably where, of course, it should be more difficult to discuss effective charges since they contain the cumulative effect of at least two quantities. The equal splitting of overlap populations to get Mulliken charges mixes in higher multipole moments (as, e.g., becomes obvious from Stone's distributed multipole analysis<sup>176</sup>) and, accordingly, lends them the character of an effective rather than a pure atomic charge.

The multipole moments of a molecule indicate anisotropies in the molecular charge distribution. Since **1** is an uncharged molecule with  $D_{3h}$  symmetry, the first non-vanishing molecular moment of **1** is its quadrupole moment, which has been determined experimentally by measuring the birefringence induced by an electric field gradient and is  $5.3 \pm 0.7 \times 10^{-40} \text{ C m}^2$  ( $1.6 \pm 0.2$  Buckingham)<sup>177</sup>. At the HF/[5s3p2d/3s1p] level, a value of  $8.4 \times 10^{-40} \text{ C m}^2$  (2.5 Buckingham) was obtained by Amos and Williams<sup>178</sup>. Since possible hyperpolarizability effects would decrease rather than increase the experimental quadrupole moment, the relatively large difference between experimental and calculated quadrupole moments could not be explained. In the same investigation, calculated values of octupole and hexadecapole moments of **1** are also given (see Table 23).

The experimental values of the polarizability  $\alpha = \frac{1}{3} (2\alpha_{xx} + \alpha_{zz})$  of **1** and its anisotropy  $\Delta\alpha = \alpha_{zz} - \alpha_{xx}$  are 5.50 and  $-0.74 \text{ \AA}^3$ , which have been obtained by extrapolating polarizabilities measured at optical frequencies to their static limits<sup>179</sup>. Amos and Williams calculated for  $\alpha$  and  $\Delta\alpha$  5.03 and  $-0.67 \text{ \AA}^3$  at the HF/[5s3p2d/3s1p] level, which are about 10% too small, typical of HF/large basis set calculations. As can be seen from Table 23,  $\alpha_{xx} = \alpha_{yy}$  (components in the ring plane) is larger than  $\alpha_{zz}$  (perpendicular to the ring plane). Since an

TABLE 23. Multipole moments and polarizability  $\alpha$  of cyclopropane<sup>a</sup>

Method	$\Theta$ ( $10^{-40}$ C m <sup>2</sup> )	$\Omega$ ( $10^{-50}$ C m <sup>3</sup> )	$\Phi$ ( $10^{-60}$ C m <sup>4</sup> )		
HF/ [5s3p2d/3s1p] <sup>178</sup>	8.40	19.05	-48.91		
exp. <sup>177</sup>	5.3 ± 0.7				
	$\alpha_{xx}$ (Å <sup>3</sup> )	$\alpha_{zz}$ (Å <sup>3</sup> )	$\Delta\alpha = \alpha_{zz} - \alpha_{xx}$ (Å <sup>3</sup> )	$\alpha = 1/3 (2\alpha_{xx} + \alpha_{zz})$ (Å <sup>3</sup> )	
HF/ [5s3p2d/3s1p] <sup>178</sup>	5.26	4.59	-0.67	5.03	
exp. <sup>179</sup>	5.74	5.00	-0.74	5.50	

<sup>a</sup>  $z$  is the threefold axis of cyclopropane and  $x$  is one of its  $C_2$  axes. With this definition,  $\Theta = \Theta_{zz}$ ,  $\Omega = \Omega_{xxx}$ , and  $\Phi = \Phi_{zzzz}$ . Other non-zero elements of the multipole tensor are related to these by symmetry.

important part of the polarizability is the flow of electrons between bonds, and since it is much easier to displace charge along a bond than across it, the component of  $\alpha$  parallel to a bond chain is always larger than those perpendicular to it. In the case of a small ring such as **1**, it is easier to move charge in the ring plane than perpendicular to it as reflected by  $\alpha_{xx}$  and  $\alpha_{zz}$ . However, compared to the polarizability component perpendicular to the  $C_2$  axis of propane in the plane of the three C atoms (and by this almost 'parallel' to the C bond chain), the  $\alpha_{zz}$  value is significantly smaller, which indicates that it is more difficult to polarize the electronic charge in the plane of **1** than along the CCC chain of propane. On the other hand, one has to consider that the molecular volume of propane is larger than that of **1**.

Assuming that the molecule can be approximated as a perfectly conducting sphere (radius  $r$ ) with volume  $V$ , the dipole moment  $\mu$  induced in the sphere upon its placement in an electric field of magnitude  $F$  is given by equation 19:

$$\mu = r^3 F \quad (19)$$

which means that the molecular polarizability is equated with a volume measure. Gough<sup>180</sup> has shown that calculated molecular volumes defined by the contour for which the electron density is 0.001 a.u. indeed correlate with the molecular polarizability calculated at the HF/(9s5p1d/4s1p)[4s2p1d/2s1p] level (see Figure 21). According to this correlation, the actual molecular polarizability of **1** is about 10% larger than that predicted from the molecular volume. This is confirmed when predicting molecular polarizabilities from  $CH_3$  (1.69 Å<sup>3</sup>) and  $CH_2$  group increments (1.47 Å<sup>3</sup>) derived from calculated polarizabilities of ethane and cyclohexane<sup>180</sup>. While  $\alpha$  values of alkanes can be accurately reproduced, the  $\alpha$  value of **1** (4.42 Å<sup>3</sup>) is smaller than the theoretical value. This is similar to the case of ethene (see also Figure 21), which suggests that the polarization of negative charge in particular in the plane of the ring is larger than for a normal alkane and that **1** and ethene are related in this respect.

Gough<sup>180</sup> has investigated polarizability derivatives associated with CH and CC bond stretching, which can be compared with parameters derived from Raman trace scattering cross sections. The mean of the CH polarizability derivative of **1** is slightly larger than that for CH ( $CH_2$ ) in propane. Components along the bond are larger than those perpendicular to the bond. From all investigated alkanes the CC polarizability derivative of **1** is the smallest one, which has to do with the fact that a CC stretching mode in **1** involves three rather than two C atoms.

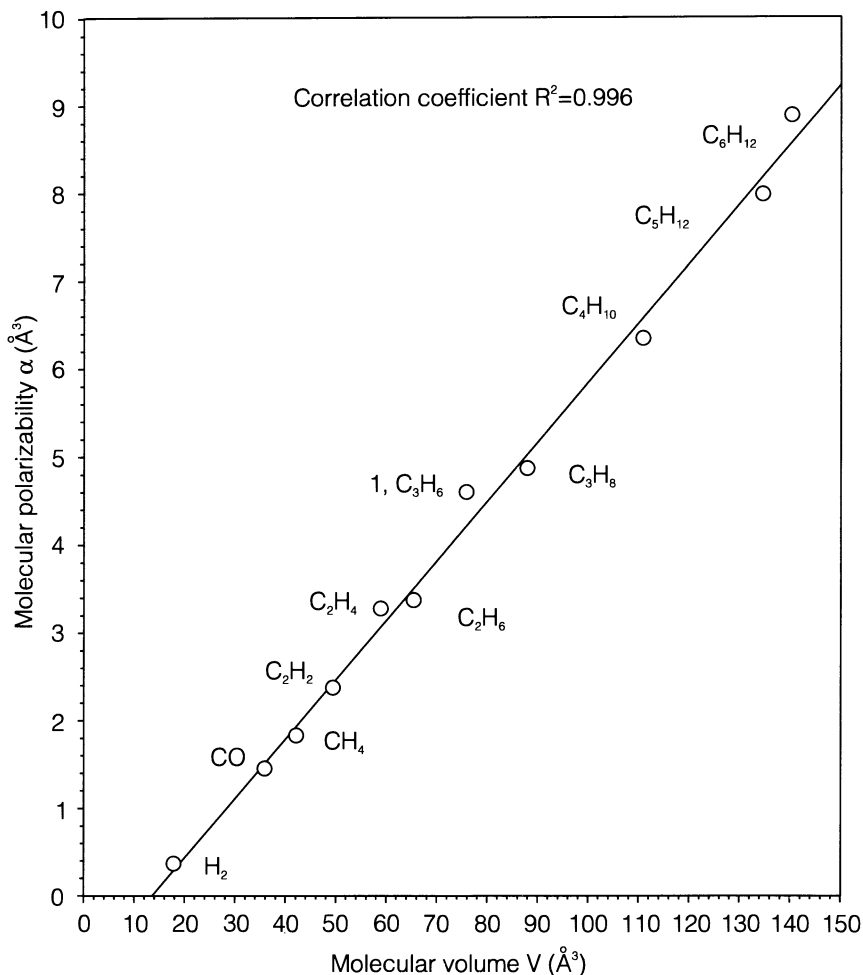


FIGURE 21. Correlation of molecular polarizabilities  $\alpha$  with molecular volumes  $V$  for a number of hydrocarbons including cyclopropane. Data from Reference 180

## IX. NMR SPECTRA

The rapid development of analytical energy gradient methods<sup>135, 167</sup> in the 70s and 80s has made accessible a large number of molecular properties to routine *ab initio* calculations. Certainly, one of the most important steps (after calculating molecular geometries and molecular vibrations) was the calculation of NMR chemical shifts by *ab initio* methods. For a long time, this information could not be provided by *ab initio* theory, since a routine calculation of NMR parameters with sufficient accuracy was not possible. There were several approaches to calculate NMR chemical shift data, of which the best known is probably the method based on *gauge independent atomic orbitals* (GIAOs)<sup>181</sup>, originally suggested by London<sup>182</sup> and later used by Pople<sup>183</sup>, Ditchfield<sup>184</sup> and others<sup>185</sup>. However, the

computer-time consuming integral evaluation over GIAOs prevented applications to larger molecules. This changed when Pulay and coworkers<sup>186</sup> improved the GIAO method by implementing modern techniques for integral and integral derivative evaluation. However, this development took place years after the routine calculation of NMR chemical shifts at the *ab initio* level was solved by Kutzelnigg and Schindler<sup>187</sup>. These authors solved the gauge problem inherent in all calculations of magnetic properties with the help of localized MOs rather than GIAOs. Accordingly, they coined their method *individual gauge for localized orbitals* (IGLO)<sup>187,188</sup>.

The work by Kutzelnigg and Schindler triggered further developments in the field of NMR chemical shift calculations. Beside the IGLO program, several other *ab initio* methods are today available for routine calculations of magnetic properties of molecules: (1) The LORG (localized orbital/local origin) method by Hansen and Bouman<sup>189</sup>; (2) GIAO-SCF in the version of Pulay and coworkers<sup>186</sup>; (3) GIAO-MBPT2 by Gauss to calculate correlation corrected NMR chemical shifts at the second-order many-body perturbation theory level<sup>190</sup>; (4) GIAO-MBPT3 and GIAO-MBPT (SDQ)-4 by Gauss to get third-order and fourth-order corrections to GIAO values<sup>191</sup>; (5) MC-IGLO by Kutzelnigg and coworkers for problems that require a MCSCF wave function<sup>192</sup>. In addition, other methods to obtain correlation-corrected NMR chemical shift values have been described in the literature<sup>193</sup>.

Since *ab initio* calculations lead to the determination of the full shielding tensor of each nucleus of **1**, one should have expected that these calculations would have helped to rationalize <sup>1</sup>H and <sup>13</sup>C NMR spectra of **1**, which are unusual with regard to measured shift values: The proton shift ( $\delta$  0.12 ppm relative to TMS<sup>194</sup>) is upfield by more than 1 ppm compared to the shift values of suitable reference compounds (cyclohexane:  $\delta$  1.44 ppm; cyclobutane:  $\delta$  1.96 ppm<sup>194</sup>) while the <sup>13</sup>C shift (isotropic shift:  $\delta$  -4.0 ppm<sup>195</sup>; shift in liquid:  $\delta$  -2.8 ppm relative to TMS<sup>196</sup>) is more than 20 ppm upfield (cyclohexane:  $\delta$  27 ppm; cyclobutane:  $\delta$  23 ppm)<sup>196</sup>. Wiberg<sup>14</sup> has summarized in his review article on the cyclopropyl group the work that has been carried out by both theoreticians and experimentalists to rationalize the <sup>13</sup>C NMR chemical shift of **1**. Today, it is clear that the observed upfield shift of more than 20 ppm is largely due to the tensor component perpendicular to the ring plane<sup>197</sup>. This is also reflected by the anisotropy and asymmetry of the <sup>13</sup>C shielding tensor of **1** calculated by Hansen and Bouman with their LORG method<sup>198</sup>. These authors suggested an analysis of shielding tensors in terms of the shielding response vector **T**, which can be displayed pictorially in the same way as one displays MOs (see Figure 6). Three-dimensional contour line diagrams of **T** were used to rationalize <sup>13</sup>C shielding tensors in cyclopropene and other three-membered rings<sup>198</sup>. However, the <sup>13</sup>C shielding tensor of **1** was not discussed in this work.

So far, speculations which attribute the observed upfield shifts of the NMR signals of **1** to a ring current of the  $\sigma$ -electrons<sup>199</sup> (in line with the idea of  $\sigma$ -aromaticity<sup>8</sup>) have not been refuted. However, a less spectacular rationalization of the NMR chemical shifts in terms of local anisotropy contributions caused by the unique electron distribution of **1** (see Section IV) may also be possible<sup>200</sup>.

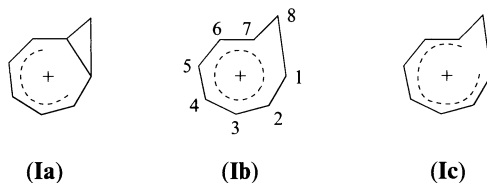
The determination of NMR chemical shifts by either IGLO, LORG or GIAO turns out to be very sensitive with regard to the geometry used<sup>201-204</sup>. Experimental geometries are not that useful in this connection since very often they are not accurate enough, represent different geometries ( $r_e$ ,  $r_g$ ,  $r_o$ ,  $r_u$ ,  $r_g$ ,  $r_v$ , etc.) or suffer from intermolecular interactions in condensed phases. *Ab initio* geometries provide a consistent description of molecules that does not suffer from the ambiguities of experimental geometries. Many calculations have shown that reasonable NMR chemical shifts are obtained if the geometry of the molecule in question has been optimized at a correlation-corrected level of theory such as second-order perturbation theory (MP2) using DZ, DZ + P or better basis sets. Since the calculated NMR chemical shifts clearly depend on the geometry, an agreement between experimental and

theoretical shifts not only means a clear identification but also a geometry determination of the molecule in question. On the other hand, if theoretical and experimental shifts differ considerably, other possible geometries or structures have to be tested<sup>205</sup>.

Schleyer was the first to fully realize the sensitivity of calculated NMR chemical shifts with regard to molecular geometry and he used this for *ab initio*/IGLO/NMR-based structural determinations in many cases including carbocations, boron and organolithium compounds<sup>201, 202</sup>. A recent assessment of this approach suggests that 'structural assignments based on the *ab initio*/IGLO/NMR method are quickly approaching a confidence level that rivals modern day X-ray diffraction determinations of molecular structures'<sup>206</sup>.

The *ab initio*/IGLO/NMR method has been used to determine the relative distribution and stability difference of the cyclopropylcarbinylium cation and cyclobutyl cation in solution<sup>207</sup>. Agreement between <sup>13</sup>C IGLO chemical shifts and experimental shifts could only be obtained when assuming a rapid equilibrium between the two cations. Over the range of temperatures considered (-61 to -132°C), a cyclobutyl cation structure with an axial H atom and short 1,3-distances of 1.65 Å (bicyclobutonium ion structure) was found to be more stable by 0.5 kcal mol<sup>-1</sup><sup>207</sup>. For the gas phase, however, the cyclopropylcarbinylium cation was calculated to be 0.26 kcal mol<sup>-1</sup> more stable [MP4/6-31G(d)//MP2/6-31G(d) calculations including vibrational corrections]<sup>207</sup>.

Cremer and coworkers investigated a number of potentially homoconjugated cyclopropyl compounds such as the monohomotropylium cation<sup>203, 205</sup>, the 1,4- and 1,3-bishomotropylium cation<sup>208</sup>, the trishomotropylium cation<sup>209</sup>, the barbaralyl cation<sup>210</sup> and the cyclobutenyl cation<sup>211</sup>. All these cations have the choice between a closed cyclopropyl structure (**Ia**), an open cyclopolyenyl structure (**Ic**) and an intermediate structure (**Ib**) as demonstrated in the case of the monohomotropylium cation.



For all cations considered, <sup>13</sup>C NMR spectra have been measured in solution while direct structural information on the question as to whether structure **Ia**, **Ib** or **Ic** corresponds to a minimum energy form was completely missing. Therefore, the structural problem was solved by utilizing the *ab initio*/IGLO/NMR method. Since results of this work will be reviewed in another chapter of this volume (see Chapter 7), we refrain from discussing calculated NMR data for potentially homoconjugated cyclopropyl compounds at this point.

There is little computational work on NMR coupling constants since the *ab initio* methods for calculating these quantities are still at an infant stage. A discussion of the experimental work on NMR coupling constants of **1** and related ring compounds can be found in the review article of Wiberg<sup>14</sup>.

## X. EXCITED STATES AND ULTRAVIOLET ABSORPTION SPECTRA

The observed ultraviolet absorption spectrum of **1**<sup>212</sup> (for a display of the recorded spectrum see Section I.G of Wiberg's review article on the cyclopropyl group<sup>14</sup>) consists of three broad bands, of which the first (60,000 to 66,000 cm<sup>-1</sup>; 7.44–8.18 eV) possesses a maximum at 63,000 cm<sup>-1</sup> (7.8 eV; oscillator strength *f* 0.12), far to the red of most saturated absorbers and in the region of the π → π\* transitions of unsaturated molecules. This observation has

been one of the reasons to bring **1** into relation with ethene and to associate  $\pi$ -character with its CC bonds. The second ultraviolet absorption band extends from 67,000 to 72,000  $\text{cm}^{-1}$  (8.3–8.9 eV) with a maximum at 70,000  $\text{cm}^{-1}$  (8.7 eV,  $f = 0.04$ ) while the third, which is the most intense band ( $f = 0.7$ ), is located at 83,000  $\text{cm}^{-1}$  (10.3 eV) extending over the range from 74,000 to 85,000  $\text{cm}^{-1}$  (9.2–10.5 eV). The first and the third band possess a discrete structure superimposed on a broad continuous background, which has been brought into connection with the Rydberg character of the first and partial Rydberg character of the third band. The second band may have either valence or Rydberg character according to experiment<sup>212</sup>.

The classic *ab initio* work on excited states of **1** is the SCF plus limited CI study by Buenker and Peyerimhoff from 1969, which gave a first basis for analysing its ultraviolet absorption spectrum and investigating ring opening to trimethylene<sup>213</sup>. A decade later, Goldstein, Vijaya and Segal carried out an extensive *ab initio* CI investigation of absorption and magnetic circular dichroism (MCD) spectra of **1** using the improved computational possibilities of the eighties<sup>52</sup>. Segal and coworkers used a (9s5p/5s)[4s2p/1s] basis augmented by diffuse s, p and d functions (exponent 0.02) located at the ring centre to describe in particular the lower Rydberg states of **1**. The CI calculations (based on 32,542 spin eigenfunctions) were carried out by using perturbational CI techniques<sup>52</sup>. Some of the results obtained in this work are summarized in Table 24.

TABLE 24. Comparison of calculated excitation energies<sup>52</sup> and experimental absorptions of cyclopropane<sup>a</sup>

State	Primary excitation	Excitation energy (eV)	$f^r$	$f^v$	$f^{r+v}$	Exp. UV spectrum <sup>212</sup>
$1^3E'$	$3e' \rightarrow 4a_1'$ (0.85)	7.47	not electric-dipole-allowed			
$1^1E'$	$3e' \rightarrow 4a_1'$ (0.90)	7.61	0.009	0.013	0.011	7.4–8.2, $f = 0.12$
$1^1A_2'$	$3e' \rightarrow 4e'$ (0.68)	8.07	not electric-dipole-allowed			
$1^1A_1'$	$3e' \rightarrow 4e'$ (0.68)	8.08	not electric-dipole-allowed			
$2E'$	$3e' \rightarrow 4e'$ (0.66)	8.11	0.127	0.101	0.113	
$1A_2''$	$3e' \rightarrow 2e''$ (0.68)	8.72	0.007	0.001	0.005	
$1A_1''$	$3e' \rightarrow 2e''$ (0.67)	8.79	not electric-dipole-allowed			
$3E'$	$3e' \rightarrow 5a_1'$ (0.95)	8.85	0.002	0.001	0.002	8.3–8.9, $f = 0.04$
$1E''$	$3e' \rightarrow 2e''$ (0.68)	8.96	not electric-dipole-allowed			
$4E'$	$3e' \rightarrow 5e'$ (0.69)	9.08	0.002	0.001	0.001	
$2A_2'$	$3e' \rightarrow 5e'$ (0.69)	9.09	not electric-dipole-allowed			
$2A_1'$	$3e' \rightarrow 5e'$ (0.69)	9.19	not electric-dipole-allowed			
$5E'$	$3e' \rightarrow 6a_1'$ (0.88)	9.92	0.001	0.004	0.002	weak Rydberg at 9.9 eV,
$6E'$	$1e'' \rightarrow 2a_2''$ (0.97)	10.56	0.135	0.076	0.102	9.2–10.5, maximum 10.3,
$2E''$	$1e'' \rightarrow 4e'$ (0.70)	10.62	not electric-dipole-allowed			
$2A_2''$	$1e'' \rightarrow 4e'$ (0.63)	10.79	0.072	0.053	0.062	valence with Rydberg
$7E'$	$3e' \rightarrow 1a_2'$ (0.64)	11.94	0.376	0.244	0.303	superimposed, $f = 0.7$

<sup>a</sup> All calculated excited states are listed together with the main contribution (corresponding CI coefficient given in parentheses).

Molecule **1** possesses a large number of degenerate electronic energy levels and an unusually high density of electronic states in the energy region between the onset of optical absorption and the first ionization potential. Because of its  $D_{3h}$  symmetry, transitions from the ground state to the  $A_2''$  and  $E'$  excited states are electric dipole allowed. CI calculations suggest that eight states (six  $E'$  + two  $A_2''$ ) are involved in the first three absorptions (Table 24)<sup>50</sup>.

The first optical absorption band is made up of two states,  $1E'$  ( $3e' \rightarrow 4a_1'$ ) and  $2E'$  ( $3e' \rightarrow 4e'$ ), which can be viewed as excitations to 3s and  $3p_{x,y}$  Rydberg orbitals<sup>52</sup>.

There are three dipole allowed singlet states in the region of the second absorption band,  $1A_2''$ ,  $3E'$  and  $4E'$ , all of which possess approximate 3d Rydberg character (Table 24). Experimental and calculated oscillator strength ( $f_{\text{exp}} = 0.04$ ,  $f_{\text{theor}} = 0.01$  for all three states) differ, which could not be resolved<sup>52</sup>. The principal transition of the third absorption has frequently been assigned to the transition  $3e' \rightarrow 1a_2'$ , but theoretical values for the energy of the state, for which the transition  $3e' \rightarrow 1a_2'$  is the primary contribution, are 2–3 eV higher than experimental values. Instead, CI calculations suggest that the third band is the result of a transition to a  $3p_z$  Rydberg state ( $6E'$ ,  $1e'' \rightarrow 2a_2''$ ; 10.56 eV;  $f = 0.135$ ), a transition to a state with partial Rydberg character ( $2A_2''$ ,  $1e'' \rightarrow 4e'$ ; 10.79 eV;  $f = 0.072$ ) and a transition to a state with valence character ( $7E'$ ,  $3e' \rightarrow 1a_2'$ ,  $1e'' \rightarrow 2e''$ ; 11.94 eV;  $f = 0.376$ ). Again, the calculated total oscillator strength (0.2) is smaller than the experimental one (0.7, Table 24), which in this case seems to be a deficiency of the basis set used to describe a possible mixing in of higher Rydberg states<sup>52</sup>.

Although the investigation of Segal and coworkers gives a first basis for the understanding of the ultraviolet absorption spectrum of **1**, it leaves a number of open questions, which can only be answered by more extended calculations. Such calculations are possible and have been done for derivatives of **1** (see, e.g., the MR-CI calculations for fluoro- and methyl-cyclopropanone with more than 50,000 spin adapted configurations<sup>214</sup>) but not for **1** itself. Therefore, further calculations are needed to get additional information on the excited states of **1**.

## XI. CHARGED CYCLOPROPYL GROUPS

### A. Cyclopropyl Anion

Rapid and significant progress in gas-phase carbanion chemistry in the last decade has promoted gas-phase acidity measurements even for such weakly acidic hydrocarbons such as **1**<sup>215</sup>. In addition, theoretical investigations of negative ions using *ab initio* MO methods have also produced new thermochemical and structural data for isolated carbanions which exhibit impressive accuracy when compared with experimental results (Table 25)<sup>216</sup>.

TABLE 25. Proton affinity (PA) and relative stability with regard to the  $\text{CH}_3^-$  anion ( $\Delta E$  of equation 20) given for cyclopropane and some other carbanions<sup>a</sup>

Carbanion	Method	$\Delta E$	Proton Affinity		Reference
			calc.	exp.	
Cyclopropyl	HF/4-31+G	-2.1	414.5	412	216
	MP2/6-31+G(d)//HF/6-31G(d)	-4.0			216
Cyclopropylmethyl	HF/4-31+G	-2.7	413.9		216
	HF/4-31+G	-9.7	406.9	408.0	216
Vinyl	HF/3-21+G	-11.2	420.5		215
	HF/4-31+G	-28.0	388.6	391.0	216
Allyl	HF/3-21+G	-27.8	403.9		215
	HF/4-31+G	-47.9	368.7	375.4	216
Ethynyl	HF/4-31+G	5.9	422.5	419.0	216
2-Propyl	HF/4-31+G				

<sup>a</sup> Energies in kcal mol<sup>-1</sup>.

Basis sets used for carbanions have to include diffuse functions because anions generally have low ionization potentials, i.e. there is a pair of (or a single) electrons in the form of a diffuse charge cloud that extends relatively far from the nuclei and therefore is easily lost. Without diffuse functions, even larger basis sets such as DZ + P are not entirely successful either in the calculation of absolute acidities or in the ordering of acidities.

Froelicher, Freiser and Squires<sup>215</sup> calculated the gas-phase geometry of the cyclopropyl anion at the HF/3-21+G level of theory. In case of C1 deprotonation, vicinal (C1C2: 1.562 Å) and distal (C2C3: 1.531 Å) bond lengths become longer than the CC bond lengths of **1** (Section VI. A). The cyclopropyl anion favours pyramidal geometry at the anionic centre to avoid additional ring strain. The calculated activation barrier for carbanion inversion is 18.4 kcal mol<sup>-1</sup>. The changes in the geometry of the cyclopropyl ring upon deprotonation can be rationalized in terms of changes in electronegativity and hybridization of atom C1. The hybrid orbital that accommodates the electron lone pair tries to adopt as much s-character as possible to stabilize the non-bonded charge distribution (see discussion of heterocyclopropanes in Section V. D). This will increase the p-character of the CH hybrid orbital which, according to a calculated HC1C2 angle of 111°, should be close to sp<sup>3</sup> hybridization.

Froelicher and coworkers<sup>215</sup> and Schleyer and coworkers<sup>216</sup> calculated the proton affinity of several carbanions (Table 25). Especially, the HF/4-31+G results are in good agreement with experimental values. Calculated proton affinities are compared to that of CH<sub>3</sub><sup>-</sup> with the help of the isodesmic reaction given in equation 20.



The ethynyl anion is calculated to be the most stable carbanion followed by the allyl, vinyl and cyclopropyl carbanion. The latter is only 2–4 kcal mol<sup>-1</sup> more stable than CH<sub>3</sub><sup>-</sup> but significantly more stable than the 2-propyl carbanion (Table 25), which is destabilized by the two methyl groups (due to 2-orbital–4-electron destabilization between the filled pπ-orbital of the carbanion and the occupied pseudo-π orbitals of the methyl groups). This is a general observation for alkyl anions with the exception of the cyclopropyl carbanion, which is stabilized by a methyl group when compared to CH<sub>3</sub><sup>-</sup> (Table 25). The effect of methyl substituents at the anionic centre depends on the electronegativity of the atom to which the CH<sub>3</sub> group is attached. The large electronegativity of C1 of the cyclopropyl anion relative to that of the anionic C of 2-propyl or methyl anion explains the observed difference in proton affinities (Table 25).

Schleyer and coworkers<sup>216</sup> calculated the electron affinity of ethyl, 2-propyl, cyclobutyl and cyclopropyl radicals. Apart from the cyclopropyl radical, these radicals have negative electron affinities suggesting that the corresponding anions cannot be observed as long-lived species in the gas phase. For the cyclopropyl radical, an electron affinity of 5.1 kcal mol<sup>-1</sup> was predicted<sup>216</sup>, in reasonable agreement with the experimental value of 8 kcal mol<sup>-1</sup><sup>217</sup>. Accordingly, it is probable that the cyclopropyl anion is the only saturated carbanion that can be observed experimentally in the gas phase.

## B. Protonated Cyclopropane

The reactivity of **1** in substitution reactions is markedly different from that of other cycloalkanes. An electrophilic substitution of **1** is followed by opening of the three-membered ring to a 2-propyl cation. Therefore, protonation of **1** as the simplest electrophilic attack has been extensively investigated, both experimentally<sup>218–220</sup> and computationally<sup>221–223</sup>.

Koch, Liu and Schleyer<sup>223</sup> explored the C<sub>3</sub>H<sub>7</sub><sup>+</sup> potential energy surface at the MP2 and MP4//MP2 level of theory using a TZ + P basis [6-311G(d,p)]. Their results are summarized in Figure 22 (structures **28**–**33**). The global minimum of the C<sub>3</sub>H<sub>7</sub><sup>+</sup> surface is occupied by the 2-propyl cation (**28**) that possesses C<sub>2</sub> symmetry rather than C<sub>2v</sub> symmetry as is com-



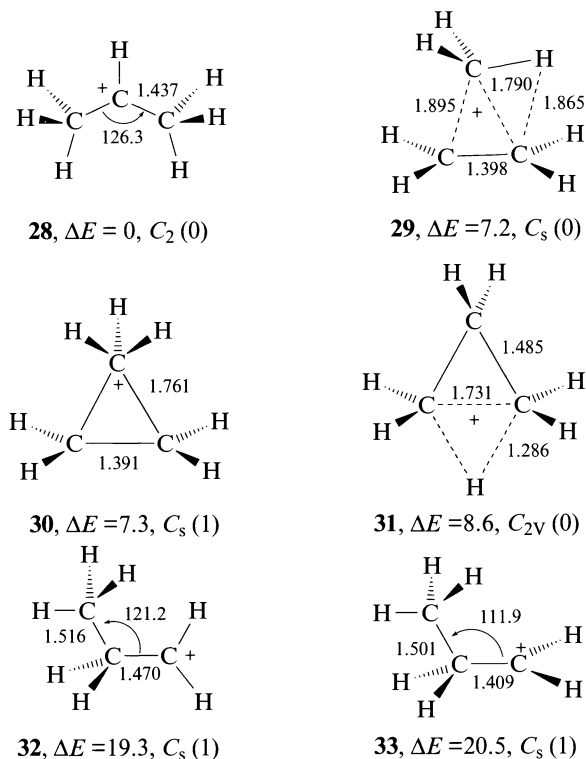


FIGURE 22. MP2/6-311G(d,p) geometries and MP4(SDQ, frozen core)/6-311G((d,p) relative energies at MP2 geometries for protonated cyclopropane and related compounds. For each geometry, the number of imaginary frequencies (0: energy minimum; 1: first-order transition state) is given in parentheses. All data from Reference 223

monly believed. Protonation of **1** may lead in the first step to the corner (**29**) or edge protonated isomers (**31**), which are 7.2 and 8.6 kcal mol<sup>-1</sup> above the global minimum (Figure 22). The C1C2 bond length of the corner protonated isomer is longer [1.895 and 1.790 Å at MP2/6-311G(d,p), Figure 22], while its C2C3 bond is shorter (1.398 Å) than the CC bonds in **1** (see Section VI. A). According to Dewar and coworkers<sup>222</sup>, **29** is best characterized as a  $\pi$ -complex between methyl cation and ethene.

Structure **30** in Figure 22 corresponds to the transition state of methyl rotation (CH<sub>3</sub> rotated by 30° with regard to **29**), which is just 0.1 kcal mol<sup>-1</sup> above cation **29** according to MP4(FC)/6-311G(d,p)//MP2/6-311G(d,p) calculations<sup>223</sup> [0.7 kcal mol<sup>-1</sup> according to MP4SDQ/6-31G(d)//MP2/6-31G(d) calculations<sup>222</sup>]. This means that **29** is essentially a symmetric species with a rapidly rotating methyl group.

Edge protonated **1** (isomer **31**) is positioned in a very flat minimum which, if zero-point energy corrections are considered, may also be a transition state<sup>223</sup>. In any case, hydrogen scrambling in **29** (via ion **31**) will be also rapid considering a barrier of just 1.4 kcal mol<sup>-1</sup>. The 1-propyl cation structures **32** and **33** are both transition states (there exists no minimum energy structure corresponding to 1-propyl cation), which are passed on the way to ring opening of **29** to give **28** (H migration takes place without any barrier). The calculated barrier for the process **28** → **29** (19.3 kcal mol<sup>-1</sup><sup>223</sup>, Figure 22) is somewhat higher than

the activation energy ( $16.3 \pm 0.4 \text{ kcal mol}^{-1}$ <sup>224</sup>) determined in non-nucleophilic (super acid) media. The calculated proton affinity of **1** is  $180.0 \text{ kcal mol}^{-1}$ <sup>223</sup>, which is in excellent agreement with the experimental value of  $179.8 \text{ kcal mol}^{-1}$ <sup>218</sup>.

### C. Cyclopropyl Radical Cation

Investigation of **1** upon removal of an electron has intrigued both theoreticians<sup>225–233</sup> and experimentalists<sup>234, 235</sup> because the properties of the formed cyclopropyl radical cation provide a basis to test MO models of three-membered rings (the Walsh MO model cannot explain the properties of the cyclopropyl radical cation<sup>233</sup>). Ejection of an electron from the  $3e'$  MOs of **1** (MOs #11,12 in Figure 6) leads to the Jahn–Teller unstable electron configuration  ${}^2E'$  (see Section X), which can be stabilized by distortion to the  $C_{2v}$ -symmetrical states  ${}^2A_1$  and  ${}^2B_2$  (first-order Jahn–Teller effect, see Figure 23).

If an electron is ejected from the  $3e'-a_1$  MO, which is C2C3 bonding, elongation of the distal bond can be expected accompanied by a lowering of the  $3e'-b_2$  MO because of reduction of its C2C3 antibonding overlap (Figure 23). The reverse effect should occur for electron removal from the  $3e'-b_2$  MO, namely (a) shortening of the distal bond, (b) lengthening of the vicinal bonds and (c) lowering of the energy of the  $3e'-a_1$  MO. Accordingly, the  ${}^2A_1$  state possesses a structure that is trimethylene-like and characterized by a short vicinal [1.474 Å at UMP2/6-31 G(d)] and a long distal [1.826 Å at UMP2/6-31G(d)] bond according to calculations by Krogh-Jespersen and Roth (see Figure 21)<sup>231</sup>. The  ${}^2B_2$  state, on the other hand, is best described as  $\pi$  complex formed between a methylene cation and ethene because of its long vicinal [1.665 Å at UMP2/6-31G(d)] and short distal [1.410 Å at UMP2/6-31G(d)] bond<sup>231</sup>.

Krogh-Jespersen and Roth<sup>231</sup> identified the  ${}^2B_2$  state as a transition state with one imaginary frequency and the  ${}^2A_1$  state as the ground state of the cyclopropyl radical cation. At

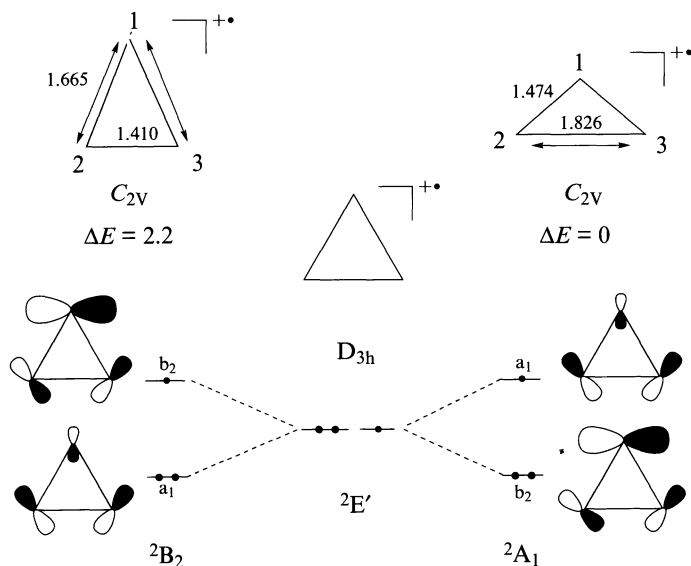


FIGURE 23. First-order Jahn–Teller distortion of  $D_{3h}$  symmetrical cyclopropyl radical cation. Geometries [UMP2/6-31G(d) calculations] and relative energy [CISD/6-31G(d)] from Reference 231

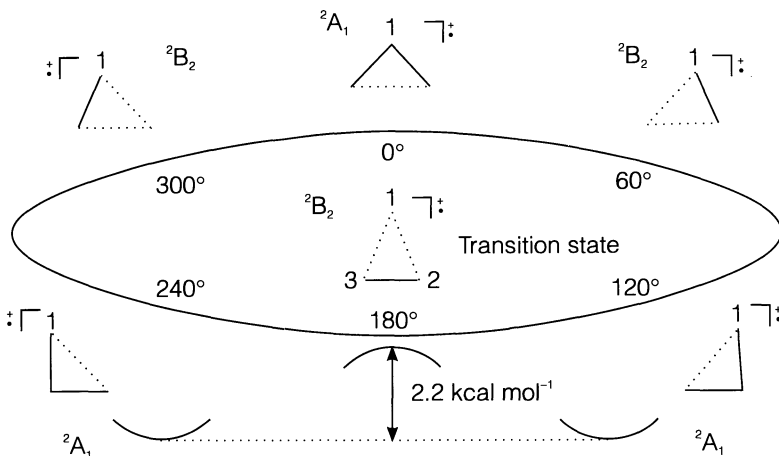


FIGURE 24. Pseudorotation cycle of the cyclopropyl radical cation. Relative energy [CISD/6-31G(d)] of the  ${}^2A_1$  ground state and the  ${}^2B_2$  transition state from Reference 231

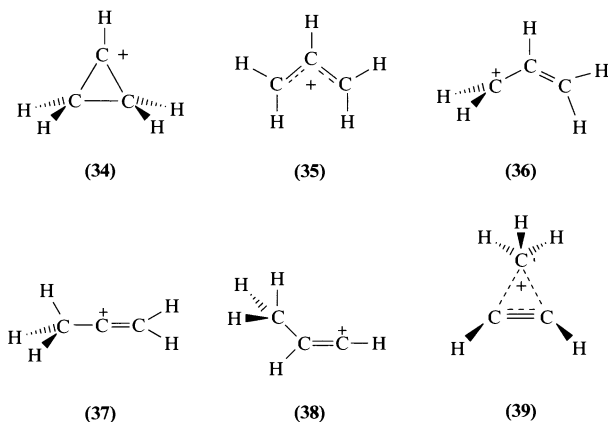
the UMP2/6-31G(d) level the energy difference between the two states is 2.5 kcal mol<sup>-1</sup>, while CI with all single and double substitutions CISD/6-31G(d)//UHF/6-31G(d) + zero point energy correction] predicts the  ${}^2B_2$ - ${}^2A_1$  energy difference to be 2.2 kcal mol<sup>-1</sup>. MP4(SDTQ)/6-31G(d,p)//ROHF/6-31G(d) calculations by Hudson and coworkers<sup>233</sup> lead to an energy difference of 2 kcal mol<sup>-1</sup>. Hence, the radical cation can undergo rapid pseudorotation (Figure 24), which is in line with ESR coupling constant measurements at 77 K<sup>234,235</sup>. Lunell and coworkers determined isotropic hyperfine coupling constants of the cyclopropyl radical cation at the CI level of theory, which turned out to be in reasonable agreement with measured values<sup>230</sup>.

Krogh-Jespersen and Roth<sup>231</sup> also investigated Jahn–Teller distortions in mono-, di- and tetramethyl substituted cyclopropyl radical cations. In all cases, the ground state of the corresponding radical cation can be considered to be derived from a  ${}^2A_1$ -type state and (the) transition state(s) of pseudorotation from (a)  ${}^2B_2$ -type state(s). Several minima and transition states were found along the pseudorotation path where the most stable form corresponds to an asymmetrical  ${}^2A_1$ -type state.

The possible existence of a trimethylene radical cation was investigated as a reaction to claims by experimentalists that this cation had been observed in the ring-opening reaction of the cyclopropyl radical cation<sup>236,237</sup>. Borden and coworkers<sup>227</sup> calculated the energy difference between these two radical cations to be as large as 19 kcal mol<sup>-1</sup> with little chance to observe the trimethylene radical cation on the  $C_3H_6^{+}$  potential energy surface. UMP2 calculations suggest that the cyclopropane radical cation can rearrange to the propane radical cation in two stages [barrier: 19 kcal mol<sup>-1</sup>, reaction energy: -10.3 kcal mol<sup>-1</sup> at UMP2/6-31G(d) + zero point energy corrections]: (a) ring opening via a conrotatory transition state and (b) migration of a H atom (with just a 0.2 kcal mol<sup>-1</sup> barrier).

#### D. Cyclopropyl Cation

The cyclopropyl cation (**34**) corresponds to a stationary point on the  $C_3H_5^+$  potential energy surface<sup>238,239</sup>, the global minimum of which is occupied by the allyl cation (**35**). Table 26 summarizes relative energies of various  $C_3H_5^+$  isomers (**34–39**) that were investigated at the HF, MP2 and MP4(SDQ) levels of theory<sup>238</sup>. Cation **34** is about 36 kcal mol<sup>-1</sup> less

TABLE 26. Relative energies (kcal mol<sup>-1</sup>) of cyclopropyl cation and other C<sub>3</sub>H<sub>5</sub><sup>+</sup> cations<sup>238</sup>

Cation	Sym	HF/6-31G(d,p) //HF/6-31G(d)	MP2/6-31G(d,p) //HF/6-31G(d)	MP4(SDQ)/6-31G(d,p) <sup>a</sup> //HF/6-31G(d)
Cyclopropyl (34)	C <sub>2v</sub>	37.8	37.0	35.0
Allyl (35)	C <sub>2v</sub>	0	0	0
Perpendicular allyl (36)	C <sub>s</sub>	33.7	37.7	34.9
2-Propenyl (37)	C <sub>s</sub>	16.1	14.2	11.6
1-Propenyl (38)	C <sub>s</sub>	32.3	33.1	30.2
Corner protonated cyclopropene (39)	C <sub>s</sub>	42.6	30.9	33.6

<sup>a</sup> Estimated from MP4(SDQ)/6-31G(d) values.

stable than cation **35**, 2 kcal mol<sup>-1</sup> less stable than corner protonated cyclopropene (**39**) and 1 kcal mol<sup>-1</sup> less stable than the perpendicular allyl cation (**36**). It has been speculated that **34** is the transition state for the stereomutation of the planar allyl cation<sup>238</sup>. This is confirmed by MP2/6-31G(d,p) calculations<sup>240</sup>, which show that the cyclopropyl cation is located at a first-order transition state possessing one imaginary frequency of *b*<sub>1</sub> symmetry that describes a disrotatory movement of the CH<sub>2</sub> groups in line with a stereomutation process of the allyl cation. Alternatively, stereomutation can also follow a stepwise route via perpendicular allyl cations **36** that are somewhat more stable than **34** (Table 26) and therefore lead to lower stereomutation barriers<sup>238</sup>.

In Figure 25, geometries and relative stabilities of some 1-substituted cyclopropyl cations are compared with the corresponding 2-allyl cations according to HF/6-31G(d)//HF/3-21G results of Lien and Hopkinson<sup>239</sup>. In all cases, the vicinal bond C<sup>+</sup>C bonds (1.43–1.46 Å) are much shorter than the distal CC bond (1.52–1.58 Å). Increase of the positive charge at C1 caused by electron-withdrawing substituents (e.g. F or CN) leads to shortening of vicinal and lengthening of the distal bond, which is in line with an increase in ring strain as a result of increased s-character at C1 and a stretching of the distal bond. Electron-donating substituents have the opposite effect and stabilize the ring.

Of the substituents considered in Figure 25, The amino group is the strongest  $\pi$ -donor and, not surprisingly, the  $\alpha$ -aminocyclopropyl cation is more stable than the 2-aminoallyl cation by 23.4 kcal mol<sup>-1</sup> at the HF/6-31G(d)//HF/3-21G level of theory. This is in line with



the observation and characterization of  $\alpha$ -dimethylamino- and  $\alpha$ -methylaminocyclopropyl cations by NMR spectroscopy<sup>241-243</sup>.

Stabilization of **34** by a hydroxy group is smaller, as is suggested by the small energy difference of 1.3 kcal mol<sup>-1</sup> between  $\alpha$ -hydroxycyclopropyl and 2-hydroxyallyl cation in favour of the latter cation (see Figure 25). Experimentally, the  $\alpha$ -methoxycyclopropyl cation appears to be a stable intermediate in substitution reactions in solution<sup>244</sup>, and there is evidence for the independent existence of both the  $\alpha$ -methoxycyclopropyl and 2-methoxyallyl cations in the gas phase<sup>245</sup>.

## XII. THE CYCLOPROPYL RADICAL

The CH bond dissociation enthalpy DH of **1** is 106.3 kcal mol<sup>-1</sup>, which is 11.2 kcal mol<sup>-1</sup> larger than that of the secondary CH bond of propane (95.1 kcal mol<sup>-1</sup>)<sup>89a</sup>. At the UMP2/6-31G(d) level, a dissociation energy DE of 107.7 kcal mol<sup>-1</sup> is calculated, which can be improved by using isogyric reactions (the number of unpaired electron spins is preserved) such as equation 21:



provided the dissociation energy (enthalpy) of the reaction given in equation 22:



is known exactly (e.g. R'H = H<sub>3</sub>CH, Table 27) and can be used to derive DE values for RH from the calculated reaction energy of reaction 21.

TABLE 27. CH dissociation enthalpies DH(298) and changes in CH dissociation enthalpies ( $\Delta$ DH) and energies ( $\Delta$ DE) of cyclopropane and various small hydrocarbons according to the reaction<sup>a</sup>:

$\text{R}-\text{H} + \text{CH}_3\cdot \longrightarrow \text{R}\cdot + \text{CH}_4$					
Radical-H	DH <sup>b</sup>	$\Delta$ DH <sup>b</sup>	$\Delta$ DH <sup>c</sup>	$\Delta$ DH <sup>d</sup>	$\Delta$ DE <sup>e</sup>
Methyl-H	105.1 $\pm$ 0.2	0	0	0	0
Ethyl-H	98.2 $\pm$ 1	-6.9	-4.6	-3.6	-3.6
<i>n</i> -Propyl-H	97.9 $\pm$ 1	-7.2	-4.0	-3.6	-3.5
<i>i</i> -Propyl-H	95.1 $\pm$ 1	-10.0	-5.8	-6.2	-6.8
Cyclopropyl-H	106.3 $\pm$ 0.3	1.2		5.2	3.2
Cyclobutyl-H	96.5 $\pm$ 1	-8.6		-3.1	
Cyclopentyl-H	94.5 $\pm$ 1	-10.6			
Cyclohexyl-H	95.5 $\pm$ 1	-9.6			
Vinyl-H	110 $\pm$ 2	4.9		5.2	10.4
Phenyl-H	110.9 $\pm$ 2	5.8		6.3	

<sup>a</sup> All energies in kcal mol<sup>-1</sup>.

<sup>b</sup> Reference 89a.

<sup>c</sup> Reference 89c.

<sup>d</sup> Reference 165.

<sup>e</sup> Reference 76a.

In Table 27, CH dissociation enthalpies and differences of DH or DE values are compared<sup>89, 165, 76a</sup>. They clearly confirm that CH dissociation for **1** requires a significantly larger energy (up to 11 kcal mol<sup>-1</sup>) than for other cycloalkanes or propane. It is just 4 kcal mol<sup>-1</sup> smaller than the CH dissociation enthalpy for ethene or benzene, as can be seen from the

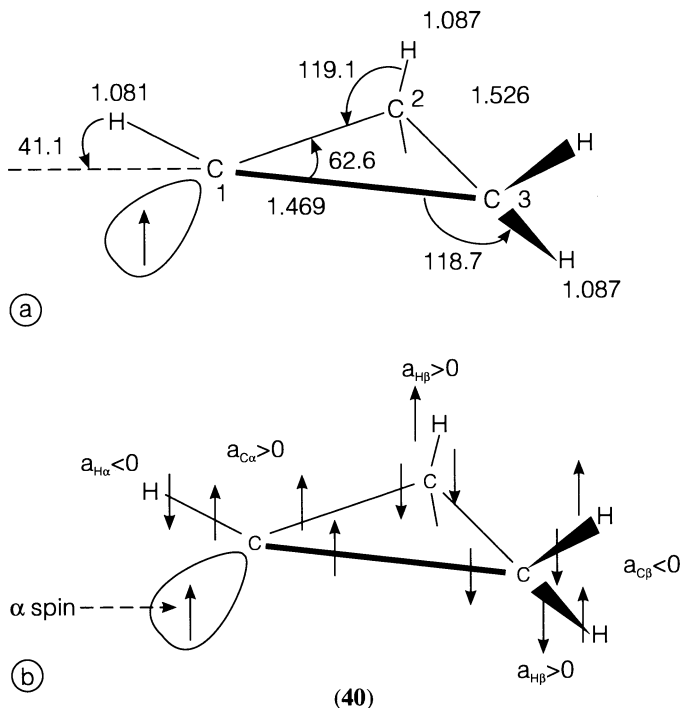


FIGURE 26 (a) MP2/6-31G(d) geometry of the cyclopropyl radical **40** according to Reference 246. (b) Spin-coupling scheme of the cyclopropyl radical according to the 'intra-atomic Hund rule' and spin coupling within bonds. Hyperfine splitting  $a_N$  at nucleus N will be  $> 0$  ( $< 0$ ) if valence electrons at N possess  $\alpha$  ( $\beta$ ) spin

data in Table 27. The relatively large value of the CH dissociation energy of **1** may partially reflect the strengthening of the CH bond, but as to the major part, it simply reflects the increase in strain energy when going to the cyclopropyl radical (**40**). In general, an alkyl radical prefers a planar trigonal geometry with bonding angles of  $120^\circ$  at the radical centre. Reduction of these angles to  $60^\circ$  in the cyclopropyl radical costs much more energy than reduction from a tetrahedral angle ( $109.5^\circ$ ) to a CCC angle to  $60^\circ$  in **1**.

This is also the reason why the cyclopropyl radical prefers a non-planar rather than a planar geometry at the radical centre. A pyramidalization angle of  $41^\circ$  has been calculated for **40** (Figure 26)<sup>246-250</sup>, which indicates a  $17^\circ$  decrease compared to the corresponding angle for **1** [ $57.1^\circ = \frac{1}{2} \alpha_c(\text{HCH})$ ]; see the MP2/6-31G(d) value in Table 11]. Hence, the s-character of the CC hybrid orbitals increases at the radical centre, thus causing a widening of the C2C1C3 angle ( $62.6^\circ$ ), shortening of the vicinal bonds (1.469 Å), lengthening of the distal bond C2C3 (1.526 Å) and increased ring strain. One can also view **40** as a derivative of **1**, which has lost an electron from the highest CH bonding MO. This is the  $\pi(\text{CH}_2)$  MO #9, which has C1C2 antibonding and C2C3 bonding character (see Figure 6, Section III.A). Accordingly, removal of an electron (as caused by an extremely strong  $\sigma$ -electron acceptor; see Section VI. B, Table 14) leads to shortening of the vicinal and lengthening of the distal CC bond.

Barone and coworkers<sup>250</sup> have investigated the inversion potential of **40** using UHF in connection with MP2, MP3, MP4, QCISD(T) correlation methods and a Huzinaga–Dunning DZ + P basis. At the highest level of theory [QCISD(T)/DZ + P], they calculated an inversion barrier of 3.66 kcal mol<sup>-1</sup>, which is somewhat larger than the inversion barrier measured for the methylcyclopropyl radical (3.11 kcal mol<sup>-1</sup><sup>251</sup>). Barone and coworkers also calculated the vibrational levels of the inverting cyclopropyl radical by treating the C1–H movement with a one-dimensional Schrödinger equation. In this way, they determined splitting of vibrational levels below the barrier top (H tunneling) ( $\nu = 0$ : 1.1 cm<sup>-1</sup>;  $\nu = 1$ : 35.9 cm<sup>-1</sup>), rate constant for inversion at 344 K ( $4 \times 10^{11}$  s<sup>-1</sup>; estimate derived from trapping experiments: 1012 s<sup>-1</sup><sup>252</sup>) and the true inversion barrier that measures from the ground vibrational level ( $\nu = 0$ ) to the first vibrational level above the barrier top ( $\nu = 2$ ). The latter value was calculated to be 3.06 kcal mol<sup>-1</sup>, in much better agreement with the experimental value of 3.11 kcal mol<sup>-1</sup> for the methylcyclopropyl radical<sup>251</sup>.

Barone and coworkers<sup>250</sup> also determined EPR hyperfine splittings  $a_N$  of the radical **40** at the UMP2/DZ + P level of theory using the Fermi contact operator and a finite field method with an increment size of 0.001 a.u. Expectation values of  $a_N$ ,  $\langle a_N \rangle$ , at higher temperatures  $T$  were calculated by assuming a Boltzmann population of vibrational levels according to equation 23:

$$\langle a \rangle_T = \sum_{j=0} \langle a \rangle_j \exp[(\epsilon_0 - \epsilon_j)/k_B T] / \sum_{j=0} \exp[(\epsilon_0 - \epsilon_j)/k_B T] \quad (23)$$

with  $k_B$  being the Boltzmann constant and  $\epsilon_j$  corresponding to the energies of the vibrational levels. In this way, the data in Table 28 were obtained, and clearly show that vibrational averaging generally improves the agreement between computed experimental hyperfine splittings  $a_N$ <sup>250</sup>.

TABLE 28. Isotropic hyperfine splittings (Gauss) of the cyclopropyl radical computed at the UMP2/DZ + P level<sup>250</sup>

Atom	$a_N$ (min)	$\langle a_N \rangle_{0+}$	$\langle a_N \rangle_{0-}$	$\langle a_N \rangle_{1+}$	$\langle a_N \rangle_{1-}$	$\langle a_N \rangle_2$	$\langle a_N \rangle_{T=302}$	$a_N$ (exp) <sup>b</sup>
H <sup>x</sup>	-5.7	-7.6	-7.5	-13.9	-11.1	-18.5	-7.8	-6.7
H <sup><math>\beta</math></sup>	18.2 <sup>a</sup>	18.8	18.8	21.0	19.9	22.6	18.9	23.5
C <sup><math>\alpha</math></sup>	116.9	111.1	111.5	91.5	101.0	77.5	77.5	95.9
C <sup><math>\beta</math></sup>	-7.3	-7.6	-7.6	-8.8	-8.3	-9.8	-9.8	—

<sup>a</sup> Mean between *syn* and *anti* values.

<sup>b</sup> Experimental values obtained at  $T = 77$  K (H <sup>$\alpha$</sup>  and H <sup>$\beta$</sup> ) and  $T = 203$  K (C <sup>$\alpha$</sup>  and C <sup>$\beta$</sup> ). From Reference 252.

Considering the spin coupling scheme shown in Figure 26, the signs of the hyperfine splittings result from (a) spin alignment according to an 'intra-atomic Hund rule'<sup>253</sup> and (b) spin coupling within a bond. The low negative value of  $a_{H\alpha}$  ( $-6.7$  G<sup>252</sup>, for methyl radical  $a_H = -23$  G<sup>253</sup>) and the relatively large positive value of  $a_{C\alpha}$  (95.9 G<sup>252</sup>, for methyl radical  $a_C = 38$  G<sup>252</sup>) confirm the pyramidal geometry at C <sup>$\alpha$</sup>  and provide a rough estimate of the inversion barrier<sup>252</sup>.

Experimental  $a_N$  values have been obtained at  $T = 77$  K<sup>252b, c</sup> (H <sup>$\alpha$</sup>  and H <sup>$\beta$</sup> ) and  $T = 203$  K<sup>252a</sup> (C <sup>$\alpha$</sup>  and C <sup>$\beta$</sup> ). They do not show any significant  $T$  dependence up to 220 K, which is in line with expectation value calculations between 0 and 200 K (Table 28). For temperatures considerably larger than 200 K, higher vibrational levels are occupied that lead to considerable H tunneling ( $\nu = 1+$ ,  $1-$ ; Table 28) or a large amplitude vibration involving pyramidal and inverted radical form ( $\nu = 2$ ), thus decreasing the hyperfine coupling constant  $a_{H\alpha}$  and  $a_{C\alpha}$  to values typical of a planar alkyl radical.

Cometta-Morini, Ha and Oth<sup>246</sup> have investigated the vibrational spectra of cyclopropyl and allyl radicals using DZ + P basis sets at the UHF and UMP2 level. Calculated harmonic



frequencies were scaled according to different procedures involving measured and calculated vibrational frequencies of propene and **1**. The authors improved previous mode assignments<sup>247</sup> and related all calculated harmonic frequencies to frequencies of the experimental infrared spectrum that had been recorded by Holtzhauer and coworkers at 18 K in the argon matrix after photochemically induced ring closure of the allyl radical to radical **40**<sup>254</sup>.

The heats of formation for allyl and cyclopropyl radical are  $66.5 \pm 2.7$  and  $43.7 \pm 2.2$  kcal mol<sup>-1</sup>, which suggests an isomerization enthalpy of  $-22.8 \pm 4.9$  kcal mol<sup>-1</sup> for radical **40**<sup>255</sup>. The activation energy of the gas-phase thermolysis of **40** leading to the allyl radical was measured to be  $22 \pm 2$  kcal mol<sup>-1</sup><sup>256, 257</sup>. The reaction can proceed with the CH<sub>2</sub> groups moving in a disrotatory or conrotatory mode. Contrary to the ring opening of cyclopropyl cation or anion, neither Woodward–Hoffmann rules, orbital and state correlation diagrams nor PMO arguments make any valid prediction with regard to the preferred ring-opening mode. Therefore, Olivella, Sole and Bofill<sup>249</sup> have studied thermal ring opening of radical **40** into the allyl radical at the UHF and the CASSCF level of theory employing a 3-21G basis. The authors demonstrate that the reaction proceeds via a highly non-symmetric transition state with unequal vicinal bond lengths (1.424 and 1.485 Å at CASSCF/3-21G<sup>249</sup>) and one CH<sub>2</sub> group having rotated by about 24° while the other is still orthogonal to the ring plane. The CC bond, being broken, has a length of 2.066 Å in the transition state<sup>249</sup>. The rotation of the second CH<sub>2</sub> group takes place in the last phase of the ring-opening process after the distal bond is fully broken and the C1C2 π-bond is formed.

The non-synchronous rotation of the two methylene groups implies a common transition state for both disrotatory and conrotatory ring opening, which may split into different transition states under the impact of a substituent. CASSCF/3-21G and CASSCF/6-31G(d) calculations lead to reaction energies which are far too negative ( $< -30$  kcal mol<sup>-1</sup>) while UMP2/6-31G(d) predicts for this process a reaction energy of  $-20.2$  kcal mol<sup>-1</sup><sup>246</sup> in good agreement with experiment<sup>255</sup>. This reflects the importance of dynamic correlation corrections and the fact that the UHF wave function provides a reasonable description of radicals. Furthermore, Olivella and coworkers<sup>249</sup> show that quartet contamination of the UHF doublet wave function leads to some useful electron correlation that helps to obtain a reasonable transition state description at the UHF level. However, an accurate prediction of the transition state energy is only obtained at the CASSCF/6-31G(d)//CASSCF/3-21G level (3 electrons in 3 active orbitals leading to 8 doublet spin-adapted configuration state functions) after zero point energy corrections (21.9 kcal mol<sup>-1</sup>)<sup>249</sup>.

### XIII. FUSED CYCLOPROPANES

#### A. Bicyclo[1.1.0]butane

This is the most strained of all bicyclic alkanes<sup>79, 258, 259</sup>. Calculated geometries of bicyclobutane (Table 12, Section VI) indicate that the bridgehead (C1C3) bond length (1.47 Å) is significantly shorter than the CC bonds in **1** while other geometrical parameters are similar to the corresponding parameters in **1**. Dependence of calculated bond lengths on the applied theoretical method and basis set agree with trends described in Section VI.A for **1**. HF/4-31G leads to the longest CC bond lengths, while inclusion of polarization functions at the HF level results in considerable shortening of the CC bonds. MP2/6-31G(d) predicts somewhat longer bond lengths than those obtained at the HF/6-31(d) level. Apart from the C1C3 bond length, the experimental value of which should be questioned, the MP2/6-31G(d) geometry is in good agreement with experimental data.

The C1C3 bridgehead bond is the most strained part of the molecule (CSE = 68.6 kcal mol<sup>-1</sup><sup>258</sup>). According to Newton and Schulman<sup>260</sup>, it is formed from hybrid orbitals of nearly pure p character inclined at an angle of *ca* 30° with respect to the bond vector; a π char-

acter of 26% has been calculated for the central bond from localized bond hybrids. This early work is largely confirmed by electron density studies of Wiberg and coworkers<sup>79</sup>, who found that C1 (C3) carries a strong negative charge. This suggests strongly increased s-character and a large electronegativity of the bridgehead carbon<sup>79</sup>. Calculation of the atomic energies with the help of the virial partitioning method predicts the methylene groups rather than the CH groups to be more destabilized, which can be easily traced to a shift of electronic charge from the former to the latter [ $q(\text{CH}_2) = 0.068$ ,  $q(\text{CH}) = -0.067$ <sup>79</sup>]. This description, however, is not very helpful since it disguises the fact that the strain of the central bond dominates the chemical behaviour of bicyclobutane.

Jackson and Allen<sup>32</sup> calculated the difference electron density (see Section IV.A) of bicyclo[1.1.0]butane. They found that the maximum of positive difference density is displaced by about 0.35 Å from the C1C3 internuclear axis, which is significantly larger than the corresponding displacement calculated for cyclopropane (0.2 Å) and suggests increased bending for the central CC bond. These authors also noted that there is accumulation of charge in the non-bonded regions of the C1C3 bond, which supports the prediction that the C1C3 bond is formed by overlap of nearly pure p orbitals.

## B. [1.1.1]Propellane

[1.1.1]propellane possesses two bridgehead C atoms (C1, C3), for which all four bonds are on one side of a plane perpendicular to the C1C3 axis and containing the bridgehead C atom. Such C atoms have been termed inverted C atoms, which should lead to large molecular strain, high reactivity, peculiar bonding features and exceptional geometries. Nevertheless, it was possible to synthesize [1.1.1]propellane and to determine many of its properties<sup>14</sup>. The strain energy of [1.1.1]propellane (CSE = 98 kcal mol<sup>-1</sup><sup>14</sup>) is indeed much larger than the sum of the strain energies (81 kcal mol<sup>-1</sup>) of the three cyclopropane rings that constitute the molecule. Contrary to bicyclo[1.1.0]butane, the bridgehead distance C1C3 [1.592 Å at MP2/6-31G(d), Table 12] is longer in [1.1.1]propellane than the CC bond in **1** while the other CC bonds (C1C2) are similar to the CC bond in **1**. Comparing published *ab initio* geometries of [1.1.1]propellane listed in Table 12, it becomes obvious that the MP2/6-31G(d) geometry agrees best with the experimental geometry.

The most intriguing aspect of [1.1.1]propellane is the nature of the interactions between its bridgehead atoms C1 and C3<sup>32, 258, 261</sup>. Newton and Schulman<sup>261</sup> were the first to point out that the localized MO associated with the central CC bond (C1C3) is non-bonding or even antibonding in the centre of the molecule. Jackson and Allen<sup>32a</sup> compared the highest occupied  $\sigma(\text{CC})$  MO in eclipsed ethane, **1**, bicyclo[1.1.0]butane and [1.1.1]propellane and demonstrated that in each of these cases the CC MO has bonding and non-bonding components, but that the latter increase and become larger than the bonding components when going to [1.1.1]propellane. While a normal bonding  $\sigma(\text{CC})$  MO increases in energy upon CC stretching, the  $\sigma(\text{CC})$  MO of [1.1.1]propellane decreases in energy. The calculated difference electron density of its central CC bond is negative (loss of electron density) while there is a relatively large positive electron density in the non-bonding region<sup>32</sup>. This is in line with other calculations<sup>258</sup> and an X-ray study of Chakrabarti, Dunitz and coworkers<sup>262</sup> that also suggested charge loss in the region between formally bonded inverted C atoms. Inspection of the calculated difference electron density reminds one of two (almost parallel) p-type charge distributions in the non-bonding region of C1C3, which are connected by three filaments of positive difference electron density resulting from contributions of the three bridging CH<sub>2</sub> groups.

Although there seems to be no direct  $\sigma$ -type (along the C1C3 axis) and  $\pi$ -type bonding between the bridgehead C atoms,  $\sigma$ -components of the CH<sub>2</sub> groups lead to a (three fold)  $\sigma$ -bridged  $\pi$ -bond<sup>32</sup> as was already discussed in Section VI.C in connection with the bonding in three-membered rings. The  $\sigma$ -bridged  $\pi$ -bond is responsible for a close-to-normal CC

bond length and the relative low reactivity of [1.1.1]propellane with an estimated stability of  $65 \text{ kcal mol}^{-1}$  with regard to its singlet biradical<sup>125b</sup>.

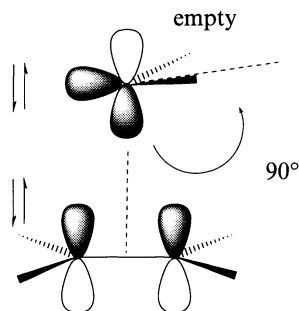
#### XIV. FORMATION AND REACTIVITY

An impressive amount of theoretical work has been carried out in recent years with regard to a computational description of reactions of **1**. We will consider here just some of the more important *ab initio* investigations and leave a detailed discussion of this work to the more specialized chapters in this volume.

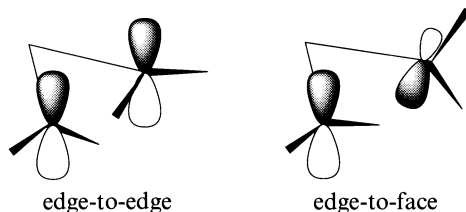
##### A. Formation Reactions

According to Woodward–Hoffmann rules, the addition of singlet methylene ( $^1A_1$ ) to alkene is symmetry-allowed in a  $C_s$  but not a  $C_{2v}$  symmetrical mode (see Scheme 6)<sup>263</sup>. The stereochemistry of the reacting alkene will be retained, thus leading to a stereospecific addition reaction. This has been confirmed by Zurawski and Kutzelnigg<sup>264</sup> on the basis of CEPA/DZ + P calculations. At large distances ( $> 1.8 \text{ \AA}$ ) the angle of approach is close to  $90^\circ$ . Electrons are transferred from ethene to methylene, which can be considered as an electrophile. At smaller distances, methylene becomes a nucleophile, which transfers electrons to the  $\pi^*$  MO of ethene. Zurawski and Kutzelnigg found no barrier for the reaction, i.e. ethene and singlet methylene form **1** in a strongly exothermic reaction [ $\Delta E(\text{CEPA/DZ} + \text{P}) = -109.2 \text{ kcal mol}^{-1}$  compared to an experimental value of  $\Delta_r H(298) = -105 \text{ kcal mol}^{-1}$ <sup>264</sup>]. An investigation on the addition of substituted carbenes to ethene was carried out by Rondan, Houk and Moss<sup>265</sup>, but the level of theory applied in this work was moderate (HF/STO-3G, HF/4-31G) and therefore results were of just qualitative value.

Moreno and coworkers<sup>266</sup> published a study on the triplet carbene–ethene addition reaction. This process should involve two steps, namely the formation of a triplet trimethylene 1,3-diradical as an intermediate followed by intersystem crossing and formation of **1**. The intermediate may live long enough to permit rotation at the CC bonds. In this way, the stereochemistry of the alkene will be lost and a non-stereospecific addition takes place. Moreno and coworkers<sup>266</sup> calculated for the first step of the reaction  $\text{CH}_2(^3B_2) + \text{H}_2\text{C} = \text{CH}_2$  a barrier of  $11 \text{ kcal mol}^{-1}$  and a reaction energy of  $-26 \text{ kcal mol}^{-1}$  at the MP2/3-21G level. (It has to be mentioned in this connection that the 3-21G basis is far too small to lead to reliable energies in correlation calculations and therefore results are just of a qualitative nature<sup>267</sup>.) Activation energies varied from 5 to  $17 \text{ kcal mol}^{-1}$  if  $\text{CH}_2$  was replaced by the triplet state of  $\text{CH}(\text{CN})$ ,  $\text{CH}(\text{BeH})$  and  $\text{CHLi}$ <sup>266</sup>.



SCHEME 6



SCHEME 7

## B. Thermal Ring-opening and Stereomutation Reactions

Both ring opening and isomerization to propene or stereomutation of **1** require activation energies of about 65 and 61 kcal mol<sup>-1</sup>, respectively<sup>268</sup>. They lead to an intermediate trimethylene singlet diradical that has attracted a lot of attention by quantum chemists because it represents a challenging test ground for *ab initio* methods involving multiple-configuration electronic states. Use of these methods has clarified that the trimethylene singlet diradical is not a stable intermediate, but that it can occur in various forms located in shallow minima along the reaction path of the stereomutation of **1**<sup>129, 132, 269–275</sup>.

The thermal stereomutation of **1** may involve one or more of the following three mechanistic possibilities: (a) rotation of a single methylene group (Smith mechanism<sup>276</sup>), (b) cleavage of a CC bond to give a trimethylene diradical intermediate in which random loss of stereochemistry is competitive with ring closure (Benson mechanism<sup>277</sup>), (c) coupled, simultaneous rotation of two methylene groups (Hoffmann mechanism<sup>263</sup>). Independent investigations by Yamaguchi, Schaefer and Baldwin<sup>132</sup> (TCSCF/TZ + 2P and CISD+Q/TZ + 2P calculations) as well as Getty, Davidson and Borden<sup>275</sup> [GVB/6-31G(d) and CISD/6-31G(d) calculations] revealed that the potential energy surface for methylene group rotation is actually much more complicated than previously believed. Both the edge-to-edge and edge-to-face conformers (Scheme 7) of the trimethylene radical are second-order transition states (hilltops in a two-dimensional space spanned by the methylene torsion angles), which are surrounded by eight (in the case of the edge-to-edge form) and two (in the case of the edge-to-face form) stationary points of lower order (minima and first-order transition states) as is shown in Figure 27<sup>275</sup>. However, differences between the energies of the stationary points are small so that one can expect that better methods and basis sets may lead to somewhat different pictures.

The barrier for stereomutation is calculated to be close to 61 kcal mol<sup>-1</sup> (CISD+Q/TZ + 2P)<sup>132, 275</sup>. Conrotatory double rotation of the methylene groups is about 1 kcal mol<sup>-1</sup> more favourable than single rotation of a methylene group. Calculations further reveal that disrotatory rotation is also possible with a barrier 0.5 kcal mol<sup>-1</sup> larger than conrotatory rotation (Figure 27).

## C. Electrophilic Ring-opening Reactions and Insertion Reactions

Electrophilic ring opening of **1** has been studied extensively experimentally and theoretically<sup>18</sup>. The simplest electrophilic ring-opening reaction is protonation of **1**, which has already been discussed in Section XI.B. The first step in this process leads to corner protonated **1**, which decomposes via a transition state with 1-propyl cation structure and subsequent H migration to form the 2-propyl cation (calculated barrier: 12.1 kcal mol<sup>-1</sup><sup>223</sup>). Edge protonated **1** is not necessarily involved in this process since its relative energy (with regard to corner protonated **1**) is 1.4 kcal mol<sup>-1</sup> and since it may correspond to a transition state (of H scrambling) rather than an energy minimum<sup>223</sup>.

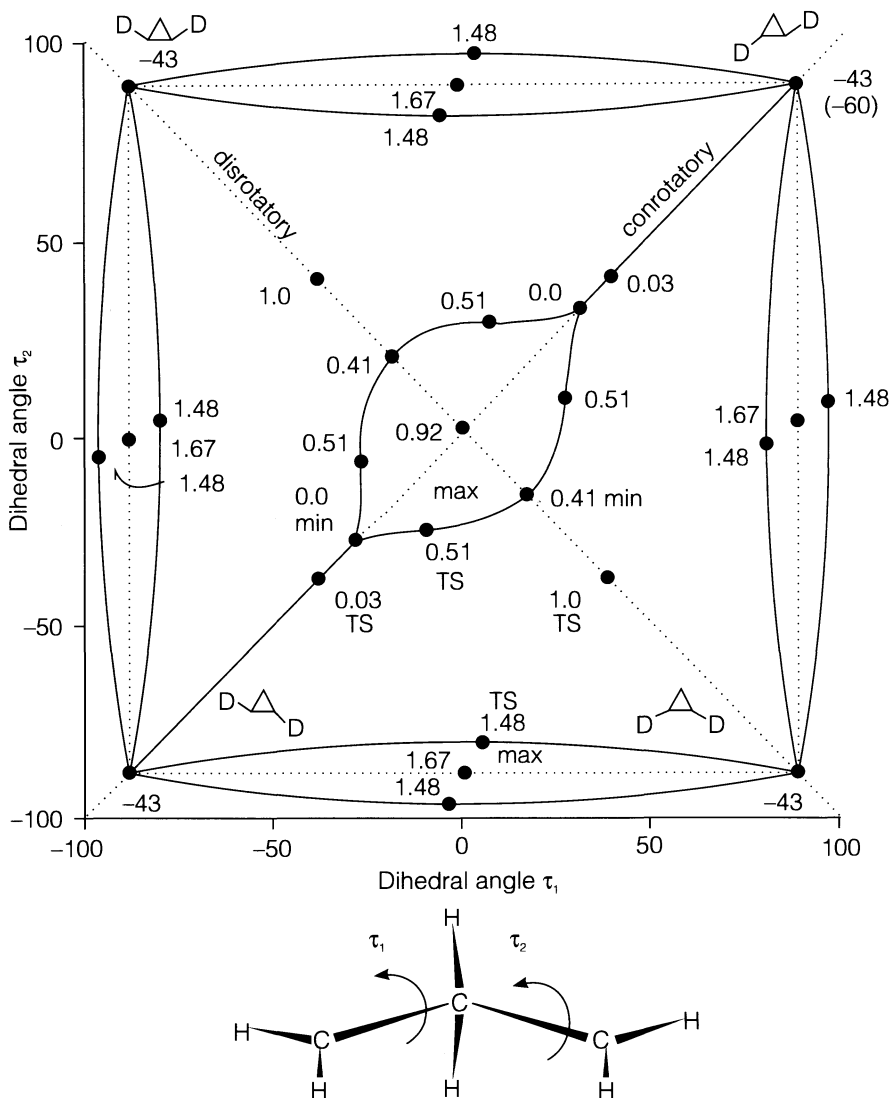


FIGURE 27. Schematic description of the potential energy surface (PES) of cyclopropane-trimethylene in terms of the two dihedral angles  $\tau_1$  and  $\tau_2$  according to GVB/6-31G(d) calculations by S. J. Getty, E. R. Davidson and W. T. Borden (Reference 275). Deuterated cyclopropane forms are shown to indicate the stereochemistry of the possible stereomutation routes (conrotatory and disrotatory) connecting the four cyclopropane forms in the  $\tau_1, \tau_2$  space shown. For each calculated stationary point (•) on the  $\tau_1, \tau_2$  PES, relative energy (in kcal mol<sup>-1</sup>) and character of the stationary point (min: minimum; max: maximum; TS: transition state) are given. Reference energy is the energy of the most stable trimethylene form with  $\tau_1 = \tau_2 = 30.6^\circ$ . Note that at the GVB level the stability of cyclopropane is underestimated by about 18 kcal mol<sup>-1</sup>. The most likely reaction paths in  $\tau_1, \tau_2$  space for cyclopropane stereomutation are given by solid lines. Note that both the edge-to-edge ( $\tau_1 = \tau_2 = 0^\circ$ ) and the edge-to-face [ $\tau_1 = 0^\circ (\pm 90^\circ), \tau_2 = \pm 90^\circ (0^\circ)$ ] conformers correspond to small local maxima on the  $\tau_1, \tau_2$  PES.

Electrophilic attack by halonium ions  $X^+$  may occur in a completely different manner according to HF and MP2 investigations of Yamabe and coworkers<sup>278</sup>, who found edge rather than corner attack the preferred reaction mode in the case of  $X^+$ . For  $X^+ = Cl^+$  or  $Br^+$ , a four-membered ring is formed which is more stable by about 20 kcal mol<sup>-1</sup> than corner complexed  $C_3H_6X^+$ . The authors explained this preference with possible charge transfer interactions between the p orbitals of  $X^+$  and the 3e' HOMOs (Figure 6, MOs #11, 12,  $w_A$  and  $w_S$ ) either in a  $\sigma$ -bridge or  $\pi$ -bridge fashion (establishing a two-fold  $\sigma$ -bridged and  $\pi$ -bridged orbital, respectively; see Sections VI.C and XII.B).

Upon attack by a nucleophile, the four-membered ring collapses in a zig-zag manner into a 3-halopropyl derivative. Alternatively, the four-membered ring can open by rotation and then react with an approaching nucleophile. Calculated energy barriers should be comparable according to modelling the reaction in the absence of nucleophile. Since the authors also investigated protonation of **1**, an assessment of the accuracy of their calculations can be made by comparison with the MP4/TZ + P calculations by Koch, Liu and Schleyer<sup>223</sup>. The latter authors obtained for edge protonated **1**, a relative energy of 1.4 kcal mol<sup>-1</sup> while Yamabe and coworkers get 12.3 kcal mol<sup>-1</sup><sup>278</sup>.

Ring opening by metals or metal complexes seems to proceed by a similar mechanism. Alex and Clark<sup>279</sup> studied ring opening and isomerization of **1** catalysed by complexation with the Be radical cation. They used the 6-31G(d) basis and various methods ranging from projected UHF to projected UMP4 and to QCISD(T). According to their computational results, the reaction leads in the first step to an edge oriented  $Be^{+}$ -cyclopropane complex ( $\Delta E = -57$  kcal mol<sup>-1</sup>), which rearranges in an endothermic step ( $\Delta E = 12.3$  kcal mol<sup>-1</sup>,  $\Delta E = 29$  kcal mol<sup>-1</sup>) to a metallacyclobutane radical cation intermediate (in line with results obtained for  $X^+$  attack<sup>278</sup>). From this intermediate, isomerization to a propene- $Be^{+}$  complex or CC bond cleavage forming a carbene-ethene- $Be^{+}$  can occur. Parallels to transition metal catalysis of the ring opening of **1** were observed<sup>279</sup>.

Ring opening by palladium(II) compounds ( $PdCl_2$ ,  $PdCl_4^{2-}$ ,  $PdCl^+$ ) were directly investigated by Blomberg, Siegbahn and Bäckvall<sup>280</sup> using CASSCF and contracted CI calculations. These authors found that the Pd compound prefers a corner attack, especially if it has the possibility of ionizing into a cationic complex. Hence, for  $PdCl^+$  an activation energy of just 5 kcal mol<sup>-1</sup> was estimated while edge activation should require about 25 kcal mol<sup>-1</sup>. In the case of Pd(0), edge activation (activation energy 17 kcal mol<sup>-1</sup>) leading to palladacyclobutane was calculated to be more favourable than corner attack (activation energy 30 kcal mol<sup>-1</sup>)<sup>281</sup>. For  $PdCl_2$  and  $PdCl_4^{2-}$ , very high barriers (25–45 kcal mol<sup>-1</sup>) were found for both corner and edge activation<sup>280</sup>. It was argued that the energy differences between the different modes of attack are directly related to excitation energies of the atomic states of Pd involved.

Gano, Gordon and Boatz<sup>282</sup> investigated singlet methylene and silylene insertion into **1** using the 3-21G\* basis at the HF, MP2, MP3, and MP4 level of theory. At the highest level of theory, activation barriers of 2.3 and 20 kcal mol<sup>-1</sup> were obtained for  $CH_2(^1A_1)$  and  $SiH_2(^1A_1)$  insertion. These values were about 40 kcal mol<sup>-1</sup> lower than for the corresponding ethane insertion reactions. Clearly, it is much easier to insert methylene or silylene in a strained rather than an unstrained bond. A similar observation was made by Siegbahn and Blomberg<sup>283</sup>, who studied a large number of transition metal insertion reactions including as reagents ethane, cyclopropane and cyclobutane. The authors used a variety of methods [CASSCF, coupled pair functional methods, CCSD(T)] and a (17s13p9d3f/9s5p1d/5s1p)[7s6p4d1f/3s2p1d/3s1p] basis set. Palladium was found to insert into **1** without any barrier while calculated barriers for ethane and cyclobutane were 23 and 7 kcal mol<sup>-1</sup><sup>283</sup>.

The work of recent years clearly indicates that many puzzles of the chemistry connected with **1** have already been solved with the aid of modern *ab initio* calculations. Many more mechanistic questions will be solved in the near future provided a quantum chemist spends enough time and computer sources to carry out the necessary *ab initio* calculations. In par-

tical, the routine calculation of equilibrium geometries combined with the determination of vibrational frequencies at relatively high levels of theory helps to avoid previous confusion that was caused by the discussion of first- or even second-order transition states as stable reaction intermediates. Important steps have already been made in the area of reactions with transition metal complexes and further *ab initio* work in this area will open new synthetic routes for experimentalists.

## XV. ACKNOWLEDGEMENTS

This work was supported by the Swedish Natural Science Research Council (NFR). K.J. Szabo thanks the NFR for a postdoctoral stipend. All calculations needed to complement data from the literature were done on the CRAY YMP/416 of the Nationellt Superdatorcentrum (NSC), Linköping, Sweden. The authors thank Z. Konkoli, L. Olsson and A. Larsson for technical assistance with the calculations and the NSC for a generous allotment of computer time.

## XVI. REFERENCES

1. M. Charton, in *The Chemistry of Alkenes: Olefinic Properties of Cyclopropanes* (Ed. J. Zabicky), Vol.2, Wiley, New York, 1970.
2. D. Wendisch, in *Methoden der Organischen Chemie*, Vol. IV, 3, E. Houben-Weyl-Müller, Thieme Verlag, Stuttgart, 1971, p. 17.
3. A. De Meijere, *Angew. Chem.*, **91**, 867 (1979); *Angew. Chem., Int. Ed. Engl.*, **18**, 809 (1979).
4. R. Gleiter, *Top. Curr. Chem.*, **86**, 197 (1979).
5. (a) J. F. Liebman and A. Greenberg, *Chem. Rev.*, **76**, 311 (1976).  
(b) J. L. Franklin, *Ind. Eng. Chem.*, **41**, 1070 (1949).  
(c) D. Van Vechten and J. F. Liebman, *Isr. J. Chem.*, **21**, 105 (1981).
6. W. A. Lathan, L. Radom, P. C. Hariharan, W. J. Hehre and J. A. Pople, *Top. Curr. Chem.*, **40**, 1 (1973).
7. M. D. Newton, in *Modern Theoretical Chemistry* (Ed. H.F. Schaefer III), Vol. 4, Plenum Press, New York, 1977, p. 223.
8. (a) M. J. S. Dewar, *J. Am. Chem. Soc.*, **106**, 669 (1984).  
(b) M. J. S. Dewar, *Bull. Soc. Chim. Belg.*, **88**, 957 (1979).  
(c) M. J. S. Dewar and M. L. McKee, *Pure Appl. Chem.*, **52**, 1431 (1980).
9. D. Cremer and E. Kraka, *J. Am. Chem. Soc.*, **107**, 3800 (1985).
10. D. Cremer and J. Gauss, *J. Am. Chem. Soc.*, **108**, 7467 (1986).
11. D. Cremer and E. Kraka, in *Molecular Structure and Energetics* (Eds. J. F. Liebman and A. Greenberg), Vol. 7, VCH Publishers, Deerfield Beach, 1988, p. 65.
12. D. Cremer, *Tetrahedron*, **44**, 7427 (1988).
13. E. Kraka and D. Cremer, in *Theoretical Models of Chemical Bonding, Part 2: The Concept of the Chemical Bond* (Ed. Z. B. Maksic), Springer-Verlag, Heidelberg, 1990, p. 453.
14. K. B. Wiberg, in *The Chemistry of the Cyclopropyl Group* (Ed. Z. Rappoport), Wiley, New York, 1987, p. 1.
15. W. Runge, in *The Chemistry of the Cyclopropyl Group* (Ed. Z. Rappoport), Wiley, New York, 1987, p. 28.
16. D. G. Morris, in *The Chemistry of the Cyclopropyl Group* (Ed. Z. Rappoport), Wiley, New York, 1987, p. 101.
17. R. E. Ballard, in *The Chemistry of the Cyclopropyl Group* (Ed. Z. Rappoport), Wiley, New York, 1987, p.213.
18. M. A. Battiste and J. M. Coxon, in *The Chemistry of the Cyclopropyl Group* (Ed. Z. Rappoport), Wiley, New York, 1987, p. 255.
19. T. T. Tidwell, in *The Chemistry of the Cyclopropyl Group* (Ed. Z. Rappoport), Wiley, New York, 1987, p. 565.
20. For a balanced account of these concepts, see V. I. Minkin, M.N. Glukhovtsev and B. Ya. Simkin, *Aromaticity and Antiaromaticity, Electronic and Structural Aspects*, Wiley, New York, 1994.

21. (a) J. B. Collins, J. D. Dill, E. D. Jemmis, Y. Apeloig, P. v. R. Schleyer, R. Seeger and J. A. Pople, *J. Am. Chem. Soc.*, **98**, 5419 (1976).  
(b) For a summary see: W. J. Hehre, L. Radom, P. v. R. Schleyer and J. A. Pople, *Ab initio Molecular Orbital Theory*, Wiley, New York, 1986.
22. K. Krogh-Jespersen, D. Cremer, D. Poppinger, J. A. Pople, P. v. R. Schleyer and J. Chandrasekhar, *J. Am. Chem. Soc.*, **101**, 4843 (1979).
23. C. A. Coulson and W. E. Moffitt, *Philos. Mag.*, **40**, 1 (1949).
24. T. Förster, *Z. Phys. Chem. B*, **43**, 58 (1939).
25. A. D. Walsh, *Trans. Faraday Soc.*, **45**, 179 (1949).
26. (a) R. Hoffmann, *Tetrahedron Lett.*, 2907 (1970).  
(b) R. Hoffmann and R. B. Davidson, *J. Am. Chem. Soc.*, **93**, 5699 (1971).  
(c) R. Hoffmann, *Special Lectures of the XXIIIrd International Congress of Pure and Applied Chemistry*, Vol. 2, Butterworths, London, 1971, p. 233.  
(d) R. Hoffmann, H. Fujimoto, J. R. Swenson and C.-C. Wan, *J. Am. Chem. Soc.*, **95**, 7644 (1973).
27. H. Günther, *Tetrahedron Lett.*, 5173 (1970).
28. R. Hoffmann and W.-D. Stohrer, *J. Am. Chem. Soc.*, **93**, 6941 (1971).
29. C. W. Jorgensen and L. Salem, *The Organic Chemist's Book of Orbitals*, Academic Press, New York, 1973.
30. R. F. Hout, Jr., W. J. Pietro and W. J. Hehre, in *A Pictorial Approach to Molecular Structure and Reactivity*, Wiley, New York, 1984.
31. (a) E. Honegger, E. Heilbronner, A. Schmelzer and W. Jian-Qi, *Isr. J. Chem.*, **22**, 3 (1982).  
(b) E. Honegger, E. Heilbronner and A. Schmelzer, *Nouv. J. Chim.*, **6**, 519 (1982).
32. (a) J. E. Jackson and L. C. Allen, *J. Am. Chem. Soc.*, **106**, 591 (1984).  
(b) D. B. Kitchen, J. E. Jackson and L. C. Allen, *J. Am. Chem. Soc.*, **112**, 3408 (1990).  
(c) C. Liang and L. C. Allen, *J. Am. Chem. Soc.*, **113**, 1878 (1991).
33. T. Clark, G. W. Spitznagel, R. Klose and P. v. R. Schleyer, *J. Am. Chem. Soc.*, **106**, 4412 (1984).
34. (a) M. J. S. Dewar, *Nature*, **156**, 748 (1945).  
(b) M. J. S. Dewar, *J. Chem. Soc.*, **406**, 777 (1946).
35. A. D. Walsh, *Nature*, **159**, 167, 712 (1947).
36. M. J. S. Dewar, *Bull. Soc. Chim. Fr.*, C71 (1951).
37. M. J. S. Dewar and A. P. Marchand, *Annu. Rev. Phys. Chem.*, **16**, 321 (1965).
38. J. Chatt and L. A. Duncanson, *J. Am. Chem. Soc.*, **75**, 2939 (1953).
39. E. Kochanski and J. M. Lehn, *Theor. Chim. Acta*, **14**, 281 (1969).
40. R. Hoffmann, H. Fujimoto, J. R. Swenson and C.-C. Wan, *J. Am. Chem. Soc.*, **95**, 7644 (1973).
41. M.-M. Rohmer and B. Roos, *J. Am. Chem. Soc.*, **97**, 2025 (1975).
42. G. L. Delker, Y. Wang, G. D. Stucky, L. R. Lambert, Jr., C. K. Haas and D. Seyferth, *J. Am. Chem. Soc.*, **98**, 1779 (1976).
43. M. J. S. Dewar and G. P. Ford, *J. Am. Chem. Soc.*, **101**, 183 (1979).
44. H. B. Yokelson, A. J. Millevolte, G. R. Gillette and R. West, *J. Am. Chem. Soc.*, **109**, 6865 (1987).
45. M. Randić and Z. B. Maksic, *Theor. Chim. Acta*, **3**, 59 (1965).
46. (a) J. Wardeiner, W. Luettker, R. Bergholz and R. Machinek, *Angew. Chem., Int. Ed. Engl.*, **94**, 872 (1982).  
(b) For a discussion of hybrid orbitals see: W. A. Bingel and W. Luettker, *Angew. Chem., Int. Ed. Engl.*, **20**, 899 (1981).
47. S. Inagaki, Y. Ishitani and T. Kakefu, *J. Am. Chem. Soc.*, **116**, 5954 (1994).
48. (a) J. M. Foster and S. F. Boys, *Rev. Mod. Phys.*, **32**, 300 (1960).  
(b) S. F. Boys, in *Localized Orbitals and Localized Adjustment Functions in Quantum Theory of Atoms, Molecules and the Solid State* (Ed. P. O. Löwdin), Academic Press, New York, 1966, p. 253.
49. N. Mueller and D. E. Pritchard, *Chem. Phys.*, **31**, 1471 (1959).
50. J. G. Hamilton and W. E. Palke, *J. Am. Chem. Soc.*, **116**, 4159 (1994).
51. P. B. Karadakov, J. Gerratt, D. L. Cooper and M. Raimondi, *J. Am. Chem. Soc.*, **116**, 7714 (1994).
52. E. Goldstein, S. Vijaya and G. A. Segal, *J. Am. Chem. Soc.*, **102**, 6198 (1980).
53. H. Basch, M. B. Robin, N. A. Kuebler, C. Baker and D. W. Turner, *J. Chem. Phys.*, **51**, 52 (1969).
54. (a) A. Skancke, *J. Mol. Struct.*, **30**, 95 (1976).  
(b) For ionization potential calculations based on the Koopmans theorem, see also J. Kao and L. Radom, *J. Am. Chem. Soc.*, **100**, 379 (1978) and  
(c) H. L. Hase, C. Mühlner and A. Schweig, *Tetrahedron*, **34**, 2983 (1978).



55. W. von Niessen, L. S. Cederbaum and W. P. Kraemer, *Theor. Chim. Acta*, **44**, 85 (1977).
56. C. Fridh, *J. Chem. Soc., Faraday Trans. 2*, **75**, 993 (1979).
57. J. R. Collins and G. A. Gallup, *J. Am. Chem. Soc.*, **104**, 1530 (1982).
58. G. Bieri, L. Åsbrink and W. von Niessen, *J. Electron Spectrosc.*, **27**, 129 (1982).
59. G. de Alti, P. Decleva and A. Lisini, *J. Mol. Struct. (Theochem)*, **108**, 129 (1984).
60. K. Kimura, S. Katsumata, Y. Achiba, T. Yamazaki and S. Iwata, in *Handbook of He (I) Photoelectron Spectra of Fundamental Organic Molecules*, Halsted Press, New York, 1981.
61. T. Koopmans, *Physica*, **1**, 280 (1931).
62. K. B. Wiberg, C. M. Hadad, S. Sieber and P. v. R. Schleyer, *J. Am. Chem. Soc.*, **114**, 5820 (1992).
63. (a) P. Becker, in *Electron and Magnetization Densities in Molecules and Crystals*, Vol. 48, NATO Advanced Study Institutes, Series B: Phys., Plenum Press, New York, 1980.  
(b) P. Coppens and M. B. Hall, in *Electron Distributions and the Chemical Bond*, Plenum Press, New York, 1981.
64. P. Hohenberg and W. Kohn, *Phys. Rev.*, **136 B**, 864 (1964).
65. P. Coppens and E. D. Stevens, *Adv. Quantum Chem.*, **10**, 1 (1977).
66. (a) A. Hartman and F. L. Hirshfeld, *Acta Crystallogr.*, **20**, 80 (1966).  
(b) C. J. Fritchie, Jr., *Acta Crystallogr.*, **20**, 27 (1966).  
(c) T. Ito and T. Sakurai, *Acta Crystallogr., Sect B*, **B29**, 1594 (1973).  
(d) D. A. Matthews and G. D. Stucky, *J. Am. Chem. Soc.*, **93**, 5954 (1971).
67. (a) R. F. W. Bader and T. T. Nguyen-Dang, *Adv. Quantum Chem.*, **63** (1981).  
(b) R. F. W. Bader, T. T. Nguyen-Dang and Y. Tal, *Rep. Prog. Phys.*, **44**, 893 (1981).  
(c) R. F. W. Bader, in *Atoms in Molecules—A Quantum Theory*, Oxford University Press, Oxford, 1990.  
(d) R. F. W. Bader, P. L. A. Popelier and T. A. Keith, *Angew. Chem.*, **106**, 647 (1994).
68. D. Cremer and E. Kraka, *Croat. Chem. Acta*, **57**, 1265 (1984).
69. D. Cremer and E. Kraka, *Angew. Chem., Int. Ed. Engl.*, **23**, 627 (1984).
70. (a) K. Ruedenberg, in *Localization and Delocalization in Quantum Chemistry* (Eds. O. Chelvet, R. Daudel, S. Diner and J. P. Malrieu), Vol. 1, Reidel, Dordrecht, 1975, p. 223.  
(b) K. Ruedenberg, *Rev. Mod. Phys.*, **34**, 326 (1962).  
(c) C. Edmiston and K. Ruedenberg, *J. Phys. Chem.*, **68**, 1628 (1963).  
(d) E. M. Layton Jr. and K. Ruedenberg, *J. Phys. Chem.*, **68**, 1654 (1963).  
(e) R. R. Rue and K. Ruedenberg, *J. Phys. Chem.*, **68**, 1676 (1963).
71. D. Cremer, J. Gauss and E. Kraka, *J. Mol. Struct. (Theochem)*, **169**, 531 (1988).
72. (a) R. F. W. Bader and H. Essén, *J. Chem. Phys.*, **80**, 1943 (1984).  
(b) R. F. W. Bader, P. L. MacDougall and C. D. H. Lau, *J. Am. Chem. Soc.*, **106**, 1594 (1984).
73. See, e.g., P. M. Morse and H. Feshbach, in *Methods of Theoretical Physics*, Vol. 1, McGraw-Hill, New York, 1953, p. 6.
74. D. K. Pan, J.-N. Gao, H.-L. Liu, M.-B. Huang and W. H. E. Schwarz, *Int. J. Quantum Chem.*, **29**, 1147 (1986).
75. R. Ahlrichs and C. Ehrhardt, *Chemie in unserer Zeit*, **19**, 120 (1985).
76. (a) P. v. R. Schleyer, in *Substituent Effects in Radical Chemistry*, Nato ASI Series (Eds. H. G. Viehe, R. Janoschek and R. Merenyi), Reidel, Dordrecht, 1986, p. 61.  
(b) P. v. R. Schleyer, A. F. Sax, J. Kalcher and R. Janoschek, *Angew. Chem.*, **99**, 374 (1987).
77. K. B. Wiberg, *Angew. Chem., Int. Ed. Engl.*, **25**, 312 (1986).
78. K. B. Wiberg, R. F. W. Bader and C. D. H. Lau, *J. Am. Chem. Soc.*, **109**, 985 (1987).
79. K. B. Wiberg, R. F. W. Bader and C. D. H. Lau, *J. Am. Chem. Soc.*, **109**, 1001 (1987).
80. S. Inagaki, N. Goto and K. Yoshikawa, *J. Am. Chem. Soc.*, **113**, 7144 (1991).
81. P. Politzer and J.-S. Murray, in *Structure and Reactivity* (Eds. J. F. Liebman and A. Greenberg), VCH Publishers, New York, 1988, p. 1.
82. T. S. Slee, in *Modern Models of Bonding and Delocalization* (Eds. J. F. Liebman and A. Greenberg), VCH Publishers, New York, 1988, p. 63.
83. B. Liu and D. Kang, *J. Chem. Inf. Comput. Sci.*, **34**, 418 (1994).
84. P. George, M. Trachtman, C. W. Bock and A. M. Brett, *Tetrahedron*, **32**, 317 (1976).
85. K. B. Wiberg, *J. Comput. Chem.*, **5**, 197 (1984).
86. M. R. Ibrahim and P. v. R. Schleyer, *J. Comput. Chem.*, **6**, 157 (1985).
87. C. Zhixing, *Theor. Chim. Acta*, **68**, 365 (1985).
88. (a) R. F. W. Bader, T. Tang, Y. Tal and F. W. Biegler-König, *J. Am. Chem. Soc.*, **104**, 946 (1982).  
(b) R. F. W. Bader, *J. Chem. Phys.*, **73**, 2871 (1980).

- (c) F. W. Biegler-König, R. F. W. Bader and T. Tal, *J. Comput. Chem.*, **3**, 317 (1982).
89. (a) D. F. McMillen and D. M. Golden, *Am. Rev. Phys. Chem.*, **33**, 493 (1982).  
(b) M. H. Baghal-Vayjooee and S. Benson, *J. Am. Chem. Soc.*, **101**, 2840 (1979).  
(c) W. Tsang, *J. Am. Chem. Soc.*, **107**, 2872 (1985).
90. (a) A. von Baeyer, *Chem. Ber.*, **18**, 2269 (1885).  
(b) For an evaluation of von Baeyer's work see: R. Huisgen, *Angew. Chem., Int. Ed. Engl.*, **25**, 297 (1986).
91. (a) R. G. Snyder and J. M. Schachtschneider, *Spectrochim. Acta*, **21**, 169 (1965).  
(b) R. G. Snyder and G. Zerbi, *Spectrochim. Acta*, **23 A**, 39 (1967).
92. (a) U. Buckert and N. L. Allinger, in *Molecular Mechanics*, ACS Monograph 177, Washington D.C., 1980.  
(b) S.-J. Chang, D. McNally, S. Shary-Tehrany, M. J. Hickey and R.H. Boyd, *J. Am. Chem. Soc.*, **92**, 3109 (1970).  
(c) N. L. Allinger, M. T. Tribble, M. A. Millerand and D. H. Wertz, *J. Am. Chem. Soc.*, **93**, 1637 (1971).  
(d) See also discussion in: F. H. Westheimer, in *Steric Effects in Organic Chemistry* (Ed. M. S. Newman), Wiley, New York, 1956, p. 523.  
(e) E. M. Engler, J. D. Andose and P. v. R. Schleyer, *J. Am. Chem. Soc.*, **95**, 8005 (1973).
93. N. L. Bauld, J. Cesak and R. L. Holloway, *J. Am. Chem. Soc.*, **99**, 8140 (1977).
94. R. S. Grev and H. Schaefer III, *J. Am. Chem. Soc.*, **109**, 6577 (1987).
95. J. D. Dill, A. Greenberg and J. F. Liebman, *J. Am. Chem. Soc.*, **101**, 6814 (1979).
96. S. Durmaz and H. Kollmar, *J. Am. Chem. Soc.*, **102**, 6942 (1980).
97. D. Cremer and E. Kraka, *J. Am. Chem. Soc.*, **107**, 3811 (1985).
98. K. B. Wiberg and K. E. Laidig, *J. Org. Chem.*, **57**, 5092 (1992).
99. For experimental geometries see:  
(a) F. H. Allen, *Acta Crystallogr., Sect. B*, **B36**, 81 (1980).  
(b) F. H. Allen, *Acta Crystallogr., Sect. B*, **B37**, 890 (1981).  
(c) F. H. Allen, *Tetrahedron*, **38**, 645 (1982).  
(d) F. H. Allen, O. Kennard and R. Taylor, *Acc. Chem. Res.*, **16**, 146 (1983).
100. R. E. Penn and J. E. Boggs, *J. Chem. Soc., Chem. Commun.*, 667 (1972).
101. R. Pearson, Jr., A. Choplin and V. W. Laurie, *J. Chem. Phys.*, **62**, 4859 (1975).
102. (a) A. Skancke and J. E. Boggs, *J. Mol. Struct.*, **51**, 267 (1979).  
(b) G. R. DeMaré and M.R. Peterson, *J. Mol. Struct.*, **89**, 213 (1982).  
(c) Also see: S.W. Staley, A. E. Howard, M. D. Harmony, S. N. Mathur, M. Kattija-Ari, J.-I. Choe and G. J. Lind, *J. Am. Chem. Soc.*, **102**, 3639, (1980).  
(d) W. J. Hehre, *J. Am. Chem. Soc.*, **94**, 6592 (1972).
103. A. Skancke, *Acta Chem. Scand., Ser. A*, **A36**, 637 (1982).
104. A. Greenberg, J. F. Liebman, W. R. Dolbier, Jr., K. S. Medinger and A. Skancke, *Tetrahedron*, **39**, 1533 (1983).
105. (a) A. T. Peretta and V. W. Laurie, *J. Chem. Phys.*, **62**, 2469 (1975).  
(b) C. A. Deakyne, L. C. Allen and N. C. Craig, *J. Am. Chem. Soc.*, **99**, 3895 (1977).  
(c) C. A. Deakyne, L. C. Allen and V. W. Laurie, *J. Am. Chem. Soc.*, **99**, 1343 (1977).  
(d) A. Skancke, E. Flood and J. E. Boggs, *J. Mol. Struct.*, **40**, 263 (1977).
106. (a) D. K. Hendricksen and M. D. Harmony, *J. Chem. Phys.*, **51**, 700 (1969).  
(b) M. D. Harmony, R. E. Bostrom and D. J. Hendricksen, *J. Chem. Phys.*, **62**, 1599 (1975).  
(c) S. N. Mathur and M. D. Harmony, *J. Chem. Phys.*, **69**, 4316 (1978).
107. A. Skancke and J. E. Boggs, *J. Mol. Struct.*, **50**, 173 (1978).
108. (a) A. Skancke, *J. Mol. Struct.*, **42**, 235 (1977).  
(b) L. Hedberg, K. Hedberg and J. E. Boggs, *J. Chem. Phys.*, **77**, 2996 (1982).
109. (a) J.-M. André, M.-C. André and G. Leroy, *Bull. Soc. Chim. Belg.*, **80**, 265 (1971).  
(b) M. Eckert-Maksic and Z. B. Maksic, *J. Mol. Struct.*, **86**, 325 (1982).
110. H. Oberhammer and J. E. Boggs, *J. Mol. Struct.*, **57**, 175 (1979).
111. M. Saunders, K. E. Laidig, K. B. Wiberg and P. v. R. Schleyer, *J. Am. Chem. Soc.*, **110**, 7652 (1988).
112. C. Kaupter, H. Heydtmann and W. Thiel, *Chem. Phys.*, **156**, 85 (1991).
113. A. Skancke, *Acta Chem. Scand.*, **A36**, 637 (1982).
114. P. Reynders and G. Schrupf, *J. Mol. Struct. (Theochem)*, **150**, 297 (1987).
115. J. R. Durig Jr., A.-Y. Wang and T. S. Little, *J. Mol. Struct. (Theochem)*, **244**, 117 (1991).

116. R. G. Ford and R. A. Beaudet, *J. Chem. Phys.*, **48**, 4671 (1968)
117. A. W. Klein and G. Schrupf, *Acta Chem. Scand., Ser. A*, **A35**, 425 (1981).
118. A. de Meijere and W. Lüttke, *Tetrahedron*, **25**, 2047 (1969).
119. V. Typke, *J. Mol. Spectrosc.*, **77**, 117 (1979).
120. R. H. Schwendman, G. D. Jacobs and T. M. Krigas, *J. Chem. Phys.*, **40**, 1022 (1964).
121. M. L. Lamm and B. P. Dailey, *J. Chem. Phys.*, **49**, 1588 (1968).
122. W. H. Taylor, M. D. Harmony, D. A. Cassada and S. W. Staley, *J. Chem. Phys.*, **81**, 5379 (1984).
123. M. Dakkouri, *J. Am. Chem. Soc.*, **113**, 7109 (1991).
124. J. A. Boatz and M. S. Gordon, *J. Phys. Chem.*, **93**, 3025 (1989).
125. H. Grützmacher and H. Pritzkow, *Angew. Chem., Int. Ed. Engl.*, **30**, 1017 (1991).
126. S. Yamamoto, M. Nakata, T. Fukayama and K. Kuchitsu, *J. Phys. Chem.*, **89**, 3298 (1985).
127. Y. Endo, M. C. Chang and E. Hirota, *J. Mol. Spectrosc.*, **126**, 63 (1987).
128. K. B. Wiberg and J. J. Wendeloski, *J. Am. Chem. Soc.*, **104**, 5679 (1982).
129. Y. Yamaguchi, Y. Osamura and H. F. Schaefer, *J. Am. Chem. Soc.*, **105**, 7506 (1983).
130. E. D. Simandiras, R. D. Amos, N. C. Handy, T. J. Lee, J. E. Rice, R. B. Remington and H. F. Schaefer, *J. Am. Chem. Soc.*, **110**, 1388 (1988).
131. J. E. Boggs and K. Fan, *Acta Chem. Scand.*, **A42**, 595 (1988).
132. Y. Yamaguchi, H. F. Schaefer and J. E. Baldwin, *Chem. Phys. Lett.*, **185**, 143 (1991).
133. D. Cremer and K. J. Szabo, Unpublished, 1994.
134. M. D. Harmony, *Acc. Chem. Res.*, **25**, 321 (1992).
135. J. Gauss and D. Cremer, *Adv. Quantum Chem.*, **27**, 101 (1990).
136. MP2: (a) C. Møller and M. S. Plesset, *Phys. Rev.*, **46**, 618 (1934).  
(b) J. A. Pople, J. S. Binkley and R. Seeger, *Int. J. Quantum Chem., Symp.*, **10**, 1 (1976).  
(c) MP3, MP4: R. Krishnan and J. A. Pople, *Int. J. Quantum Chem.*, **14**, 91 (1978).  
(d) R. Krishnan, M. J. Frisch and J. A. Pople, *J. Chem. Phys.*, **72**, 4244 (1980).
137. K. Raghavachari, G. W. Trucks, J. A. Pople and M. Head-Gordon, *Chem. Phys. Lett.*, **157**, 479 (1989).
138. (a) Z. He and D. Cremer, *Theor. Chim. Acta*, **84**, 305 (1993).  
(b) Z. He and D. Cremer, *Int. J. Quantum Chem., Symp.*, **25**, 43 (1991).
139. (a) M. D. Harmony, V. W. Laurie, R. L. Kuczkowski, R. H. Schwendeman, D. A. Ramsay, F. J. Lovas, W. A. Lafferty and A. G. Maki, *J. Phys. Chem. Ref. Data*, **8**, 619 (1979).  
(b) For C<sub>2</sub>H<sub>4</sub> see: K. Kuchitsu, *J. Chem. Phys.*, **44**, 906 (1966).
140. A. Almenningen, O. Bastiansen and P. N. Skancke, *Acta Chem. Scand.*, **15**, 711 (1961).
141. K. B. Wiberg, *J. Am. Chem. Soc.*, **105**, 1227 (1983).
142. K. W. Cox, M. D. Harmony, G. Nelson and K. B. Wiberg, *J. Am. Chem. Soc.*, **90**, 3395 (1968).
143. L. Hedberg and K. Hedberg, *J. Am. Chem. Soc.*, **107**, 7257 (1985).
144. (a) E. R. Davidson, *J. Chem. Phys.*, **46**, 3320 (1967).  
(b) K. R. Roby, *Mol. Phys.*, **27**, 81 (1974).
145. A. R. Mochel, C. O. Britt and J. E. Boggs, *J. Chem. Phys.*, **58**, 3221 (1973).
146. J. R. Holtzclaw, W. C. Harris and S. F. Bush, *J. Raman Spectrosc.*, **9**, 257 (1980).
147. B. K. Stalick and J. A. Ibers, *J. Am. Chem. Soc.*, **93**, 3779 (1971).
148. D. A. Horner, R. S. Grev and H. F. Schaefer III, *J. Am. Chem. Soc.*, **114**, 2094 (1992).
149. Y. Xie and H. F. Schaefer, *J. Am. Chem. Soc.*, **112**, 5393 (1990).
150. R. H. Nobes, W. R. Rodwell, W. J. Bouma and L. Radom, *J. Am. Chem. Soc.*, **103**, 1913 (1981).
151. P. H. M. Buldelaar, A. J. Kos, T. Clark and P. v. R. Schleyer, *Organometallics*, **4**, 429 (1985).
152. M. Bühl, P. v. R. Schleyer, M. A. Ibrahim and T. Clark, *J. Am. Chem. Soc.*, **113**, 2466 (1991).
153. J.-S. Murray, J. M. Seminario, P. Lane and P. Politzer, *J. Mol. Struct. (Theochem)*, **207**, 193 (1990).
154. J. L. Duncan and D. C. McKean, *J. Mol. Spectrosc.*, **27**, 117 (1968).
155. J. L. Duncan and D. Ellis, *J. Mol. Spectrosc.*, **28**, 540 (1968).
156. J. L. Duncan and G. R. Burns, *J. Mol. Spectrosc.*, **30**, 253 (1969).
157. I. W. Levin and R. A. R. Pearce, *J. Chem. Phys.*, **69**, 2196 (1978).
158. A. Komornicki, F. Pauzat and Y. Ellinger, *J. Phys. Chem.*, **87**, 3847 (1983).
159. Y. Yamaguchi, H. F. Schaefer III and J. E. Baldwin, *Chem. Phys. Lett.*, **185**, 143 (1991).
160. For a discussion of scaling factors, see Reference 21.
161. J. A. Boatz and M. S. Gordon, *J. Phys. Chem.*, **93**, 1819 (1989).
162. Z. Konkoli, A. Larsson and D. Cremer, *J. Chem. Phys.*, to be published.
163. Z. Konkoli, A. Larsson and D. Cremer, *J. Phys. Chem.*, to be published.

164. (a) E. B. Wilson, Jr., J. C. Decius and P. C. Cross, in *Molecular Vibrations*, Dover, New York, 1980.  
(b) W. D. Gwinn, *J. Chem. Phys.*, **55**, 477 (1971).
165. D. C. McKean, *Chem. Soc. Rev.*, **7**, 399 (1978).
166. (a) J. A. Berson, L. D. Pedersen and B. K. Carpenter, *J. Am. Chem. Soc.*, **98**, 122 (1976).  
(b) S. W. Benson, in *Thermochemical Kinetics*, Wiley, London, 1976.
167. For reviews on analytical derivative methods, See:  
(a) P. Jørgensen and J. Simons (Eds.), *Geometrical Derivatives of Energy Surfaces and Molecular Properties*, Reidel, Dordrecht, 1986.  
(b) P. Pulay, *Adv. Chem. Phys.*, **67**, 241 (1987).  
(c) H. B. Schlegel, *Adv. Chem. Phys.*, **67**, 249 (1987).  
(d) R. D. Amos, *Adv. Chem. Phys.*, **67**, 99 (1987).
168. HF second derivatives:  
(a) J. A. Pople, R. Krishnan, H. B. Schlegel and J. S. Binkley, *Int. J. Quantum Chem., Symp.*, **13**, 325 (1979).  
MP2 second derivatives:  
(b) N. C. Handy, R. D. Amos, J. F. Gaw, J. E. Rice and E. D. Simandiras, *Chem. Phys. Lett.*, **120**, 151 (1985).  
(c) R. J. Harrison, G. B. Fitzgerald, W. D. Laidig and R. J. Bartlett, *Chem. Phys. Lett.*, **124**, 291 (1986).
169. For a review see:  
(a) C. Castiglioni, M. Gussoni and G. Zerbi, *J. Mol. Struct.*, **141**, 341 (1986).  
(b) M. Gussoni, C. Castiglioni and G. Zerbi, *J. Mol. Struct. (Theochem)*, **138**, 203 (1986).  
(c) M. Gussoni, C. Castiglioni, M. N. Ramos, M. Rui and G. Zerbi, *J. Mol. Struct.*, **224**, 445 (1990) and references cited therein.
170. (a) W. B. Person and J. H. Newton, *J. Chem. Phys.*, **61**, 1040 (1974).  
(b) J. H. Newton and W. B. Person, *J. Chem. Phys.*, **64**, 3036 (1976).  
(c) J. H. Newton, R. A. Levine and W. R. Person, *J. Chem. Phys.*, **67**, 3282 (1977).  
(d) W. B. Person and J. Overend, *J. Chem. Phys.*, **66**, 1442 (1977).
171. K.-M. Marstokk and H. Møllendal, *Acta Chem. Scand.*, **45**, 354 (1991).
172. (a) G. Holzawrth, E. C. Hsu, H. S. Mosher, T. R. Faulkner and A. Moscovitz, *J. Am. Chem. Soc.*, **96**, 251 (1974).  
(b) L. A. Nafie, J. C. Cheng and P. J. Stephens, *J. Am. Chem. Soc.*, **97**, 3842 (1975).  
(c) L. A. Nafie, T. A. Keiderling and P. J. Stephens, *J. Am. Chem. Soc.*, **98**, 2715 (1976).
173. P. J. Stephens, *J. Phys. Chem.*, **89**, 748 (1985).
174. K. J. Jalkanen, P. J. Stephens, R. D. Amos and N. C. Handy, *J. Am. Chem. Soc.*, **109**, 7193 (1987).
175. P. Lazzeretti, R. Zanasi, T. Prosperi and A. Lapicciarella, *Chem. Phys. Lett.*, **150**, 515 (1988).
176. A. J. Stone, *Chem. Phys. Lett.*, **83**, 233 (1981).
177. J. H. Williams, Ph.D. Thesis, University of Cambridge (1980).
178. R. D. Amos and J. H. Williams, *Chem. Phys. Lett.*, **84**, 104 (1981).
179. M. P. Bogaard, A. D. Buckingham, R. K. Pierens and A. H. White, *J. Chem. Soc., Faraday Trans. 1*, **74**, 3008 (1978).
180. K. M. Gough, *J. Chem. Phys.*, **91**, 2424 (1989).
181. (a) H. Hameka, *Mol. Phys.*, **1**, 203 (1958).  
(b) H. Hameka, *Rev. Mod. Phys.*, **34**, 87 (1962).  
(c) D. Zeroka and H. F. Hameka, *J. Chem. Phys.*, **45**, 300 (1966).
182. (a) F. London, *Naturwissenschaften*, **15**, 187 (1937).  
(b) F. London, *J. Phys. Rad.*, **8**, 397 (1937).
183. (a) J. A. Pople, *J. Chem. Phys.*, **37**, 53 (1962).  
(b) J. A. Pople, *J. Chem. Phys.*, **37**, 60 (1962).
184. (a) R. Ditchfield, *J. Chem. Phys.*, **56**, 5688 (1972).  
(b) R. Ditchfield, *J. Chem. Phys.*, **65**, 3123 (1976).  
(c) R. Ditchfield, *Mol. Phys.*, **27**, 789 (1974).  
(d) R. Ditchfield, in *Topics in Carbon-13 NMR Spectroscopy*, Vol. I, Wiley, New York, 1974.
185. (a) V. Galasso, *Theor. Chim. Acta*, **63**, 35 (1983).  
(b) M. Jaszunski and L. Adamowicz, *Chem. Phys. Lett.*, **79**, 133 (1981).  
(c) P. Lazzeretti and R. Zanasi, *J. Chem. Phys.*, **105**, 12 (1983).
186. K. Wolinski, J. F. Hinton and P. Pulay, *J. Am. Chem. Soc.*, **112**, 8251 (1990).

187. (a) W. Kutzelnigg, *Isr. J. Chem.*, **19**, 193 (1980).  
(b) M. Schindler and W. Kutzelnigg, *J. Chem. Phys.*, **76**, 1919 (1982).
188. (a) M. Schindler and W. Kutzelnigg, *J. Am. Chem. Soc.*, **105**, 1360 (1983).  
(b) M. Schindler and W. Kutzelnigg, *Mol. Phys.*, **48**, 781 (1983).  
(c) M. Schindler and W. Kutzelnigg, *J. Am. Chem. Soc.*, **109**, 1021 (1987).  
(d) M. Schindler, *J. Am. Chem. Soc.*, **109**, 5950 (1987).  
(e) M. Schindler, *Magn. Res. Chem.*, **26**, 394 (1988).  
(f) M. Schindler, *J. Am. Chem. Soc.*, **110**, 6623 (1988).  
(g) M. Schindler, *J. Chem. Phys.*, **88**, 7638 (1988).  
(h) W. Kutzelnigg, M. Schindler and U. Fleischer, in *NMR, Basic Principles and Progress* (Eds. P. Diehl, E. Fluck, H. Günther, R. Kosfeld and J. Seelig), Vol. 23, Springer, Berlin, 1991, p. 165.
189. A. E. Hansen and T. D. Bouman, *J. Chem. Phys.*, **82**, 5035 (1985).
190. (a) J. Gauss, *Chem. Phys. Lett.*, **191**, 614 (1992).  
(b) J. Gauss, *J. Chem. Phys.*, **99**, 3629 (1993).
191. J. Gauss, *Chem. Phys. Lett.*, in press.
192. (a) W. Kutzelnigg, C. van Wüllen, U. Fleischer and R. Franke, *Proceedings of the NATO Advanced Workshop on the Calculation of NMR Shielding Constants and their Use in the Determination of the Geometric and Electronic Structures of Molecules and Solids*, 1992.  
(b) C. van Wüllen and W. Kutzelnigg, *Chem. Phys. Lett.*, **205**, 563 (1993).
193. (a) T. D. Bouman and A. E. Hansen, *Chem. Phys. Lett.*, **175**, 292 (1990).  
(b) J. Geertsen and J. Oddershede, *J. Chem. Phys.*, **90**, 301 (1984).  
(c) J. Geertsen, P. Jørgensen and D. L. Yaeger, *Comp. Phys. Rep.*, **2**, 33 (1984).  
(d) G. T. Darborn and N. C. Handy, *Mol. Phys.*, **49**, 1277 (1983).  
(e) M. Jaszunski and A. Sadlej, *Theor. Chim. Acta*, **40**, 157 (1975).
194. J. W. Emsley, J. Feeney and L. H. Sutcliffe, *High Resolution Magnetic Resonance*, Vol. 2, Pergamon, Oxford, 1966.
195. K. W. Zilm, A. J. Beller, D. M. Grant, J. Michl, T. C. Chou and E. L. Allred, *J. Am. Chem. Soc.*, **103**, 2119 (1981).
196. G. C. Levy, R. L. Lichter and G. L. Nelson, in *Carbon-13 Nuclear Magnetic Resonance Spectroscopy*, 2nd ed., Wiley-Interscience, New York, 1980.
197. A. M. Orendt, J. C. Facelli, M. D. Grant, J. Michl, F. H. Walker, W. P. Daily, S. T. Waddell, K. B. Wiberg, M. Schindler and W. Kutzelnigg, *Theor. Chim. Acta*, **68**, 421 (1985).
198. A. E. Hansen and T. D. Bouman, *J. Chem. Phys.*, **91**, 3552 (1989).
199. (a) See Reference 8a  
(b) C. D. Poulter, R. S. Boikess, J. I. Brauman and S. Winstein, *J. Am. Chem. Soc.*, **94**, 2291 (1972).  
(c) W. R. Bley, *Mol. Phys.*, **20**, 491 (1971).  
(d) R. C. Benson and W. H. Flygare, *J. Chem. Phys.*, **58**, 2651 (1973).
200. R. F. Childs, M. J. McGlinchey and A. Varadarajan, *J. Am. Chem. Soc.*, **106**, 5974 (1984).
201. See, e.g.:  
(a) P. Buzek, P.v.R. Schleyer and S. Sieber, *Chemie in unserer Zeit*, **26**, 116 (1992).  
(b) M. Bühl and P.v.R. Schleyer, in *Electron Deficient Boron and Carbon Clusters* (Eds. G.A. Olah, K. Wade and R.E. Williams), Wiley, New York, 1991.  
(c) M. Bühl, N. J. R. v. E. Hommes, P. v. R. Schleyer, U. Fleischer and W. J. Kutzelnigg, *J. Am. Chem. Soc.*, **113**, 2459 (1991).
202. See e.g.:  
(a) D. Hnyk, E. Vajda, M. Buehl and P. v. R. Schleyer, *Inorg. Chem.*, **31**, 2464 (1992).  
(b) M. Buehl and P.v.R. Schleyer, *J. Am. Chem. Soc.*, **114**, 477 (1992).  
(c) M. Buehl, P.v.R. Schleyer and M. L. McKee, *Heteroat. Chem.*, **2**, 499 (1991).  
(d) M. Buehl and P.v.R. Schleyer, *Angew. Chem.*, **102**, 962 (1990).  
(e) P.v.R. Schleyer, M. Büehl, U. Fleischer and W. Koch, *Inorg. Chem.*, **29**, 153 (1990).  
(f) P.v.R. Schleyer, W. Koch, B. Liu and U. Fleischer, *J. Chem. Soc., Chem. Commun.*, 1098 (1989).  
(g) M. Bremer, K. Schoetz, P.v.R. Schleyer, U. Fleischer, M. Schindler, W. Kutzelnigg, W. Koch and P. Pulay, *Angew. Chem.*, **101**, 1063 (1989).
203. D. Cremer, F. Reichel and E. Kraka, *J. Am. Chem. Soc.*, **113**, 9459 (1991).
204. F. Reichel, Ph.D. Dissertation, University of Köln, 1991.
205. D. Cremer, L. Olsson, F. Reichel and E. Kraka, *Isr. J. Chem.*, **33**, 369 (1993).

206. T. Onak, J. Tseng, M. Diaz, D. Tran, J. Arias, S. Herrera and D. Brown, *Inorg. Chem.*, **32**, 487 (1993).
207. M. Saunders, K. E. Laidig, K. B. Wiberg and P.v.R. Schleyer, *J. Am. Chem. Soc.*, **110**, 7652 (1988).
208. D. Cremer, P. Svensson, E. Kraka, Z. Konkoli and P. Ahlberg, *J. Am. Chem. Soc.*, **115**, 7457 (1993).
209. D. Cremer, P. Svensson and K.J. Szabo, to be published.
210. D. Cremer, P. Svensson, E. Kraka and P. Ahlberg, *J. Am. Chem. Soc.*, **115**, 7445 (1993).
211. S. Sieber, P.v.R. Schleyer, A. H. Otto, J. Gauss, F. Reichel and D. Cremer, *J. Phys. Org. Chem.*, **6**, 445 (1993).
212. (a) P. Wagner and A. B. F. Duncan, *J. Chem. Phys.*, **21**, 516 (1953).  
(b) M. B. Robin, *Higher Excited States of Polyatomic Molecules*, Vol. I, Academic Press, New York, 1975.
213. R. J. Buenker and S. D. Peyerimhoff, *J. Phys. Chem.*, **73**, 1299 (1969).
214. T.-K. Ha and W. Cencek, *Chem. Phys. Lett.*, **177**, 463 (1991).
215. S. W. Froelicher, B. S. Freiser and R. R. Squires, *J. Am. Chem. Soc.*, **108**, 2853 (1986).
216. P.v.R. Schleyer, G. W. Spitznagel and J. Chandrasekhar, *Tetrahedron Lett.*, **27**, 4411 (1986).
217. C. H. DePuy, V. M. Bierbaum and M. Damrauer, *J. Am. Chem. Soc.*, **106**, 4051 (1984).
218. S. G. Lias, J. L. Liebman and R. D. Levin, *J. Phys. Chem. Ref. Data*, **13**, 695 (1984).
219. S.-L. Chon and J. L. Franklin, *J. Am. Chem. Soc.*, **94**, 6347 (1972).
220. J. C. Schulz, F. A. Houle and J. L. Beauchamp, *J. Am. Chem. Soc.*, **106**, 3917 (1984).
221. K. Raghavachari, R. A. Whiteside, J. A. Pople and P.v.R. Schleyer, *J. Am. Chem. Soc.*, **103**, 5649 (1981).
222. M. J. S. Dewar, E. F. Healy and J. M. Ruiz, *J. Chem. Soc., Chem. Commun.*, 943 (1987).
223. W. Koch, B. Liu and P. v. R. Schleyer, *J. Am. Chem. Soc.*, **111**, 3479 (1989).
224. M. Saunders, P. Vogel, E. L. Hagen and J. Rosenfeld, *Acc. Chem. Res.*, **6**, 53 (1973).
225. W. J. Bouma, D. Poppinger and L. Radom, *Isr. J. Chem.*, **23**, 21 (1983).
226. D. D. M. Wayner, R. J. Boyd and D. R. Arnold, *Can. J. Chem.*, **63**, 3283 (1985).
227. P. Du, D. A. Hrovat and W. T. Borden, *J. Am. Chem. Soc.*, **110**, 3405 (1988).
228. C. E. Hudson, M. S. Ahmed, J. C. Traeger, C. S. Giam and D. J. McAdoo, *Int. J. Mass Spectrom. Ion Processes*, **113**, 117 (1992).
229. J. A. Booze and T. Baer, *J. Phys. Chem.*, **96**, 5710 (1992).
230. S. Lunell, L. Yin and M.-B. Huang, *Chem. Phys.*, **139**, 293 (1989).
231. K. Krogh-Jespersen and H. D. Roth, *J. Am. Chem. Soc.*, **114**, 8388 (1992).
232. L. A. Eriksson and S. Lunell, *J. Am. Chem. Soc.*, **114**, 4532 (1992).
233. C. E. Hudson, C. S. Giam and D. J. McAdoo, *J. Org. Chem.*, **58**, 2017 (1993).
234. (a) M. Iwasaki, K. Toriyama and K. Nunome, *J. Chem. Soc., Chem. Commun.*, 202 (1983).  
(b) K. Ohta, H. Nakatsuji, H. Kubodera and T. Shida, *Chem. Phys.*, **76**, 271 (1983).
235. S. Lunell, M.-B. Huang and A. Lund, *Faraday Discuss. Chem. Soc.*, **78**, 35 (1984).
236. (a) X.-Z. Qin and F. Williams, *Chem. Phys. Lett.*, **112**, 79 (1984).  
(b) X.-Z. Qin and F. Williams, *Tetrahedron*, **42**, 6301 (1986).
237. T. M. Sack, D. L. Miller and M. L. Gross, *J. Am. Chem. Soc.*, **107**, 6795 (1985).
238. (a) K. Raghavachari, R. A. Whiteside, J. A. Pople and P.v.R. Schleyer, *J. Am. Chem. Soc.*, **103**, 5649 (1981).  
(b) L. Radom, J. A. Pople and P.v.R. Schleyer, *J. Am. Chem. Soc.*, **95**, 8193 (1973).  
(c) For a summary, see Reference 21b, Chapter 7.
239. M. H. Lien and A. C. Hopkinson, *J. Phys. Chem.*, **88**, 1513 (1984).
240. D. Cremer and K. J. Szabo, unpublished results.
241. E. Jongejan, W. J. M. van Tilborg, Ch. H. V. Dusseau, H. Steinberg and Th. J. deBoer, *Tetrahedron Lett.*, 2359 (1972).
242. E. Jongejan, H. Steinberg and Th. J. deBoer, *Tetrahedron Lett.*, 397 (1972).
243. E. Jongejan, H. Steinberg and Th. J. DeBoer, *Recl. Trav. Chim. Pays-Bas*, **98**, 66 (1979).
244. J. R. van der Vecht, H. Steinberg and Th. J. deBoer, *Recl. Trav. Chim. Pays-Bas*, **96**, 313 (1977).
245. M. W. M. van Tilborg, R. van Doorn and N. M. M. Nibbering, *J. Am. Chem. Soc.*, **101**, 7617 (1979).
246. C. Cometta-Morini, T.-K. Ha and J. F. M. Oth, *J. Mol. Struct. (Theochem)*, **188**, 79 (1989).
247. M. Dupuis and J. Pacansky, *J. Chem. Phys.*, **76**, 2511 (1982).
248. M. M. H. Lien and A. C. J. Hopkinson, *J. Comput. Chem.*, **6**, 2764 (1985).
249. S. Olivella, A. Solé and J. M. Bofill, *J. Am. Chem. Soc.*, **112**, 2160 (1990).

250. V. Barone, C. Minichino, H. Faucher, R. Subra and A. Grand, *Chem. Phys. Lett.*, **205**, 324 (1993).
251. (a) S. Deycars, L. Hughes, J. Lustzyk and K. U. Ingold, *J. Am. Chem. Soc.*, **109**, 4954 (1987).  
(b) See also: R. W. Fessenden and R. H. Schuler, *J. Chem., Phys.*, **39**, 2147 (1963).  
(c) K. S. Chen, D. G. Edge and G. K. Kochi, *J. Am. Chem. Soc.*, **95**, 7036 (1973).
252. L. J. Johnston and K. U. Ingold, *J. Am. Chem. Soc.*, **108**, 2343 (1986).
253. J. E. Wertz and J. R. Bolton, *Electron Spin Resonance*, McGraw-Hill, New York, 1972.
254. (a) K. Holtzhauer, Ph.D. Thesis, ETH, Zürich, 1987.  
(b) K. Holtzhauer, C. Cometta-Morini and J. F. M. Oth, *J. Phys. Org. Chem.*, **3**, 219 (1990).
255. D. J. DeFrees, R. T. McIver and W. J. Hehre, *J. Am. Chem. Soc.*, **102**, 3334 (1980).
256. (a) G. Greig and J. C. C. Thynne, *Trans. Faraday Soc.*, **62**, 3338 (1966).  
(b) G. Greig and J. C. C. Thynne, *Trans. Faraday Soc.*, **63**, 1369 (1967).  
(c) J. A. Kerr, A. Smith and A. F. Trotman-Dickenson, *J. Chem. Soc. (A)*, 1400 (1969).
257. R. Walsh, *Int. J. Chem. Kinet.*, **2**, 71 (1970).
258. K. B. Wiberg, *J. Am. Chem. Soc.*, **105**, 1227 (1983).
259. P. H. M. Budzelaar, E. Kraka, D. Cremer and P.v.R. Schleyer, *J. Am. Chem. Soc.*, **108**, 561 (1986).
260. M. D. Newton and J. M. Schulman, *J. Am. Chem. Soc.*, **94**, 767 (1972).
261. M. D. Newton and J. M. Schulman, *J. Am. Chem. Soc.*, **94**, 773 (1972).
262. P. Chakrabarti, P. Seiler, J. D. Dunitz, A.-D. Schluter and G. J. Szejmies, *J. Am. Chem. Soc.*, **103**, 7378 (1981).
263. R. Hoffmann, *J. Am. Chem. Soc.*, **90**, 1475 (1968).
264. B. Zurawski and W. Kutzelnigg, *J. Am. Chem. Soc.*, **100**, 2654 (1978).
265. N. G. Rondan, K. N. Houk and R. A. Moss, *J. Am. Chem. Soc.*, **102**, 1770 (1980).
266. M. Moreno, J. M. Lluch, A. Oliva and J. Bertrán, *J. Mol. Struct. (Theochem)*, **164**, 17 (1988).
267. See, e.g., A. Szabo and N. S. Ostlund, *Modern Quantum Chemistry, Introduction to Advanced Electronic Structure Theory*, MacMillan, New York, 1982 and references cited therein.
268. (a) Activation energy for the reaction to give propene: I. E. Klein and B. S. Rabinovitch, *Chem. Phys.*, **35**, 439 (1978).  
(b) B. S. Rabinovitch, *Chem. Phys.*, **67**, 201 (1982).  
(c) The difference between the activation energies was determined to be  $3.7 \text{ kcal mol}^{-1}$ : E. V. Waag and B. S. Rabinovitch, *J. Phys. Chem.*, **76**, 1965 (1972).  
(d) See also: W. Doering, *Proc. Natl. Acad. Sci. U.S.A.*, **78**, 5279 (1982).
269. C. Doubleday, J.W. McIver and M. Page, *J. Am. Chem. Soc.*, **104**, 6533 (1982).
270. Y. Yamaguchi and H. F. Schaefer III, *J. Am. Chem. Soc.*, **106**, 5115 (1984).
271. T. R. Furlani and H. F. King, *J. Chem. Phys.*, **82**, 5577 (1985).
272. L. Carlucci, C. Doubleday, T. R. Furlani, H. F. King and J. W. McIver, *J. Am. Chem. Soc.*, **109**, 5323 (1987).
273. C. Doubleday, J. W. McIver and M. Page, *J. Phys. Chem.*, **92**, 4367 (1988).
274. S. Olivella and J. Salvadori, *Int. J. Quantum Chem.*, **37**, 713 (1990).
275. S. J. Getty, E. R. Davidson and W. T. Borden, *J. Am. Chem. Soc.*, **114**, 2085 (1992).
276. (a) F. T. Smith, *J. Chem. Phys.*, **29**, 235 (1958).  
(b) H. Kollmar, *J. Am. Chem. Soc.*, **95**, 966 (1973).
277. (a) S. W. Benson, *J. Chem. Phys.*, **34**, 521 (1961)  
(b) S. W. Benson and P. S. Nangia, *J. Chem. Phys.*, **38**, 18 (1963).  
(c) H. E. O'Neil and S. W. Benson, *J. Chem. Phys.*, **72**, 1866 (1968).  
(d) H. E. O'Neil and S. W. Benson, *Int. J. Chem. Kinet.*, **2**, 42 (1970).  
(e) S. W. Benson, *Thermochemical Kinetics*, Wiley, New York, 1971, p. 83.
278. S. Yamabe, T. Minato, M. Seki and S. Inagaki, *J. Am. Chem. Soc.*, **110**, 6047 (1988).
279. A. Alex and T. Clark, *J. Am. Chem. Soc.*, **114**, 10897 (1992).
280. M. R. A. Blomberg, P. E. M. Siegbahn and J.-E. Bäckvall, *J. Am. Chem. Soc.*, **109**, 4450 (1987).
281. J.-E. Bäckvall, E. E. Björkman, L. Pettersson, P. E. M. Siegbahn and A. Strich, *J. Am. Chem. Soc.*, **107**, 7408 (1985).
282. D. R. Gano, M. S. Gordon and J. A. Boatz, *J. Am. Chem. Soc.*, **113**, 6711 (1991).
283. P. E. M. Siegbahn and M. R. A. Blomberg, *J. Am. Chem. Soc.*, **114**, 10548 (1992).